



**HAL**  
open science

## Dynamic combinatorial chemistry for the multiplexed identification of glyco-dyn[n]arenes in an anti-adhesive strategy against *Pseudomonas aeruginosa*

Fanny Demontrond, Yoann Pascal, Marion Donnier-Maréchal, Corentin Raillon, Baptiste Luton, Clara de la Tramblais, Laurent Vial, David Gueyrard, Wessam Galia, Emmanuelle Berger, et al.

### ► To cite this version:

Fanny Demontrond, Yoann Pascal, Marion Donnier-Maréchal, Corentin Raillon, Baptiste Luton, et al.. Dynamic combinatorial chemistry for the multiplexed identification of glyco-dyn[n]arenes in an anti-adhesive strategy against *Pseudomonas aeruginosa*. 2024. hal-04738302

**HAL Id: hal-04738302**

**<https://hal.science/hal-04738302v1>**

Preprint submitted on 15 Oct 2024

**HAL** is a multi-disciplinary open access archive for the deposit and dissemination of scientific research documents, whether they are published or not. The documents may come from teaching and research institutions in France or abroad, or from public or private research centers.

L'archive ouverte pluridisciplinaire **HAL**, est destinée au dépôt et à la diffusion de documents scientifiques de niveau recherche, publiés ou non, émanant des établissements d'enseignement et de recherche français ou étrangers, des laboratoires publics ou privés.



Distributed under a Creative Commons Attribution - NonCommercial - NoDerivatives 4.0 International License

# Dynamic combinatorial chemistry for the multiplexed identification of glyco-dyn[n]arenes in an anti-adhesive strategy against *Pseudomonas aeruginosa*

Fanny Demontrond,<sup>a</sup> Yoann Pascal,<sup>a</sup> Marion Donnier-Maréchal,<sup>a</sup> Corentin Raillon,<sup>a</sup> Baptiste Luton,<sup>b</sup> Clara De la Tramblais,<sup>c</sup> Laurent Vial,<sup>a</sup> David Gueyrard,<sup>a</sup> Wessam Galia,<sup>b</sup> Emmanuelle Berger,<sup>b</sup> Alain Géloën,<sup>b</sup> Benoit Cournoyer,<sup>b</sup> Julien Leclaire,<sup>a</sup> and Sébastien Vidal<sup>a,c\*</sup>

<sup>a</sup> Institut de Chimie et Biochimie Moléculaires et Supramoléculaires, UMR 5246, CNRS, Université Claude Bernard Lyon 1, Université de Lyon, INSA Lyon, CPE Lyon, Villeurbanne, 69622, France

<sup>b</sup> UMR Ecologie Microbienne, CNRS 5557, INRAE 1418, Research Group «Bacterial Opportunistic Pathogens and Environment», VetAgro Sup, Aisle 3, 1st Floor, 69280 Marcy L'Etoile, France

<sup>c</sup> Institut de Chimie des Substances Naturelles, UPR 2301, CNRS, Université Paris-Saclay, Gif-sur-Yvette, 91198, France, [sebastien.vidal@cnrs.fr](mailto:sebastien.vidal@cnrs.fr)

This article is dedicated to Sir James Fraser Stoddart and Prof Jeremy K. M. Sanders who have inspired this work through their pioneering studies in supramolecular chemistry.

**Abstract:** Carbohydrate-protein interactions are of prime importance in cell-cell communication, signal transduction, cancer, bacterial or viral infection. Chemists have designed multivalent systems to mimic these recognition phenomena and provide potent ligands of these proteins with foreseen therapeutic applications. Dynamic combinatorial chemistry provides access to a library of chemical species in equilibrium through reversible covalent bonds. This strategy can be readily applied to the rapid and efficient identification of multivalent glycoclusters by introducing a protein into the equilibrating library for the selection of the fittest glycocluster for this protein. 1,4-Dithiophenols conjugated to monosaccharides were equilibrated into dynamic combinatorial libraries providing a diverse mixture of glycoclusters. Selection of the best ligand for different lectins (ConA, LecA and LecB from *Pseudomonas aeruginosa*) could increase the concentration of glyco-dyn[3]arenes and glyco-dyn[4]arenes. A key aspect of this strategy is that multiplexing can be readily achieved by using two building blocks (galactosylated and fucosylated 1,4-dithiophenols) to interrogate several lectins at once in a single experiment. These macrocyclic glycoclusters could be synthesized, isolated, then evaluated as ligands of the lectins and displayed nanomolar dissociation constants. Furthermore, while no toxicity could be detected against human cells or bacteria, their evaluation as anti-adhesive agents could be confirmed through a virulence assay on human A549 lung epithelial cells.

## Introduction

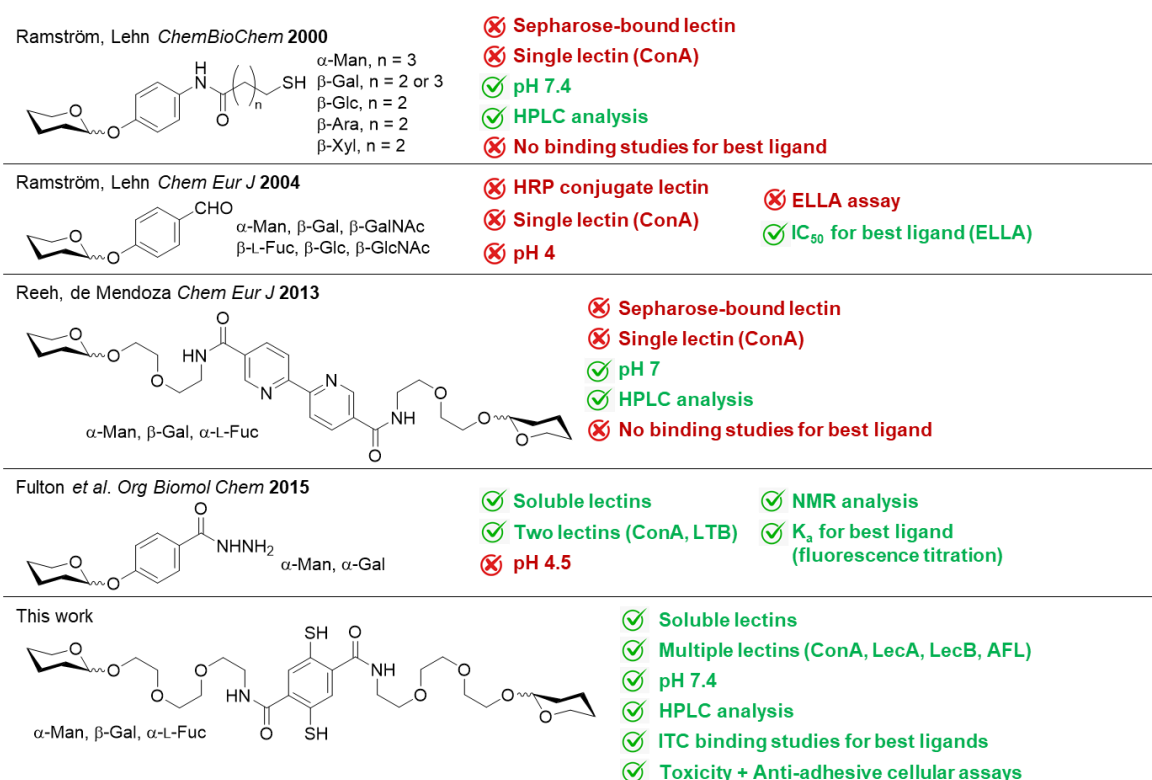
Carbohydrates are present at the cell surface and are taking part to the cell's communication with other healthy cells.<sup>1-4</sup> But they are also involved in the recognition by pathogens (bacteria, viruses) for the very first step of infection, i.e. adhesion to the host cell.<sup>5-7</sup> Bacteria will take advantage of a series of proteins (lectins or adhesins) present at their membrane, at the tip of their flagellum or pili to recognize specific oligosaccharidic structures at the host cell surface. When adhesion is secured, the bacteria will be internalized and deliver their cytotoxins or will reach a density that will trigger an

41 accumulation of quorum sensing molecules (e.g. homoserinelactones), then hasten their cell division,  
42 generate a biofilm, release toxins and become problematic or fatal to the host cells. The carbohydrate-  
43 lectin interactions are usually quite weak in terms of affinity, typically in the millimolar range.<sup>8-9</sup> Such  
44 interactions in nature are governed by multivalent interactions through lectin clustering at the cell  
45 surface, most of lectins being multimeric as the assembly of four and up to six monomeric units. Such  
46 multivalent interactions can provide a stronger carbohydrate-lectin interaction through multivalency.  
47 Chemists have designed a series of biomimetic strategies to tackle bacterial infections through two  
48 approaches.<sup>10-12</sup> The first one resides on a “medicinal chemistry” strategy in which the structure of the  
49 lectin and its natural ligand are known. The chemist and biochemist would then team up to generate  
50 a series of carbohydrate analogues of the natural ligand, largely termed as glycomimetics, and identify  
51 the most potent ligand of the lectin through intensive structure-activity relationship studies. This  
52 approach has been successfully applied for the design of potent FimH ligands against *Escherichia coli*  
53 urinary tract infections,<sup>13-19</sup> or targeting Galectin-3 in pulmonary fibrosis.<sup>20-24</sup> Another competitive  
54 strategy for the design of high affinity ligands of lectins is based on multivalency, meaning the design  
55 of multivalent glycoconjugates displaying multiple copies of the same and simple monosaccharide on  
56 a central core. The multivalent glycoconjugates can be based on small organic molecules (e.g.  
57 calixarene, pillararene, fullerene, porphyrin, peptide) and will be called a glycocluster.<sup>11-12, 25</sup> Several  
58 glycoclusters have been demonstrated as protective against bacterial infection up to the animal model  
59 and are very promising approaches.<sup>26-28</sup> While antibiotics are killing the bacteria and create a selection  
60 of the most resistant bacterial strains during a medical treatment, multivalent glycoconjugates are  
61 limiting the bacterial infection through anti-adhesion of the bacteria to the host cell, thus avoiding  
62 selective pressures on the bacterial strain and the emergence of resistance phenotypes.<sup>29-32</sup> For these  
63 reasons, glycoscientists have designed a large series of multivalent systems for interfering with  
64 bacterial adhesion. Nevertheless, like in every drug design process, the synthesis of each candidate  
65 with subtle structural variations can be time consuming prior a production of the additional datasets  
66 required to progress from a “hit” to a “lead” candidate.

67 This is where dynamic combinatorial chemistry (DCC) comes into play, offering the possibility to  
68 reversibly assemble simple building blocks into multivalent architectures under mild conditions.<sup>33</sup> In  
69 dynamic combinatorial libraries (DCLs), thermodynamic control implies that altering experimental  
70 conditions can induce changes in library composition. In theory, DCLs are sensitive to many external  
71 influences, such as temperature, pressure or light.<sup>34</sup> In practice, the response of libraries to a template  
72 target has been the most studied. Introducing a template (e.g., a protein) within a thermodynamically-  
73 controlled library of multivalent ligands was shown to shift the equilibrium towards the best binder(s),  
74 in an amplification process that is, after all, the way in which biomolecules have evolved their  
75 sophisticated functions.<sup>35-36</sup> If amplification is selective for the compound(s) that binds most strongly  
76 to the template, then DCC conveniently enables both the detection and the isolation of hit  
77 candidate(s).

78 A scarce number of examples of dynamic combinatorial chemistry applied for the identification of  
79 lectin ligands have been reported (Figure 1). The very first study by Ramström and Lehn used glycoside  
80 appended with a thiol-functionalized linker arm.<sup>37</sup> The disulfide exchange DCL was analyzed by reverse  
81 phase HPLC through UV absorption of the aromatic aglycon. Selection of the bis-mannoside ligand was  
82 observed when adding a sepharose-bound Concanavalin A (ConA), a lectin binding to mannose  
83 epitopes. While a valency of only two carbohydrate epitopes could be reached in the latter study, a  
84 follow-up investigation by the same group took advantage of acyl-hydrazone reversible covalent bond  
85 formation to explore higher valencies based on benzaldehyde aglycons and mono- di- or tri-hydrazide  
86 core scaffolds.<sup>38</sup> DCLs of up to 474 constituents were generated and the identification of the best ligand  
87 for ConA was performed through a novel assay involving an enzyme-linked lectin assay (ELLA). This

88 assay was implemented in a 96-well plate and dynamic deconvolution was applied based on the  
 89 removal of a single building block from the complete library. A trivalent ligand with micromolar affinity  
 90 towards ConA was finally identified through this strategy. A few years later, Reeh and de Mendoza  
 91 designed a DCL library of glycoclusters based on Fe(II)-bipyridine complexes providing valencies of six  
 92 carbohydrate epitopes.<sup>39</sup> Analysis of the DCL was readily performed by reverse phase HPLC through  
 93 UV absorption of the bipyridine moiety. Sepharose-bound ConA was incorporated into the  
 94 equilibrating DCLs and a hexa-mannoside glycocluster was clearly identified as the best ligand for  
 95 ConA. Fulton et al. have used a polyacrylamide appended with benzaldehyde groups for the reversible  
 96 covalent condensation with hydrazide-functionalized carbohydrates.<sup>40</sup> DCLs were studied by <sup>1</sup>H NMR  
 97 and the incorporation of galactose or mannose moieties was analyzed in the presence of either ConA  
 98 (for mannose) or *Escherichia coli* heat labile toxin (LTB, for galactose). The best binding polymers could  
 99 be isolated and their association constants with lectins evaluated.



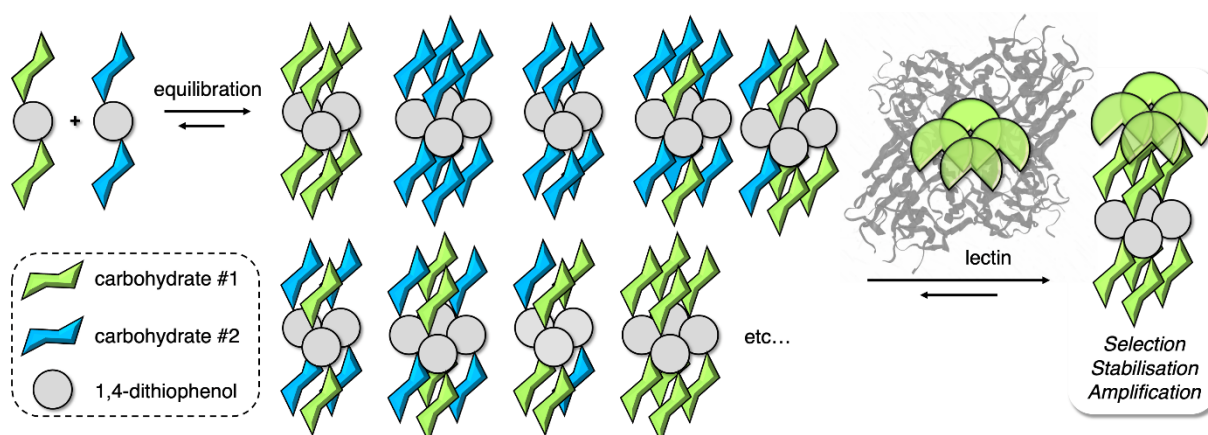
100

101 **Figure 1.** Pioneering studies on dynamic combinatorial chemistry with glycosylated architectures and  
 102 their conditions and results

103 These precedents have paved the way to further studies in the context of dynamic combinatorial  
 104 chemistry applied to the rapid and efficient identification of glycoclusters as high affinity ligands of  
 105 lectins. Nevertheless, they suffer from a few drawbacks such as the use of sepharose-bound lectins  
 106 which does not allow for an easy analysis of a large array of lectins since these are not always  
 107 commercially available either as pure biomaterials or as polymer-supported. The best ligands  
 108 identified were not always assayed against the lectin to clearly demonstrate their improved binding  
 109 properties. The only lectin studied was thus the model lectin ConA which is typically used as a proof of  
 110 concept but has no therapeutic implications, and a rather tedious ELLA assay was required to fully  
 111 deconvolute the properties of the glycoclusters in the DCLs.<sup>38</sup> Acyl-hydrazone exchange is typically  
 112 performed at pH 4.0-4.5 and is not always perfectly compatible with the stability of the lectin.<sup>38, 40</sup>  
 113 Spontaneous disulfide bond formation and exchange take place in aqueous solutions within pH range  
 114 7 to 9, and can be halted by reducing the pH below the pKa of the thiols involved. This inherent

115 thermodynamic sensitivity has been harnessed by researchers such as Prof Jeremy K. M. Sanders<sup>41-43</sup>  
116 and others<sup>44-45</sup> to create intricate molecular architectures and receptors in aqueous media. In this  
117 world of disulfide exchange-based DCC,<sup>46</sup> some also explored and developed over the last decade a  
118 new family of dynamic cyclophanes named dyn[n]arenes, which are based on mono- to tetra-  
119 functionalized 1,4-dithiophenol units linked by disulfide bridges.<sup>47</sup> We have recently demonstrated  
120 that a set of driving forces such as templating, folding and stacking lead to the selection and  
121 amplification of dyn[n]arenes of different composition, size and stereochemistry.<sup>48-51</sup> Furthermore, the  
122 unraveling of interactions involved in the dyn[n]arenes assembly processes not only led to the  
123 identification of novel physicochemical phenomena like the hydrophilic effect,<sup>52</sup> but also to innovative  
124 applications such as chiroptical sensing of biomolecules.<sup>53</sup>

125 Here, we describe an innovative approach for the design of high affinity lectin ligands through dynamic  
126 combinatorial chemistry which will address drawbacks reported before (Figure 2). The reversible  
127 covalent bond is a disulfide exchange of 1,4-dithiophenols that can equilibrate in buffer solution  
128 compatible with lectins stability and at neutral pH. Our approach reconsidered several aspects of the  
129 experimental setup developed so far to provide improved DCL conditions and generate novel outputs  
130 for glycoscience applications (Figure 1). The lectins used in the assays were not bound to sepharose or  
131 other polymer, nor conjugated to a horse radish peroxidase (HRP) for ELLA assay, but rather used in  
132 their native form in buffer solutions. Multiple lectins were readily used in the present study with a  
133 possibility for multiplexing several lectins with a single reference DCL for a rapid identification of the  
134 best glycoclusters in a single experimental process. Lectins of therapeutic interest from *Pseudomonas*  
135 *aeruginosa* have been studied and very high affinity glycoclusters could be identified, isolated and  
136 assayed against the lectin by ITC for a confirmation of their nanomolar affinities and also in a cellular  
137 assay to monitor their anti-adhesive properties.



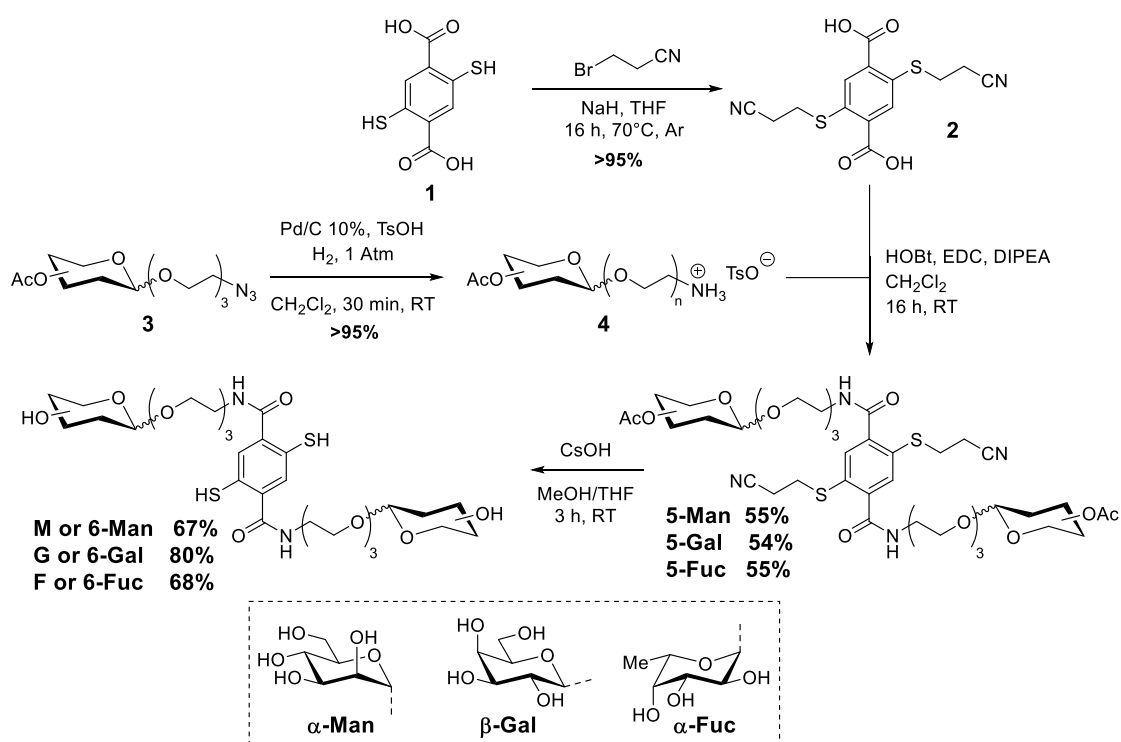
138  
139 **Figure 2.** Schematic representation of the 1,4-dithiophenol equilibration of dynamic combinatorial  
140 libraries of glycosylated dyn[n]arenes and influence of a lectin on the composition of the library

## 141 142 **Results and Discussion**

### 143 *Synthesis of 1,4-dithiophenol building blocks*

144 The glycosylated 1,4-dithiophenol building blocks were obtained through amide bond formation  
145 between an amino-functionalized glycoside and a protected dicarboxylic acid (Scheme 1). 1,4-  
146 dithiophenol-2,5-dicarboxylic acid **1**<sup>54</sup> required a protection of the thiols with 2-cyanoethyl to the bis-  
147 carboxylic acid **2** to provide a robust and reproducible amidation. Previous attempts of amidation with  
148 the bis-thiocarbamates protected thiols afforded only low yields for the desired amides. Then, the

149 azido-functionalized glycoside precursor was initially conjugated with the bis-acid **2** under Staudinger-  
 150 Villarasa conditions but with only low yields (20-30%) and concomitant formation of partially  
 151 deacetylated byproducts. The azido moiety was then reduced into the amine but further amidation  
 152 again produced up to 15% of deacetylated byproducts very difficult to separate from the desired  
 153 amine. To avoid deacetylation, an ammonium tosylate intermediate **4** was obtained by reduction of  
 154 the azido-carbohydrates **3** under hydrogenation conditions with a stoichiometric amount of *p*-  
 155 toluenesulfonic acid (TsOH).<sup>55</sup> The subsequent amidation using the diacid **2** afforded the desired  
 156 glycosylated 1,4-dithiophenol intermediates **5** in good yields and high purity. The simultaneous  
 157 deprotection of acetate esters on the carbohydrate moiety and the 2-cyanoethyl groups at the  
 158 thiophenol was performed in a single step using cesium hydroxide<sup>56</sup> to afford the desired fully  
 159 deprotected glycosylated 1,4-dithiophenol building blocks **6**.



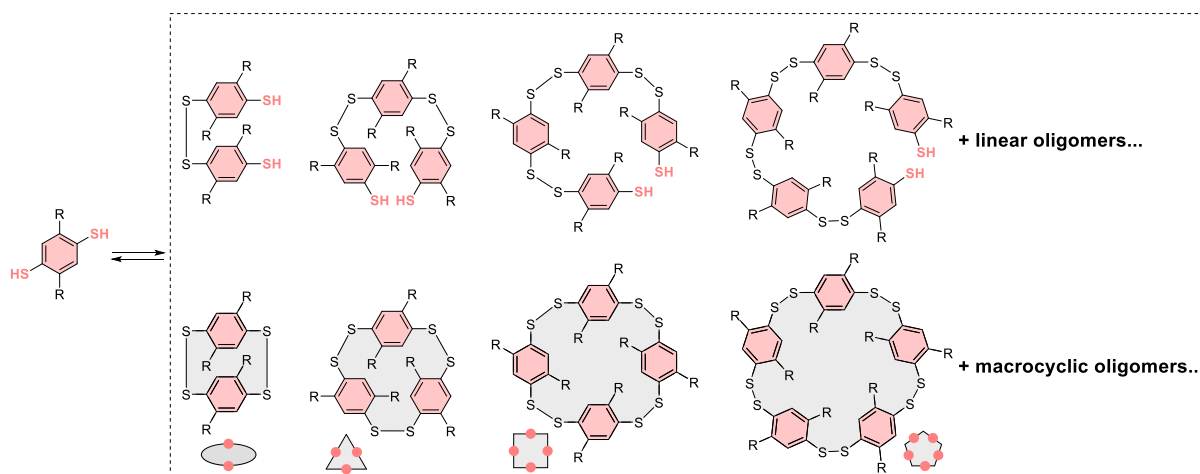
160

161 **Scheme 1.** Synthesis of the glycosylated 1,4-dithiophenol building blocks

162

163 *Equilibration and study of dynamic combinatorial libraries (DCLs)*

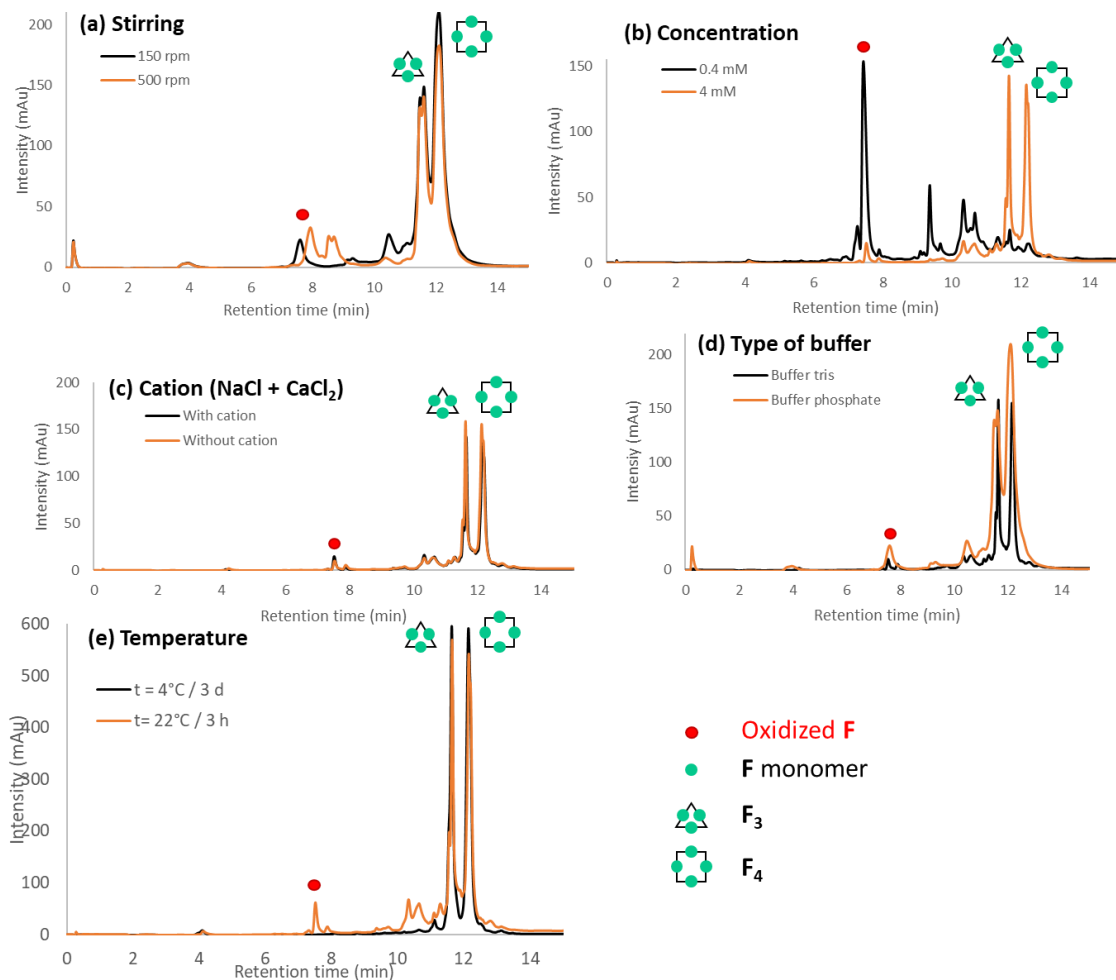
164 Disulfides are prone to oligomerization under neutral pH in solution, and oxidation can occur with the  
 165 assistance of oxygen dissolved in the solvent. 1,4-Dithiophenols will similarly generate linear oligomers  
 166 in solution with two residual thiophenols which can trigger cyclization for trimers, tetramers, or  
 167 pentamers and so on (Figure 3). One reason is that dihedral angle around the S-S bond is typically close  
 168 to 90° creating a helicoidal-type conformation bringing the residual thiophenols in close vicinity thus  
 169 favoring the ring closing of such oligomers. Equilibration is in general considered as complete when  
 170 the composition of the DCL is not evolving anymore and can be analyzed by reverse phase UHPLC using  
 171 the UV absorbance of the aromatic 1,4-dithiophenol core.



172

173 **Figure 3.** Schematic representation of the oligomerization process for 1,4-dithiophenols in the DCLs

174 The DCL equilibration was studied using the fucosylated 1,4-dithiophenol building block **F** alone in  
 175 solution with a particular attention for the determination of the operating conditions (Figure 4).  
 176 Stirring rate of the solution did not influence the equilibration of the **F**-DCL (Figure 4a), nor did the  
 177 addition of NaCl and CaCl<sub>2</sub> since most lectins require exogenous Ca<sup>2+</sup> for proper binding (Figure 4b) or  
 178 the type of buffer used (Figure 4c, Tris or PBS). Concentration of **F** in solution had a strong influence  
 179 on the DCL equilibration since at low concentration (0.4 mM) a large proportion of the **F** building block  
 180 was oxidized to sulfenic (RSOH) or sulfinic acids (RSO<sub>2</sub>H) with characteristic mass spectrometry *m/z*  
 181 values of M+16 or M+32 (Figure 4d). The oxidation into two sulfenic acids on both thiols or one thiol  
 182 remaining with a sulfinic acid could not be distinguished. This is problematic since oxidized **F** species  
 183 cannot participate to the DCL equilibration as they are not thiols anymore and hence their presence  
 184 must be reduced to the lowest proportion as possible. This was readily achieved by using higher  
 185 concentration (4 mM) of 1,4-dithiophenol **F** in the DCL solution. Thus, the amount of oxygen dissolved  
 186 in the solvent was much less important in comparison to the concentration of the equilibrating **F**  
 187 building block and the oxidized species were limited to less than 5% in relative quantity. Finally,  
 188 temperature of equilibration of the DCL did not have a major impact other than extending the time  
 189 required for equilibration (3 h at 22°C, 72 h at 4°C) but the low temperature conditions allowed the  
 190 complete removal of oxidized species (Figure 4e). A typical DCL equilibration was finally performed at  
 191 room temperature in a few hours, using the required buffer solution for the lectin and at 4 mM  
 192 concentration of 1,4-dithiophenol the building block with stirring.

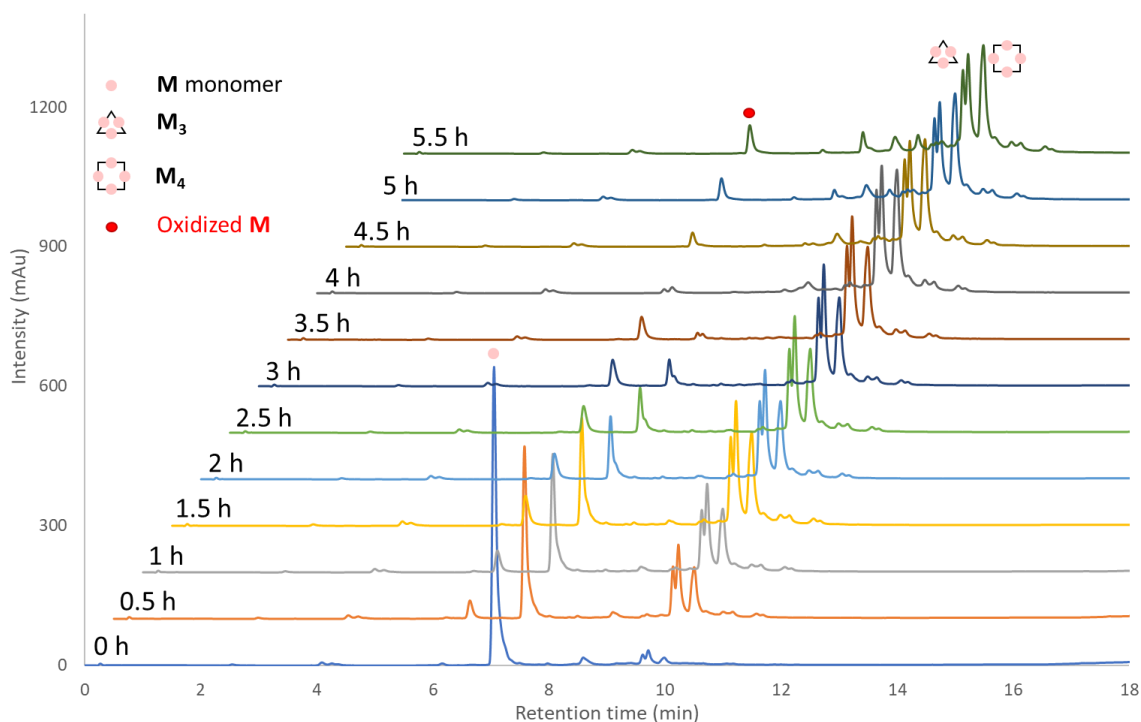


193

194 **Figure 4.** Influence of several parameters on an equilibrated DCL of **F** after > 7 h. (a) stirring ( $[F] = 4$   
 195 mM, 200 mM PBS, 22°C), (b) addition of  $\text{Na}^+$  or  $\text{Ca}^{2+}$  ( $[F] = 4$  mM, 200 mM Tris, 22°C, 100 mM NaCl, 100  
 196  $\mu\text{M}$   $\text{CaCl}_2$ ), (c) type of buffer ( $[F] = 4$  mM 200 mM PBS or 200 mM Tris, 22°C), (d) concentration ( $[F] =$   
 197 0.4 or 4 mM, 200 mM Tris, 22°C), or (e) temperature ( $[F] = 4$  mM, 200 mM Tris, 4°C or 22°C).

198 The kinetic analysis of the DCL equilibration was performed with the mannosylated 1,4-dithiophenol  
 199 **M** (Figure 5). At  $t=0$ , the monomer **M** can be observed at ca. 7 min retention time (RT) with a very tiny  
 200 amount of oligomerized species (ca. 10 min at RT). Equilibration then takes place in a few hours to  
 201 reach the disappearance of the monomer **M** after 3.5 h. After 0.5 h, a portion of oxidized **M** species  
 202 appeared and stayed constant over the course of the equilibration. Oligomeric species are growing  
 203 over the course of the equilibration of the DCL and appear at ca. 10 min at RT and are mainly composed  
 204 of macrocyclic **M**<sub>3</sub> and **M**<sub>4</sub>. The retention times had enough difference to clearly identify these species  
 205 and their mass spectrometry data were matching their molecular formula and composition. Therefore,  
 206 DCLs can be readily equilibrated at room temperature in a buffer solution and the equilibrium can be  
 207 reached within 3 to 4 hours. The DCL composition can be determined from UHPLC-MS data and a series  
 208 of macrocyclic oligomers are typically observed.

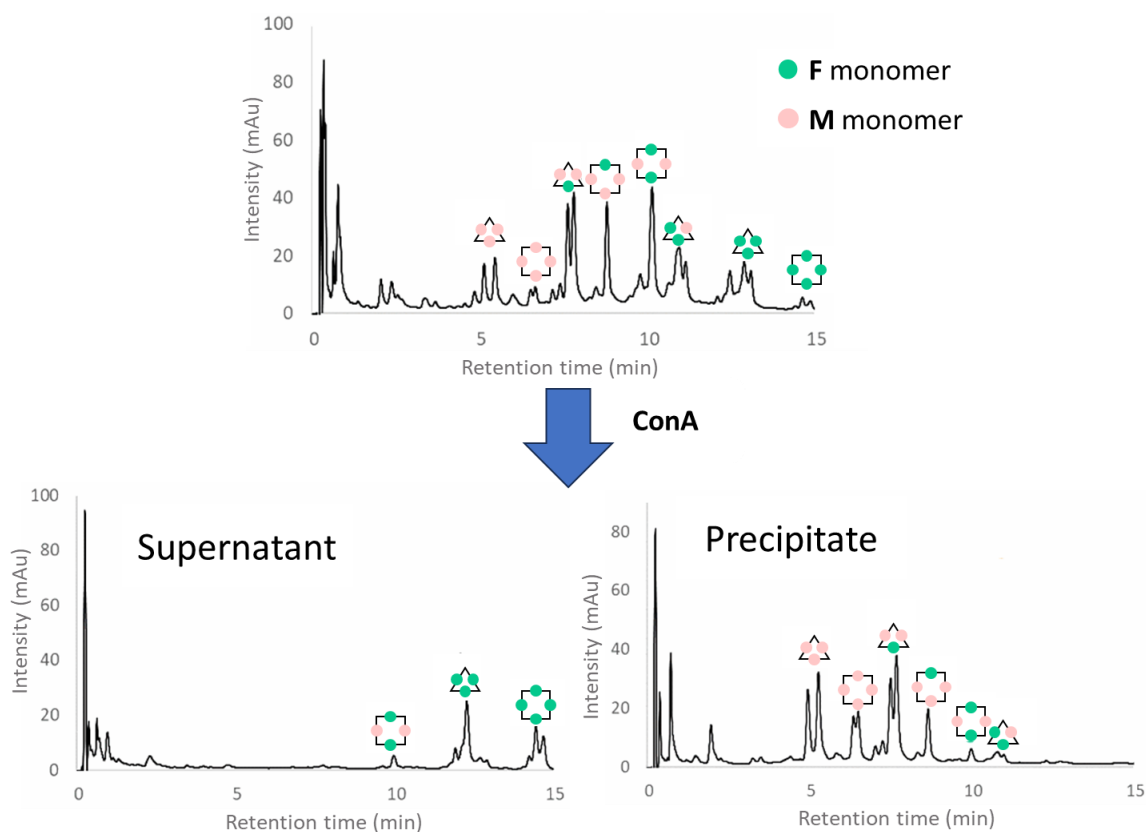




209  
 210 **Figure 5.** UHPLC-MS analysis of the DCL using the **M** building block (RT, [**M**] = 4 mM, 200 mM Tris  
 211 buffer)

212  
 213 *Study of DCL composed of **M** and **F** building blocks in the presence of ConA*

214 DCLs containing two different 1,4-dithiophenol building blocks have been studied. Their equilibration  
 215 with and without lectin will provide information about the identification of the best ligand for that  
 216 lectin in solution if the proportion of one of these species is increased. A (**M**+**F**)-DCL containing  
 217 equimolar amounts of each building block at a total concentration of 4 mM (2 mM each) was  
 218 equilibrated to reach equilibrium within a few hours. The resulting DCL composition was determined  
 219 by UHPLC-MS analysis (Figure 6). The first important observation is that all possible heteroglycoclusters  
 220 based on trimers and tetramers can be observed and characterized in the UHPLC-MS data. They all  
 221 appeared at different retention times from 5 to 15 minutes, due to the difference in polarity between  
 222 the mannose and fucose moieties: fucose building block **F** being more apolar than the mannosylated  
 223 one **M**, the retention time increased with the increasing number of **F** in the macrocycles.



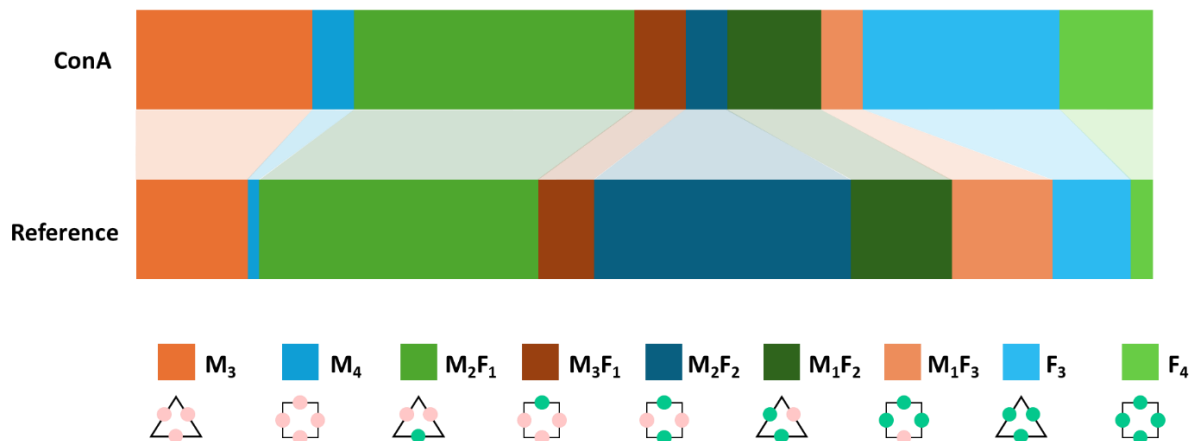
224

225 **Figure 6.** Equilibration of DCLs composed of **M** and **F** building blocks and influence of ConA on the  
 226 composition. **M:F** (1:1, 4 mM), ConA (4 mM) in buffer Tris 200 mM, NaCl 100 mM, CaCl<sub>2</sub> 100 μM, at RT

227 The same (**M+F**)-DCL equilibration was performed in the presence of ConA in the solution. A reference  
 228 (**M+F**)-DCL was equilibrated during 3.5 h at room temperature and with a concentration of 4 mM (to  
 229 minimize oxidation of the thiols). After that, this reference DCL was aliquoted into a new DCL and  
 230 diluted 10x with buffer to reach 0.4 mM concentration of **M+F**. The lectin (ConA, 0.4 mM) was then  
 231 added and the DCL equilibrated for an additional 2.5 h and a precipitate appeared in the solution. The  
 232 precipitate was recovered by centrifugation and the supernatant separated. The precipitate contained  
 233 the macrocycles with high affinity to the lectin that created a large three-dimensional network of  
 234 aggregated proteins and glycoclusters that crushed out of the solution. This precipitate was treated  
 235 with 1M HCl to unfold the protein and release the glycoclusters in solution that could be analyzed by  
 236 UHPLC-MS. This precipitate was composed mainly of **M<sub>3</sub>** and **M<sub>4</sub>** glycoclusters. As a consequence, the  
 237 supernatant contained mostly the fucosylated species that could not bind to the mannose-specific  
 238 ConA lectin.

239 The relative proportions of each macrocycle can be obtained through the area under the curve (AUC)  
 240 of the UHPLC chromatograms and allow the monitoring of the increase/decrease of each macrocycle  
 241 in the (**M+F**)-DCL with or without the ConA lectin (Figure 7). The increase of the **M<sub>3</sub>** can be clearly  
 242 identified along with an increase in **M<sub>4</sub>** while the proportion of most of the heteroglycoclusters  
 243 composed of **M** and **F** building blocks decrease in the DCL. The increased proportion of **M<sub>3</sub>** and **M<sub>4</sub>** can  
 244 be attributed to the selection of these high affinity ligands by the ConA lectin. This will be later  
 245 confirmed by ITC studies of these glycoclusters with ConA. Hence, ConA triggered the re-organization  
 246 of the (**M+F**)-DCL to favor the organization of the **M** building blocks into homoglycoclusters **M<sub>3</sub>** and **M<sub>4</sub>**  
 247 by decreasing the amount of heteroglycoclusters which displayed a poorer affinity for the lectin. As a  
 248 consequence, the increased proportion of fucosylated species (**F<sub>3</sub>** and **F<sub>4</sub>**) could be attributed to the

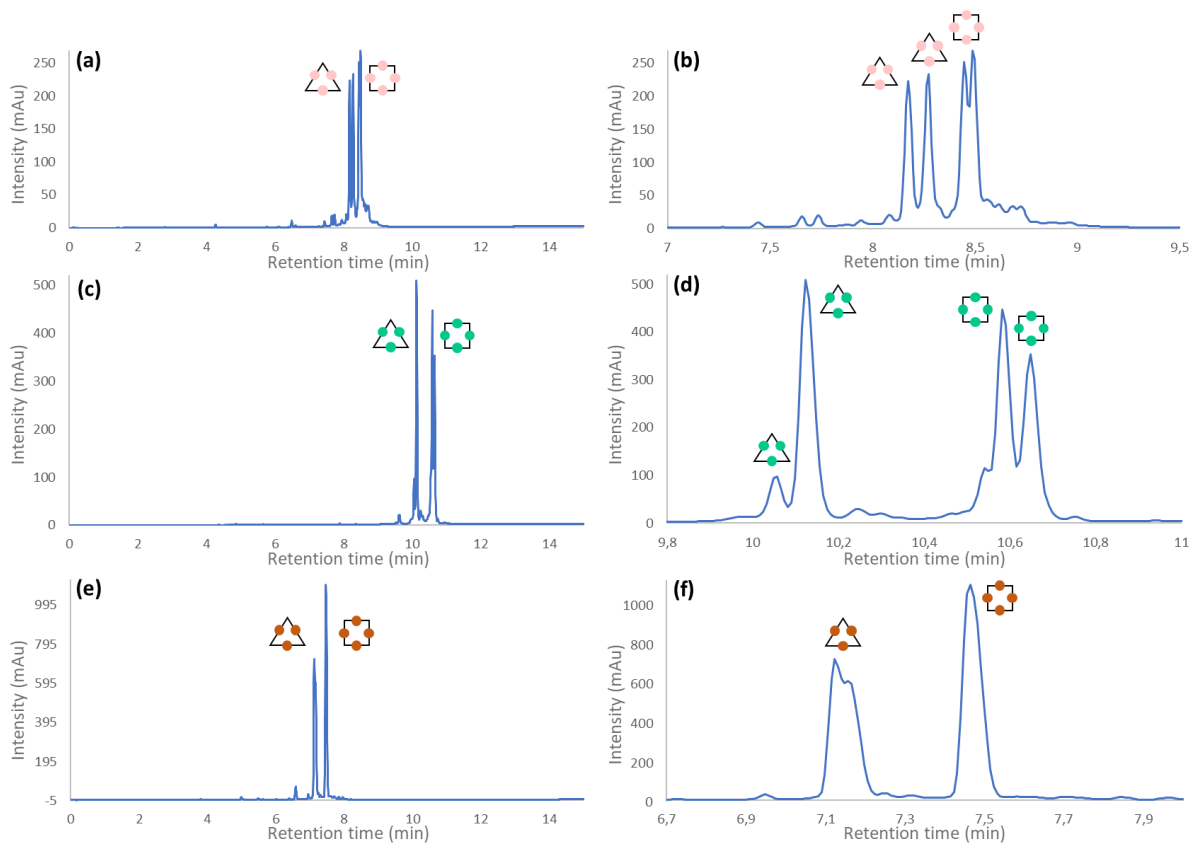
249 fact that if the **M** building blocks are brought together by ConA, then the remaining **F** building blocks  
 250 do not have any other outcome than to assemble together into macrocyclic oligomers **F<sub>3</sub>** and **F<sub>4</sub>**. ITC  
 251 binding studies of the fucosylated macrocycles **F<sub>3</sub>** and **F<sub>4</sub>** were performed to demonstrate that these  
 252 compounds have no affinity for the ConA lectin and therefore could not be selected by the lectin in  
 253 the equilibrating (**M+F**)-DCL.



254  
 255 **Figure 7.** Comparison of the reference DCL to the ConA amplified DCL combining materials from the  
 256 supernatant and precipitate fractions. Measurements were performed in triplicate and did not differ  
 257 by more than 5%.

258  
 259 *Purification of the macrocyclic glycoclusters **X<sub>3</sub>**/**X<sub>4</sub>***

260 The trimeric and tetrameric macrocycles **X<sub>3</sub>**/**X<sub>4</sub>** had to be purified from the equilibrated DCLs. For that  
 261 purpose, DCLs of **M**, **G** or **F** building blocks were equilibrated at low temperature (4°C) during 72 h to  
 262 limit oxidation, and the resulting DCL composed mostly of **X<sub>3</sub>**/**X<sub>4</sub>** was purified by preparative HPLC to  
 263 collect the macrocycles (Figure 8). It is worth pointing out that the macrocycles **X<sub>3</sub>** and **X<sub>4</sub>** were obtained  
 264 pure after preparative HPLC, but rearrangements were always observed during evaporation of solvents  
 265 from the collected fractions and also after a few hours in solution, preventing ITC studies with lectins.  
 266 Two sets of peaks were typically observed in the UHPLC chromatogram for each species (**X<sub>3</sub>** or **X<sub>4</sub>**) and  
 267 were due to the intrinsic chirality of the S-S bond which provides diastereoisomers for each disulfide  
 268 linkage.<sup>48</sup> Due to these limitations in reaching pure macrocycles, the mixture of **X<sub>3</sub>**/**X<sub>4</sub>** was analyzed by  
 269 ITC and the exact composition of the solution was determined for each individual measurement. The  
 270 molecular weight of **X<sub>3</sub>**/**X<sub>4</sub>** was calculated as the ratio of each macrocycle and according to the AUC  
 271 proportion in the UHPLC chromatogram.

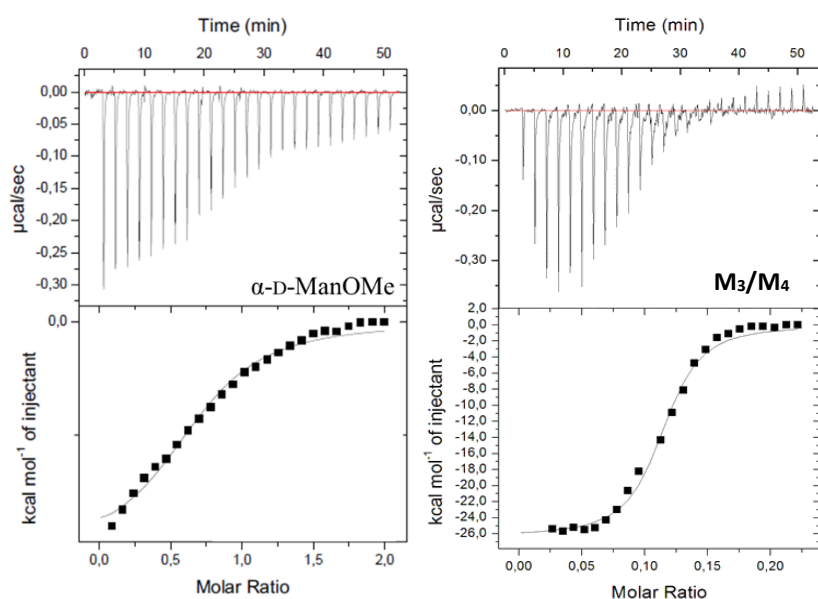


272

273 **Figure 8.** UHPLC chromatograms of glycosylated dyn[n]arenes after typical equilibration and  
 274 purification by preparative HPLC. (a,b) **M<sub>3</sub>/M<sub>4</sub>**, (c,d) **F<sub>3</sub>/F<sub>4</sub>** and (e,f) **G<sub>3</sub>/G<sub>4</sub>** in buffer Tris 200 mM, NaCl  
 275 100 mM, CaCl<sub>2</sub> 100 μM, at RT.

276 *ITC binding studies of M<sub>3</sub>/M<sub>4</sub> with ConA*

277 The affinity of the mannosylated glycoclusters **M<sub>3</sub>/M<sub>4</sub>** was verified by isothermal titration  
 278 microcalorimetry (ITC) to quantify the multivalent interactions between ConA and the ligands. Titration  
 279 provided a sigmoidal curve which is representative of a strong affinity of the ligands for ConA with a  
 280 60-fold improvement of affinity ( $\beta$ ) in comparison to the monovalent reference ligand methyl  $\alpha$ -D-  
 281 mannopyranoside ( **$\alpha$ -D-ManOMe**) (Figure 9).



282

283 **Figure 9.** Isothermal titration microcalorimetry (ITC) analysis of the binding properties toward ConA  
 284 (0.12 mM) for  **$\alpha$ -D-ManOMe** (1.8 mM, left panel) and the association titration curve obtained with a  
 285 1:1 binding model (lower left panel). ITC data obtained for injections of  **$M_3/M_4$**  (0.2 mM, 1:1) into a  
 286 solution of ConA (0.12 mM) and the associated titration curve (lower right panel).

287 Analysis of the ITC data (Table 1) also provided information about the stoichiometry of the  
 288 glycoclusters' complexes with ConA, and the  $n$  value of 0.09 indicates that, theoretically, up to 11 lectin  
 289 monomers can be involved in binding events simultaneously with the glycoclusters. Since the valency  
 290 of  **$M_3$**  is of 6 mannose units and 8 for the  **$M_4$**  macrocycle, this  $n$  value indicates that nearly all  
 291 mannosides are involved in an interaction with ConA, and thus a multivalent interaction is responsible  
 292 for the improvement of affinity ( $\beta$ ). This result indicates that the higher multivalency (6 to 8 valency)  
 293 reached with the oligomerized  **$M_3/M_4$**  is indeed responsible for the sharp increase in affinity ( $\beta = 61$ )  
 294 towards ConA reaching nanomolar affinity. For comparative purposes, it is to be noted that the affinity  
 295 of a calixarene-based tetravalent ligand (**Calix-Man<sub>4</sub>**, Figure S1) of ConA was reported in the nanomolar  
 296 range,<sup>26</sup> similar to the macrocycles  **$M_3/M_4$** , meaning that both are high affinity ligands for this lectin.

297 **Table 1.** ITC data for the binding properties of glycosylated dyn[n]arenes  **$M_3/M_4$**  and tetravalent **Calix-**  
 298 **Man<sub>4</sub>** towards ConA

Ligand	$n$	$-\Delta H$ (kJ.mol <sup>-1</sup> )	$-\Delta S$ (kJ.mol <sup>-1</sup> )	$K_d$ (nM)	$\beta^a$
<b><math>\alpha</math>-D-ManOMe</b>	$0.67 \pm 0.02$	$8.53 \pm 0.06$	$18.6 \pm 0.4$	18 000	1
<b><math>M_3/M_4^b</math></b>	$0.09 \pm 0.02$	$106.6 \pm 24.7$	$5.8 \pm 2.1$	294	61
<b>Calix-Man<sub>4</sub></b>	$0.25 \pm 0.02$	$104.6 \pm 4.2$	$68.7 \pm 3.9$	540	33.3

299 <sup>a</sup>  $\beta$  is the binding potency calculated as the ratio of the monovalent  **$\alpha$ -D-ManOMe** reference  $K_d$  value to the  $K_d$   
 300 value of the multivalent compound. <sup>b</sup> Values obtained from four independent measurements.

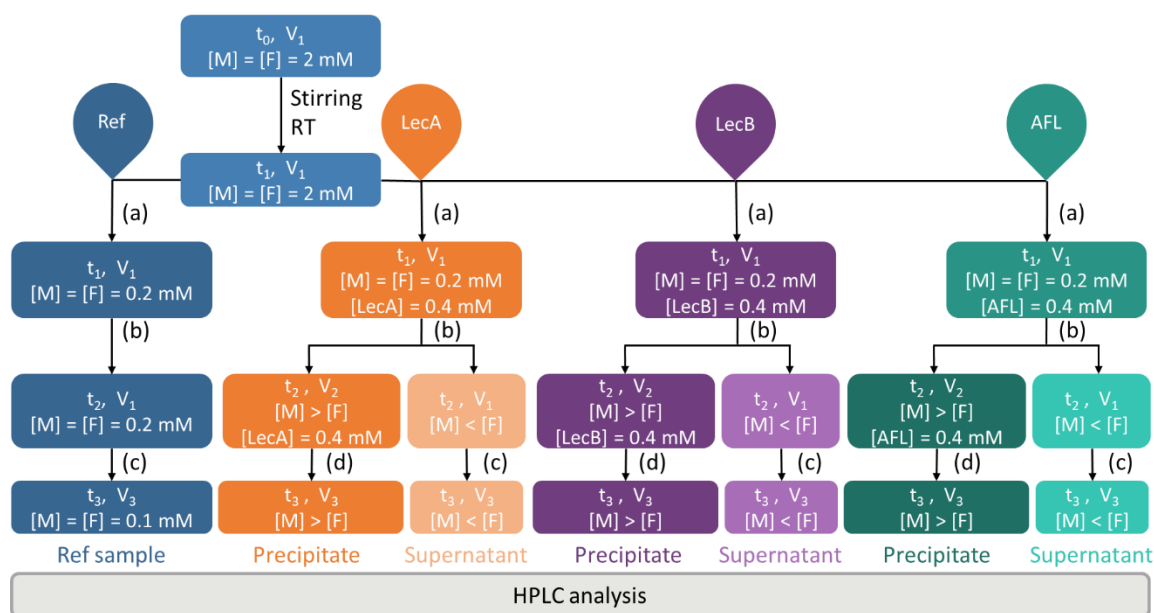
301

302 *Multiplexing of DCLs for the simultaneous rapid identification of high affinity ligands of three lectins*  
 303 *(LecA, LecB and AFL)*

304 Having demonstrated that 1,4-dithiophenol building blocks could oligomerize in solution and that the  
 305 resulting DCL could be influenced by the addition of an external stimulus (lectin) to generate the best  
 306 fit ligands of that protein, the concept was then pushed one step further by designing a multiplexed

307 experiment in which several lectins were used as external stimuli for the identification of their best  
 308 ligands, in a single experiment. First, a selection of three lectins from pathogens has been selected.  
 309 *Pseudomonas aeruginosa* is a bacterium responsible for lung infections and is highly resistant to  
 310 antimicrobials. Two lectins have been reported as virulence factors in this species, namely LecA which  
 311 has a strong affinity for galactose ligands, and LecB for fucose. *Aspergillus fumigatus*, a fungus,  
 312 responsible for lung infections, was also found to bind host cells through an AFL lectin which has affinity  
 313 for fucose. Both pathogens are significant infectious agents that can benefit from the design of  
 314 innovative therapeutic approaches. By using the galactosylated and fucosylated building blocks **G** and  
 315 **F**, respectively, a multiplexed system of DCL can be readily setup for the identification in a single  
 316 experiment of each high affinity ligand for all three lectins (Figure 10 and Figure S7).

317

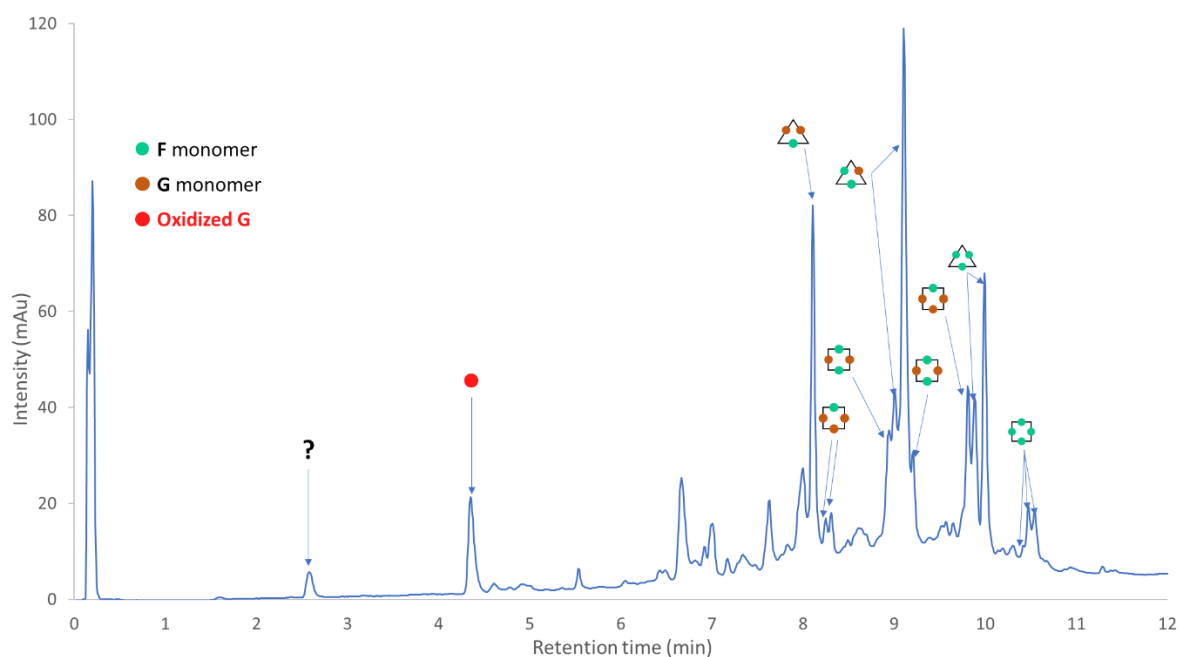


318

319 **Figure 10.** Simultaneous analysis of the DCL equilibration for three different lectins (LecA, LecB and  
 320 AFL) and comparison to a reference DCL in buffer Tris 200 mM, NaCl 100 mM,  $\text{CaCl}_2$  100  $\mu\text{M}$ , at RT.  $V_1$   
 321 = 500  $\mu\text{L}$ ;  $V_2$  = 0  $\mu\text{L}$ ;  $V_3$  = 1000  $\mu\text{L}$ ; (a) Dilution  $\times 10$  - Stirring, RT; (b) Centrifugation; (c) Dilution with HCl  
 322 1M; (d) Dilution with HCl 1M, Dilution  $\times 2$  Buffer. For complete information, please see supporting  
 323 information.

324 A (**G+F**)-DCL was equilibrated at 4 mM and the progress of equilibration of monitored by UHPLC. When  
 325 the amount of **G** and **F** monomers reached less than 15% of the DCL composition, the reference (**G+F**)-  
 326 DCL was diluted 10x then separated into four different 0.4 mM DCLs and each of them were exposed  
 327 to 0.4 mM of the lectin to be studied (LecA, LecB and AFL) or a reference DCL buffer. The reactions  
 328 were monitored by UHPLC, and when the **G** and **F** monomers were totally consumed, DCLs were  
 329 centrifuged to separate the precipitate containing the lectins and the high affinity ligands from the  
 330 supernatant (containing the non-specific macrocycles). UHPLC-MS analyses were used to quantify the  
 331 amount of each macrocycle in the respective DCL reactions.

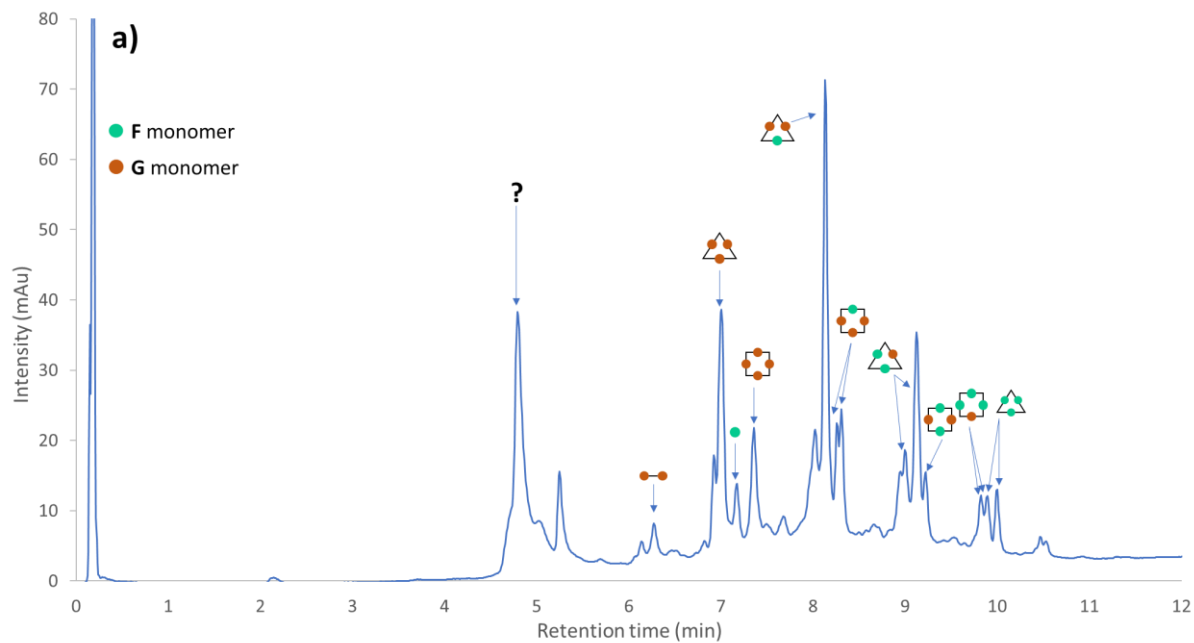
332 UHPLC-MS analyses of the reference DCL revealed that galactosylated macrocycles could not be  
 333 detected, but several heteroglycoclusters could be identified clearly as well as homoglycoclusters  
 334 (Figure 11). Some compounds could not be assigned to any structure (e.g.  $t = 2.6 \text{ min}$ ,  $m/z = 661$ ,  
 335 representing 1.6% in the mixture), and oxidized building block **G** could be observed at a retention time  
 336 of ca. 4.3 min which represented less than 5% in the DCL constituents.



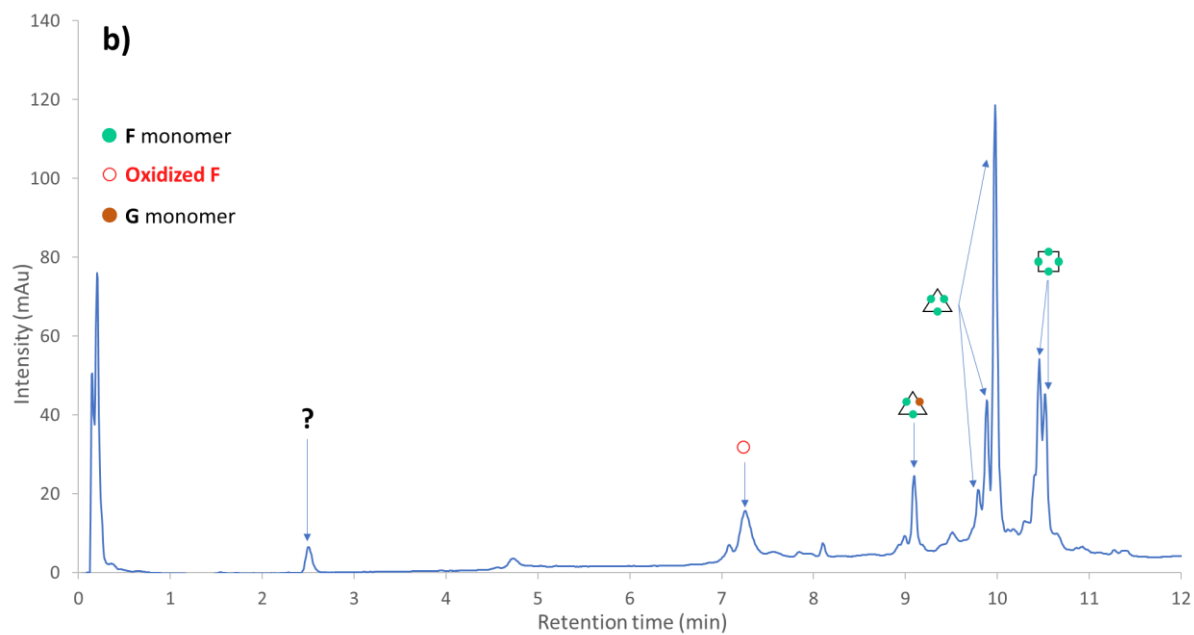
337

338 **Figure 11.** Equilibration of the reference DCL composed of **G/F** building blocks (1:1, 4 mM) in buffer  
 339 Tris 200 mM, NaCl 100 mM, CaCl<sub>2</sub> 100 μM, at RT during 36 h

340 The LecA-(**G+F**)-DCL was analyzed by UHPLC from its precipitate and supernatant samples (Figure 12).  
 341 The overall composition of the DCL was changed in comparison to the reference DCL. The first  
 342 observation was an emergence of **G**<sub>3</sub> and **G**<sub>4</sub> macrocycles in the precipitate sample. The addition of the  
 343 LecA lectin therefore modified the distribution of the hetero- and homoglycoclusters with the hetero-  
 344 species decreasing drastically in proportion and the homoglycoclusters becoming the major species in  
 345 the DCL. Some changes are important such as the heteroglycocluster **G**<sub>2</sub>**F**<sub>2</sub> which decreased by ca. 80%  
 346 in the presence of LecA, but also **G**<sub>1</sub>**F**<sub>2</sub> (74% decrease) and **G**<sub>1</sub>**F**<sub>3</sub> (50% decrease) while homoglycoclusters  
 347 such as **F**<sub>3</sub> and **F**<sub>4</sub> have increased by 69% and 174%, respectively (Figure 13). As previously observed in  
 348 the ConA-DCLs, the addition of the galactose-specific LecA lectin triggered the scrambling of the (**G+F**)-  
 349 DCL favoring the formation of **G**<sub>3</sub> and **G**<sub>4</sub> glycoclusters, along with the corresponding **F**<sub>3</sub> and **F**<sub>4</sub>  
 350 macrocycles that would rearrange together. A peak at t = 4.8 min could not be assigned to a compound  
 351 and displayed a molecular weight of 1159 g.mol<sup>-1</sup> that represented 20% in the precipitate sample  
 352 (Figure 12a). In the supernatant, an unknown compound at t = 2.5 min was also observed with a  
 353 molecular weight of 648 g.mol<sup>-1</sup> (Figure 12b).



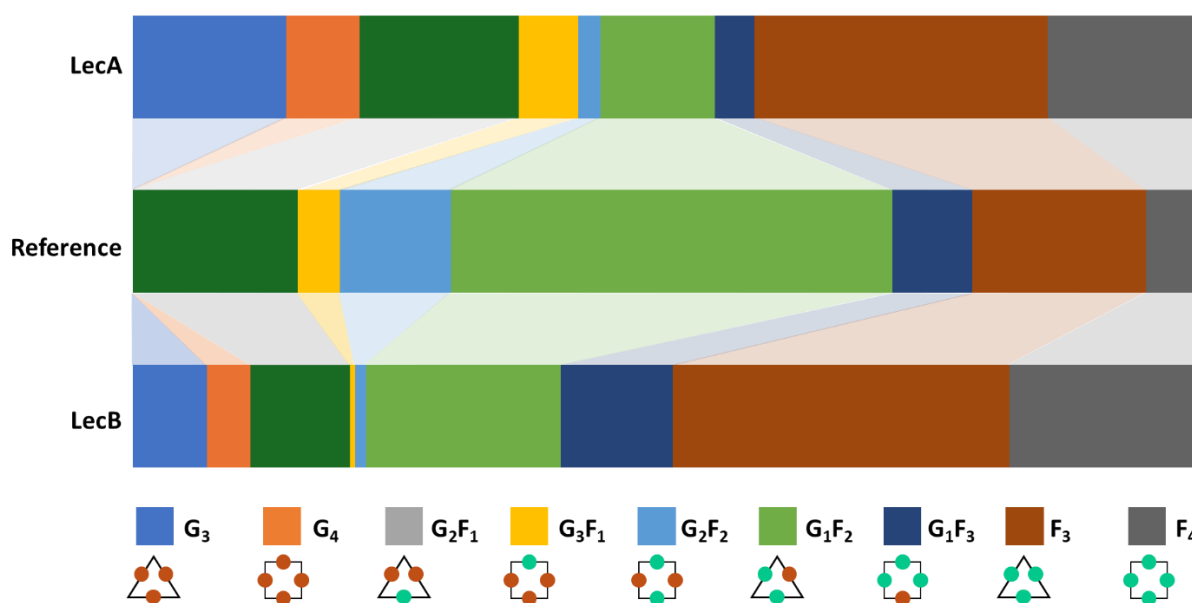
354



355

356 **Figure 12.** UHPLC analysis of the **G/F** (1:1, 0.4 mM) DCL after incubation with LecA (0.4 mM) with the  
 357 (a) precipitate and (b) supernatant





358  
 359 **Figure 13.** Comparison of the reference **G/F** DCL to the LecA (top) and LecB (bottom) amplified DCL  
 360 combining materials from the supernatant and precipitate fractions. Measurements were performed  
 361 in triplicate and did not differ by more than 5%.

362 The LecB-(**G+F**)-DCL was then analyzed similarly by UHPLC-MS (Figure S2) using precipitate and  
 363 supernatant samples. A modification of the reference DCL composition was clearly observed with the  
 364 appearance of **G<sub>3</sub>** and **G<sub>4</sub>** species in the supernatant as non specific LecB ligands (Figure S2b).  
 365 Heteroglycoclusters **G<sub>2</sub>F**, **G<sub>3</sub>F**, **G<sub>2</sub>F<sub>2</sub>** and **G<sub>1</sub>F<sub>2</sub>** decreased quite drastically in the DCL mixture (52%, 79%,  
 366 82% and 55% respectively) while the homoglycoclusters **F<sub>3</sub>** and **F<sub>4</sub>** increased by 73% 272% respectively  
 367 (Figure 13). The same unknown compounds at t = 2.6 min (4%) and t = 4.8 minutes (5%) observed with  
 368 LecA could be detected but at a very limited proportion in the whole DCL (Figure S2b).

369 Finally, the AFL-(**G+F**)-DCL was setup and processed as the other DCLs. Nevertheless, after equilibration  
 370 and centrifugation, the supernatant tended to further precipitate and lead to suspended matters  
 371 (Figure S3). A filtration through Amicon filters provided a filtrate but their UHPLC-MS analyses could  
 372 not provide exploitable data. AFL displayed low nanomolar affinities for the multivalent ligands  
 373 designed here (see ITC studies, *vide infra*). Therefore, the precipitation of AFL with the multivalent  
 374 ligands in the DCL library might occur at much lower concentrations in comparison to LecA or LecB  
 375 rendering the processing of the DCL analysis more complex and unsuccessful so far. The same DCL  
 376 could have been performed with lower amounts of lectin but a minimum amount of 0.2 mM in lectin  
 377 was necessary for the proper analysis of the DCLs to reach a reliable signal-to-noise ratio in the UHPLC-  
 378 MS analyses (data not shown).

379

### 380 *ITC binding studies of G<sub>3</sub>/G<sub>4</sub> and F<sub>3</sub>/F<sub>4</sub> with LecA, LecB and AFL*

381 The **G<sub>3</sub>/G<sub>4</sub>** macrocycles could be purified by preparative UHPLC and then assayed by ITC to determine  
 382 their binding properties towards LecA, the galactose-specific lectin from *Pseudomonas aeruginosa*  
 383 (Figure S4, Table 2). The stoichiometry of the **G<sub>3</sub>/G<sub>4</sub>** to LecA complexes was measured as n = 0.10. This  
 384 value indicates that up to ten lectin monomers can interact simultaneously with the glycoclusters. The  
 385 maximum valency of the **G<sub>4</sub>** glycocluster was 8 which would suggest a stoichiometry of n = 0.125. This  
 386 n value suggested that nearly all galactose ligands were interacting with a lectin. This slight difference  
 387 could be explained by the low precipitation observed in the ITC titration experiment within the last

388 injections of the titration (Figure S4). A dissociation constant of 185 nM was measured which  
 389 represented an increase in affinity ( $\beta$ ) of 378 in comparison to the monovalent LecA ligand reference  
 390 methyl  $\beta$ -D-galactopyranoside ( **$\beta$ -D-GalOMe**). This high affinity was very much comparable to the **Calix-**  
 391 **Gal<sub>4</sub>** (Figure S1) that displayed nanomolar affinity for LecA. A negative control was measured with the  
 392 **F<sub>3</sub>/F<sub>4</sub>** glycoclusters that did not display any binding to LecA with a titration curve that was totally flat  
 393 (Figure S4). The strong binding to LecA observed for the **G<sub>3</sub>/G<sub>4</sub>** glycoclusters was indeed due to the  
 394 specific binding of galactoside epitopes since the core framework of the glycocluster of **F<sub>3</sub>/F<sub>4</sub>**  
 395 glycoclusters did not interact with the lectin.

396 **Table 2.** ITC data for the binding properties of glycosylated dyn[n]arenes **G<sub>3</sub>/G<sub>4</sub>** towards LecA

Ligand	<i>n</i>	$-\Delta H$ (kJ.mol <sup>-1</sup> )	$-\Delta S$ (kJ.mol <sup>-1</sup> )	<i>K<sub>d</sub></i> (nM)	$\beta^a$
<b><math>\beta</math>-D-GalOMe<sup>b</sup></b>	0.80	39.0	15.0	70 000	1
<b>G<sub>3</sub>/G<sub>4</sub><sup>c</sup></b>	0.10 ± 0.01	158.3 ± 8.3	119.7	185	378
<b>Calix-Gal<sub>4</sub><sup>d</sup></b>	0.24 ± 0.01	104 ± 1	65.0	176	398

397 <sup>a</sup>  $\beta$  is the binding potency calculated as the ratio of the monovalent  **$\beta$ -D-GalOMe** reference *K<sub>d</sub>* value to the *K<sub>d</sub>*  
 398 value of the multivalent compound. <sup>b</sup> Values obtained from the literature.<sup>57</sup> <sup>c</sup> Values obtained from duplicate  
 399 measurements. <sup>d</sup> Values obtained from the literature.<sup>26</sup>

400 The similar ITC study was then performed with the **F<sub>3</sub>/F<sub>4</sub>** glycoclusters towards LecB (Figure S5, Table  
 401 3). The affinity measured was in the low nanomolar range (*K<sub>d</sub>* = 90 nM) and does compare very  
 402 favorably with the previously reported high affinity ligands for LecB such as the **Calix-Fuc<sub>4</sub>** glycocluster  
 403 (Figure S1). The increase in affinity observed was more moderate for LecB than for LecA since the  $\beta$   
 404 value was of only 6 for the **F<sub>3</sub>/F<sub>4</sub>** glycoclusters. This was already the case for the **Calix-Fuc<sub>4</sub>** glycocluster  
 405 and was explained by the LecB organization which harbors distant multimeric binding sites too far  
 406 apart to interact simultaneously with two fucoside epitopes in a chelate binding mode.<sup>12</sup> Similarly, the  
 407 negative control measurement was performed with the **G<sub>3</sub>/G<sub>4</sub>** glycocluster which did not display any  
 408 affinity towards LecB (Figure S5).

409

410 **Table 3.** ITC data for the binding properties of glycosylated dyn[n]arenes **F<sub>3</sub>/F<sub>4</sub>** towards LecB

Ligand	<i>n</i>	$-\Delta H$ (kJ.mol <sup>-1</sup> )	$-\Delta S$ (kJ.mol <sup>-1</sup> )	<i>K<sub>d</sub></i> (nM)	$\beta^a$
<b><math>\alpha</math>-L-FucOMe<sup>b</sup></b>	1.00 ± 0.07	31.5 ± 0.8	-6.2	555	1
<b>F<sub>3</sub>/F<sub>4</sub><sup>c</sup></b>	0.10 ± 0.01	225.8 ± 6.3	184.1	90	6
<b>Calix-Fuc<sub>4</sub><sup>b</sup></b>	0.32 ± 0.02	89.6 ± 2.1	47.8	48	11.6

411 <sup>a</sup>  $\beta$  is the binding potency calculated as the ratio of the monovalent  **$\alpha$ -L-FucOMe** reference *K<sub>d</sub>* value to the *K<sub>d</sub>*  
 412 value of the multivalent compound. <sup>b</sup> Values obtained from the literature.<sup>26</sup> <sup>c</sup> Values obtained from triplicate  
 413 measurements.

414

415 The **F<sub>3</sub>/F<sub>4</sub>** glycoclusters were then assayed against AFL, another fucose-specific lectin from the  
 416 *Aspergillus fumigatus* fungal pathogen.<sup>58</sup> This lectin is a hexamer displaying six fucose binding sites in  
 417 a propeller-like spatial arrangement. The cooperativity in binding to several binding sites  
 418 simultaneously has been demonstrated by the group of Renaudet using a cyclic peptide scaffold with  
 419 six fucoside epitopes (Figure S6).<sup>59</sup> The affinity towards LecB was in the low nanomolar range (Table 4)  
 420 and these ligands displayed the highest affinity ligands for AFL reported to date. A similar approach  
 421 was reported by Gouin *et al.* with octavalent glycoclusters displaying fucoside epitopes on a  
 422 silsesquioxane core scaffold (Figure S6).<sup>60</sup> Again, the *K<sub>d</sub>* value of 40 nM (Table 4) ranked this type of  
 423 glycocluster in the highest affinity for AFL.

424 The **F<sub>3</sub>/F<sub>4</sub>** glycoclusters displayed a  $K_d$  value of 38 nM (Figure S7, Table 4) which is in line with the  
 425 multivalent glycoclusters previously reported. The negative control with **G<sub>3</sub>/G<sub>4</sub>** glycoclusters confirmed  
 426 that no non-specific binding could be attributed to the macrocyclic core scaffolds.

427

428 **Table 4.** ITC data for the binding properties of glycosylated dyn[n]arenes **F<sub>3</sub>/F<sub>4</sub>** towards AFL

Ligand	<i>n</i>	$-\Delta H$ (kJ.mol <sup>-1</sup> )	$-\Delta S$ (kJ.mol <sup>-1</sup> )	$K_d$ (nM)	$\beta^a$
<b><math>\alpha</math>-L-FucOMe<sup>b</sup></b>	2.98	32.8	7.7	40 300	1
<b>F<sub>3</sub>/F<sub>4</sub><sup>b</sup></b>	0.11 ± 0.03	335.0 ± 0.0	292.5 ± 0.5	38	1060
<b>Cyclodecapeptide<sup>c</sup></b>	0.77 ± 0.01	154.5 ± 3.5	109.5	18.5	2178
<b>Silsesquioxane<sup>d</sup></b>	0.71 ± 0.04	-247.2 ± 16.0	205.0 ± 16.2	40	1007

429 <sup>a</sup>  $\beta$  is the binding potency calculated as the ratio of the monovalent  **$\alpha$ -L-FucOMe** reference  $K_d$  value to the  $K_d$   
 430 value of the multivalent compound. <sup>b</sup> Values obtained from duplicate measurements. <sup>c</sup> Values obtained from the  
 431 literature.<sup>59</sup> <sup>d</sup> Values obtained from the literature.<sup>60</sup>

432

433 As a conclusion for these ITC binding studies, the **X<sub>3</sub>/X<sub>4</sub>** glycoclusters identified after lectin-selection in  
 434 the equilibrating DCLs could be purified and their binding properties studied by ITC. All these dynarene  
 435 glycoclusters displayed high affinity for their respective lectins and can be considered as candidates to  
 436 prevent or reduce bacterial interactions with epithelial cells. They were found to have binding affinities  
 437 similar to those of the calixarene-based glycoclusters that were demonstrated as efficient bio-mimetics  
 438 reducing mouse lung infection by *Pseudomonas aeruginosa*.<sup>26</sup> Similarly, the fucosylated glycoclusters  
 439 **F<sub>3</sub>/F<sub>4</sub>** appeared as valuable candidates to reduce the outcome of *Aspergillus fumigatus* lung infections  
 440 (in immuno-compromised patients), based on their high affinity for the AFL lectin. Given the potential  
 441 of these compounds for biological applications, their toxicity and anti-adhesive properties against  
 442 *Pseudomonas aeruginosa* were evaluated on A549 lung epithelial cells.

443

#### 444 *Incidence of dynarenes on Pseudomonas aeruginosa PAO1 cells and lung epithelial cells*

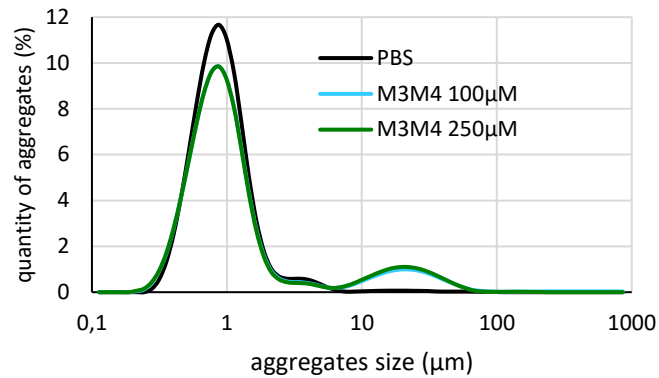
445 The toxicity of the designed **X<sub>3</sub>/X<sub>4</sub>** glycoclusters was evaluated against *P. aeruginosa* strain PAO1 (the  
 446 main strain model used in virulence studies) using two different assays. The growth of PAO1 was not  
 447 inhibited by the exposure to the **X<sub>3</sub>/X<sub>4</sub>** dynarenes (up to 10 mM) on Muller-Hinton agar plates. In  
 448 parallel, a Live-Dead assay monitoring dead cells (through their permeability to propidium iodide)  
 449 indicated that no toxicity could be observed against PAO1 for the **X<sub>3</sub>/X<sub>4</sub>** dynarenes used up to 10 mM,  
 450 over incubation times of 4 hours.

451

#### 452 *Aggregation bacterial cell assays*

453 The absence of toxicity on *P. aeruginosa* allowed to test the abilities of **X<sub>3</sub>/X<sub>4</sub>** dynarenes to induce the  
 454 formation of PAO1 cell aggregates. The presence of LecA, LecB or other adhesins at the surface of the  
 455 bacterial cells can trigger their aggregation in the presence of the multivalent **X<sub>3</sub>/X<sub>4</sub>** dynarenes acting  
 456 as cross-linking agents between cells through carbohydrate-lectin interactions. Our previously  
 457 reported procedure<sup>61</sup> was used to test the formation of cellular aggregates induced by multivalent  
 458 **X<sub>3</sub>/X<sub>4</sub>** dynarenes ligands. This procedure was slightly modified by performing an analysis of the relative  
 459 numbers of aggregates through a Malvern mastersizer 3000 diffraction laser system (Figure 14) rather  
 460 than flow cytometry. A shoulder is observed at 6  $\mu$ m suggesting the presence of aggregates of about 3  
 461 cells in the control experiment with PBS. The blue and green curves showed the impact of adding  
 462 mannosylated dynarenes **M<sub>3</sub>/M<sub>4</sub>** (100 or 250  $\mu$ M) generating larger aggregates of a few tens of microns  
 463 with nearly no influence of the concentration used.

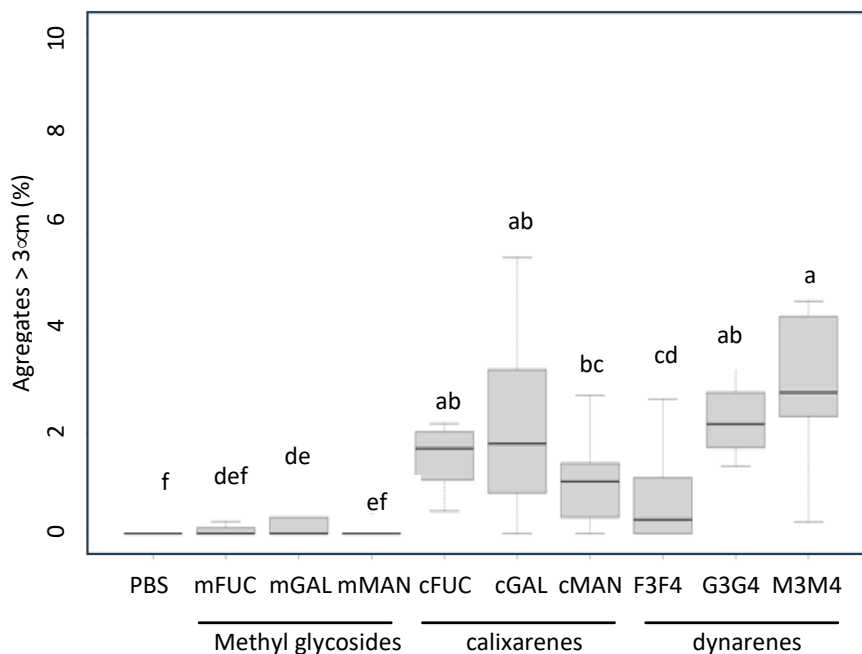
464



465  
 466 **Figure 14.** Illustration of aggregate size distribution patterns observed in a *P. aeruginosa* PAO1 cell  
 467 broth exposed to two concentrations (100  $\mu$ M, 250  $\mu$ M) of mannosylated dynarenes. Two cell  
 468 categories can be defined through the analysis of the cell size distribution patterns: (1) planktonic  
 469 PAO1 cells (< 3  $\mu$ m), and (2) aggregated PAO1 cells (> 3  $\mu$ m).

470  
 471 The aggregation assays clearly showed the ability of multivalent  $X_3/X_4$  dynarenes at inducing the  
 472 formation of PAO1 cell aggregates (Figure 15). The glycosylated dynarene aggregation potential was  
 473 compared with those of glycosylated calixarenes which have been reported as highly efficient  
 474 multivalent ligands for inducing the formation of PAO1 cell aggregates.<sup>26</sup> Interestingly, these  
 475 aggregation levels were correlated to an anti-adhesive effect reducing the formation of aggregates  
 476 when PAO1 cells are exposed to glyco-conjugate concentrations above 1 mM.<sup>26</sup> This anti-adhesive  
 477 effect was considered to result from a saturation of adhesins at the bacterial cell surface preventing  
 478 interactions with the neighboring cells. Mannosylated ( $M_3/M_4$ ) and galactosylated ( $G_3/G_4$ ) dynarenes  
 479 were found to generate as much aggregates than the calixarene-based glycoclusters (Figure S1, cFUC,  
 480 cGAL, cMAN) but not the fucosylated ( $F_3/F_4$ ) dynarenes (Figure 15).

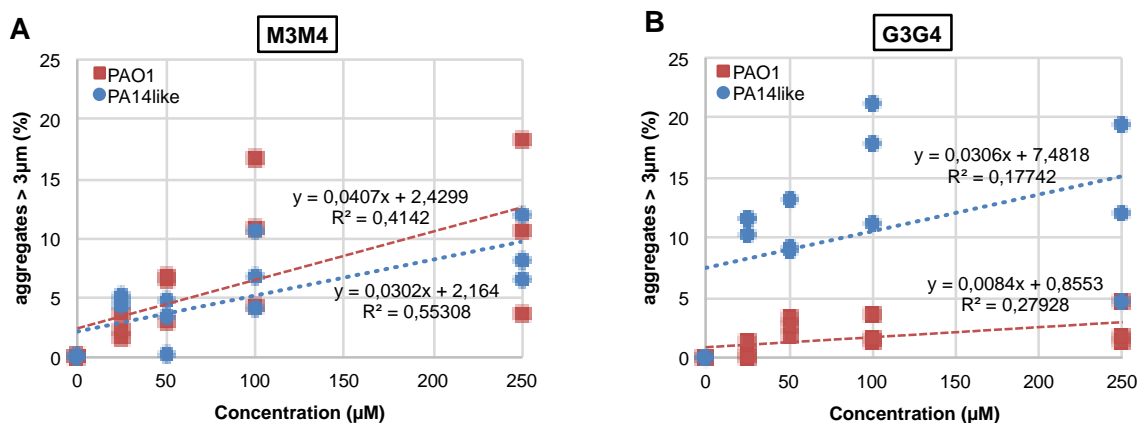
481



482  
 483 **Figure 15.** Boxplot of *P. aeruginosa* PAO1 cells aggregation levels induced through interactions with  
 484 100  $\mu$ M of methyl glycosides (monovalent ligands – mFUC = methyl  $\alpha$ -L-fucopyranoside, mGAL =  
 485 methyl  $\beta$ -D-galactopyranoside, mMAN = methyl  $\alpha$ -D-mannopyranoside), tetravalent calixarene-based  
 486 glycoclusters (cFUC, cGAL, cMAN) and the multivalent  $X_3/X_4$  dynarene glycoclusters. Size of the  
 487 aggregates were estimated using a Malvern MasterSizer. Boxplots were used to show the minimum,

488 first quartile (Q1), median, third quartile (Q3), and maximum relative abundances for PAO1 aggregates  
 489 with a size > 3  $\mu\text{m}$  among a cell population. 100  $\mu\text{M}$  of all compounds were used per assay. Boxplots  
 490 with distinct letter codes showed significant differences ( $p$ -values < 0.05 using Kruskal-Wallis (KW)  
 491 Dunn tests). Aggregates observed among control PAO1 cells in PBS were subtracted from the results;  
 492 PBS values were thus transformed into zero. At least three independent aggregation assays were  
 493 performed per assay, and more than five technical Mastersizer readings were performed per replicate.  
 494

495 Similar results were obtained with the bpoe6656 strain<sup>61-62</sup> which belongs to the PA14 clade of *P.*  
 496 *aeruginosa* expressing ExoU-based virulence behaviors rather than ExoS-based ones of the PAO1 clade  
 497 (Figure 16). Aggregation of these PA14 bpoe6656 cells was found higher with the galactosylated **G<sub>3</sub>/G<sub>4</sub>**  
 498 dynarene (Figure 16B) than the mannosylated **M<sub>3</sub>/M<sub>4</sub>** dynarenes (Figure 16A). Interestingly, a positive  
 499 linear response between the number of aggregates and the concentrations of **M<sub>3</sub>/M<sub>4</sub>** dynarenes could  
 500 be observed with these two strains but was less significant with the **G<sub>3</sub>/G<sub>4</sub>** dynarenes. This confirmed  
 501 the trends reported on Figure 15 where mannosylated **M<sub>3</sub>/M<sub>4</sub>** dynarenes induced the formation of a  
 502 greater number of aggregates.  
 503



504  
 505 **Figure 16.** Linear regression analysis of the effect of **M<sub>3</sub>/M<sub>4</sub>** and **G<sub>3</sub>/G<sub>4</sub>** dynarene concentrations ( $\mu\text{M}$ )  
 506 on the relative number of aggregates > 3  $\mu\text{m}$  in cell populations of PAO1 and PA14-like strain bpoe6656.  
 507 (A) Mannosylated dynarene **M<sub>3</sub>/M<sub>4</sub>** and (B) galactosylated dynarene **G<sub>3</sub>/G<sub>4</sub>**. The linear model fitting the  
 508 observed relation is indicated on the curve with its  $R^2$  value of goodness-of-fit.  $R^2$  indicates the  
 509 percentage of the response variable explained by the model. Three independent aggregation assays  
 510 were performed per dynarene concentration (matching the coloured square or circles), and more than  
 511 five technical Mastersizer readings were performed per replicate.  
 512

513 *P. aeruginosa* virulence cell assays using A549 lung epithelial cells  
 514 In our previous study,<sup>26</sup> calixarene-based glycoclusters were found to inhibit PAO1 adhesion on A549  
 515 epithelial cells after 3 hours of co-culture. We have now optimized these virulence assays to evaluate  
 516 the protective effects of multivalent **X<sub>3</sub>/X<sub>4</sub>** dynarene glycoclusters against PAO1 virulence. xCELLigence  
 517 monitorings, using E96-microtiter plates harboring gold electrodes (Acea Biosciences, San Diego, USA)  
 518 were implemented to test the changes in PAO1 virulence properties triggered by **X<sub>3</sub>/X<sub>4</sub>** dynarenes.  
 519 These monitorings implied real-time analyses (RTCA) of impedance changes over time for epithelial  
 520 cell monolayers, which are expressed as cell index (CI) arbitrary units. These cell index values are  
 521 reflecting changes in A549 epithelial cell adhesion forces over the electrodes which are triggered by  
 522 morphological and A549 cell number changes over time. Cell indexes were normalized at time of  
 523 treatments (i.e. presented as delta cell indexes).

524 To perform these RTCA, the toxicity of **X<sub>3</sub>/X<sub>4</sub>** dynarene glycoclusters on A549 epithelial cells was first  
 525 investigated. No toxicity effect on the A549 was observed using dynarenes (data not shown).

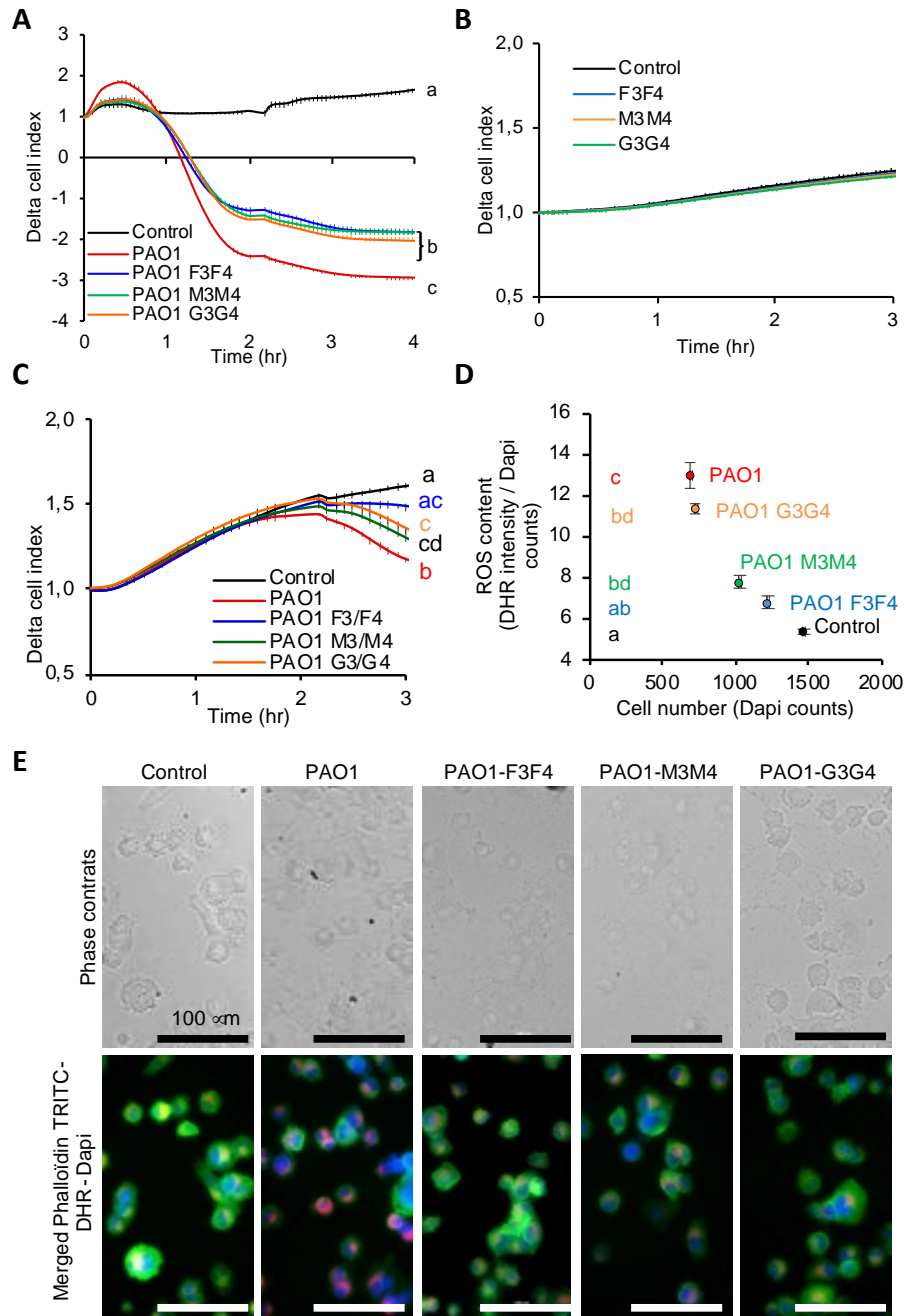
526 Experiments testing the incidence of  $X_3/X_4$  dynarenes on the PAO1 infection of A549 cells monitored  
527 by the xCELLigence system were then undertaken. PAO1 cells were grown as reported above, washed  
528 with PBS, and pre-incubated for 15 min with the  $X_3/X_4$  dynarene glycoclusters (1 mM) as performed  
529 in our previous study.<sup>26</sup> These PAO1 cells were then diluted to obtain a multiplicity of infection (MOI)  
530 of 10 according to the number of A549 cells prepared for the RTCA in the culture media without  
531 antibiotics.

532 The impact of  $X_3/X_4$  dynarene glycoclusters on *P. aeruginosa* virulence was tested on A549 cell  
533 monolayers after 2 hours of co-cultures. Since dynarenes did not exert any significant toxicity on PAO1  
534 cells, their high proliferation rate (approx. 40 min.) could interfere with pre-treated bacteria. In order  
535 to avoid excess PAO1 proliferation, remaining PAO1 cells in suspension were removed after 2 hours of  
536 co-culture and replaced by fresh cell culture media in order to amplify the effect of adherent bacteria  
537 (Figure 17A).

538 In comparison to control A549 cells, PAO1 adhesion to epithelial cells induced a drastic reduction of  
539 cell index according to time with respect of high alteration of A549 cell number, adhesion force and/or  
540 morphology (Figure 17A). This effect was significantly counterbalanced in co-cultures with PAO1 pre-  
541 exposed to either three  $X_3/X_4$  dynarenes, suggesting that PAO1 adherence and/or virulence was  
542 altered by  $X_3/X_4$  dynarene glycoclusters. In order to test whether PAO1 adhesion to epithelial cells was  
543 involved in alteration of epithelial cell index, a second approach was used to monitor A549 cell  
544 adhesion rate by RTCA of cells in suspension loaded onto the E-Plate. During this adhesion phase, the  
545 cell index (normalized to media alone) increases according to cell adhesion at the bottom of plate  
546 wells, which occurs within a few hours.<sup>63</sup> Since at MOI10,  $X_3/X_4$  dynarenes are present in the co-culture  
547 media at 4.13  $\mu$ M, their toxicity was checked on A549 cells in suspension and they did not alter cell  
548 adhesion rate and/or force (Figure 17B). Pre-incubation of A549 cells in suspension with PAO1 (MOI10)  
549 was found to drastically affect epithelial cell adhesion (Figure 17C). Pre-incubation of PAO1 with  $X_3/X_4$   
550 dynarenes (1 mM on MOI100) was found to exert a protective effect against this alteration of epithelial  
551 cell adhesion. In order to analyze the mechanisms involved in PAO1 virulence, at the end of experiment  
552 (3-4 hours), A549 cells were fixed in a 5% PBS formalin solution and kept at least 1 hour at 4°C. Then  
553 they were labeled with PBS 0.1% Triton containing Phalloidin-Atto488 for cytoskeleton labeling, DAPI  
554 for cell nuclei counts and dihydroxyrhodamine (DHR) to evaluate stress induced reactive oxygen  
555 species (ROS) during five minutes then washed twice in PBS and analyzed through automated image  
556 analyses ( $\times 4$ ) (Figure 17D). PAO1 adhesion/infection was found to affect A549 cell adhesion by  
557 reducing the number of adherent cells and induction of oxidative stress (i.e. increased intracellular  
558 ROS). Image acquisitions at higher magnification ( $\times 20$ ) with identical parameters highlight  
559 morphological changes such as reduction of adhesion surfaces (spheric cells) and loss of phalloidin  
560 fluorescence intensity reflecting destabilization of actin polymerization (Figure 17E). These data are in  
561 accordance with the effect of PAO1 adhesion on oxidative stress and consequent alteration of cell  
562 adhesion.<sup>64</sup> All  $X_3/X_4$  dynarene glycoclusters protect at least partially ( $G_3/G_4$ ) or to a large extent ( $F_3/F_4$ )  
563 A549 cells from the anti-adhesive activity of PAO1 in RTCA experiments confirmed by the  
564 counterbalancing effect on cell number adhesion, ROS induction and morphological alterations.

565 In conclusion,  $X_3/X_4$  dynarene glycoclusters could be demonstrated to exert a protective effect against  
566 PAO1 virulence on lung epithelial cells. The exact mechanism of protection is still to be further  
567 investigated but it is probably through inhibition of their adhesion on epithelial cells by inducing  
568 bacterial aggregation.

569



570  
 571 **Figure 17.** *Pseudomonas aeruginosa* PAO1 anti-adhesive assays using  $X_3/X_4$  dynarene glycoclusters and  
 572 A549 epithelial cells. (A) Real-time monitoring of A549 cell monolayer in co-culture with PAO1 pre-  
 573 treated with  $X_3/X_4$  dynarenes (1 mM). Co-cultures were washed out after 2 hours and replaced by fresh  
 574 culture media then monitored during 2 hours. Data were obtained with 8 replicates of 3 independent  
 575 preparations of each PAO1- $X_3/X_4$  dynarenes. (B) Real-time monitoring of A549 cell adhesion after pre-  
 576 incubation with  $X_3/X_4$  dynarenes (4.13  $\mu$ M) and (C) with PAO1 pre-treated with  $X_3/X_4$  dynarene (1 mM)  
 577 ( $n= 8$  replicates). (D-E) After PAO1 exposure, A549 cells were fixed and labeled with either DAPI (blue color)  
 578 for nuclei counts, phalloidin-Atto488 (green color) for cytoskeleton and dihydroxyrhodamine  
 579 (DHR, red color) for reactive oxygen species (ROS). (D) Cell number (i.e. DAPI counts) and mean ROS  
 580 content per cell (i.e. DHR intensity normalized to DAPI counts) were obtained by automated analysis  
 581 of at least 16 images (magnification  $\times 4$ ). (E) Phase contrast and merged fluorescence images at  
 582 objective  $\times 20$ . Data are presented as mean values  $\pm$  SEM, different letters represent significant  
 583 differences according to Kruskal Wallis followed by Mann Whitney (Wilcoxon) tests ( $p < 0.05$ ).

584

## 585 **Conclusion**

586 Carbohydrates are decorated at the surface of cells and play a major role in biological processes more  
587 specifically in several diseases. The very first step of bacterial or viral infection is the attachment of the  
588 pathogen to the cell surface through carbohydrate-lectin interactions, carbohydrates being present at  
589 the host cell surface in the glycocalyx and proteins being used by pathogens for infection. The design  
590 of multivalent glycoconjugates to lure pathogens and prevent adhesion to host cells is a general  
591 strategy that has found several illustrations over the past decades. The design and synthesis of  
592 multivalent glycoconjugates as potent ligands of such proteins has required intensive research work  
593 from chemists and biochemists to identify drug candidates. One main drawback is the synthesis of a  
594 large panel of analogues in a family of compounds for the structure-activity relationship study and to  
595 reach the best candidate after testing all compounds separately in a time and material consuming  
596 process. Dynamic combinatorial chemistry can provide a rapid and efficient access to a large variety of  
597 multivalent glycoconjugates and speed up drastically the process of drug discovery in this context. One  
598 major advantage is to setup an equilibrating dynamic combinatorial library of glycoclusters and then  
599 introduce a lectin for the *in situ* selection of the fittest ligand of the protein. Glycosylated 1,4-  
600 dithiophenols were equilibrated through disulfide exchange to reach a library of glycoclusters. A model  
601 study was performed with concanavalin A (ConA) to demonstrate the selection of the best ligands in  
602 this dynamic combinatorial library. More importantly, this strategy allowed the identification of the  
603 best ligands for more than one lectin in a single experimental setup by using two simple 1,4-  
604 dithiophenols building blocks. High affinity glycoclusters could be amplified in the equilibrating  
605 mixtures using LecA or LecB, leading to glyco-dyn[3]arenes and glyco-dyn[4]arenes. The glycoclusters  
606 could then be synthesized, isolated for their evaluation as lectin ligands and anti-adhesive agents  
607 against *Pseudomonas aeruginosa*. Dissociation constants in the nanomolar range could be measured  
608 by ITC which places these compounds in the same range of “classical” calixarene-based glycoclusters  
609 which among the best ligands for these pathogenic lectins. These glyco-dynarenes did not display any  
610 toxicity towards neither human cells, nor *Pseudomonas aeruginosa*. Their evaluation as anti-adhesive  
611 agents could be validated in a virulence assay on human A549 lung epithelial cells which indicated that  
612 glyco-dynarenes could perform similarly to our previous calixarene-based glycoclusters model.

613

## 614 **Acknowledgements**

615 The authors thank the Université Lyon 1 and the CNRS for financial support. This work was supported  
616 by the Agence Nationale de la Recherche (DynaSweet ANR-17-CE07-0054). Dr Florian Albrieux, Dr  
617 Alexandra Berlioz-Barbier, Christian Duchamp, and Antoine Vauchez are gratefully acknowledged for  
618 UHPLC-MS analyses at the Centre Commun de Spectrométrie de Masse of Université Lyon 1, along  
619 with Dr Nathalie Hue and Vincent Steinmetz at the ICSN mass spectrometry department.

620

## 621 **References**

622

- 623 1. Barchi, J. J., *Comprehensive Glycoscience, 2nd Edition*. Elsevier: 2021.
- 624 2. Bertozzi, C. R.; Kiessling; L., L., *Chemical Glycobiology. Science* **2001**, *291* (5512), 2357-2364.



625 3. Gabius, H.-J.; Cudic, M.; Diercks, T.; Kaltner, H.; Kopitz, J.; Mayo, K. H.; Murphy, P. V.; Oscarson,  
626 S.; Roy, R.; Schedlbauer, A.; Toegel, S.; Romero, A., What is the Sugar Code? *ChemBioChem* **2022**, *23*  
627 (13), e202100327.

628 4. Varki, A.; Cummings, R. D.; Esko, J. D.; Stanley, P.; Hart, G. W.; Aebi, M.; Mohnen, D.; Kinoshita,  
629 T.; Packer, N. H.; Prestegard, J. J.; Schnaar, R. L.; Seeberger, P. H., *Essentials of Glycobiology, 4th edition*.  
630 Cold Spring Harbor New York, 2022.

631 5. Cummings, R. D., Stuck on sugars – how carbohydrates regulate cell adhesion, recognition, and  
632 signaling. *Glycoconj. J.* **2019**, *36* (4), 241-257.

633 6. Mason, C. P.; Tarr, A. W., Human Lectins and Their Roles in Viral Infections. *Molecules* **2015**,  
634 *20* (2), 2229-2271.

635 7. Meiers, J.; Siebs, E.; Zahorska, E.; Titz, A., Lectin antagonists in infection, immunity, and  
636 inflammation. *Curr. Opin. Chem. Biol.* **2019**, *53*, 51-67.

637 8. Lee, Y. C.; Lee, R. T., Carbohydrate-Protein Interactions: Basis of Glycobiology. *Acc. Chem. Res.*  
638 **1995**, *28* (8), 321-327.

639 9. Lis, H.; Sharon, N., Lectins: Carbohydrate-Specific Proteins That Mediate Cellular Recognition.  
640 *Chem. Rev.* **1998**, *98* (2), 637-674.

641 10. Valverde, P.; Ardá, A.; Reichardt, N.-C.; Jiménez-Barbero, J.; Gimeno, A., Glycans in drug  
642 discovery. *MedChemComm* **2019**, *10* (10), 1678-1691.

643 11. Bernardi, A.; Jimenez-Barbero, J.; Casnati, A.; De Castro, C.; Darbre, T.; Fieschi, F.; Finne, J.;  
644 Funken, H.; Jaeger, K.-E.; Lahmann, M.; Lindhorst, T. K.; Marradi, M.; Messner, P.; Molinaro, A.;  
645 Murphy, P. V.; Nativi, C.; Oscarson, S.; Penades, S.; Peri, F.; Pieters, R. J.; Renaudet, O.; Reymond, J.-L.;  
646 Richichi, B.; Rojo, J.; Sansone, F.; Schaffer, C.; Turnbull, W. B.; Velasco-Torrijos, T.; Vidal, S.; Vincent, S.;  
647 Wennekes, T.; Zuilhof, H.; Imberty, A., Multivalent glycoconjugates as anti-pathogenic agents. *Chem.*  
648 *Soc. Rev.* **2013**, *42* (11), 4709-4727.

649 12. Cecioni, S.; Imberty, A.; Vidal, S., Glycomimetics versus Multivalent Glycoconjugates for the  
650 Design of High Affinity Lectin Ligands. *Chem. Rev.* **2015**, *115* (1), 525-561.

651 13. Mousavifar, L.; Roy, R., Recent development in the design of small ‘drug-like’ and nanoscale  
652 glycomimetics against Escherichia coli infections. *Drug Discov. Today* **2021**, *26* (9), 2124-2137.

653 14. Mousavifar, L.; Touaibia, M.; Roy, R., Development of Mannopyranoside Therapeutics against  
654 Adherent-Invasive Escherichia coli Infections. *Acc. Chem. Res.* **2018**, *51* (11), 2937-2948.

655 15. Chalopin, T.; Alvarez Dorta, D.; Sivignon, A.; Caudan, M.; Dumych, T. I.; Bilyy, R. O.; Deniaud,  
656 D.; Barnich, N.; Bouckaert, J.; Gouin, S. G., Second generation of thiazolylmannosides, FimH antagonists  
657 for E. coli-induced Crohn's disease. *Org. Biomol. Chem.* **2016**, *14* (16), 3913-3925.

658 16. Schönemann, W.; Cramer, J.; Mühlethaler, T.; Fiege, B.; Silbermann, M.; Rabbani, S.; Dätwyler,  
659 P.; Zihlmann, P.; Jakob, R. P.; Sager, C. P.; Smieško, M.; Schwardt, O.; Maier, T.; Ernst, B., Improvement  
660 of Aglycone  $\pi$ -Stacking Yields Nanomolar to Sub-nanomolar FimH Antagonists. *ChemMedChem* **2019**,  
661 *14* (7), 749-757.

662 17. Kleeb, S.; Jiang, X.; Frei, P.; Sigl, A.; Bezençon, J.; Bamberger, K.; Schwardt, O.; Ernst, B., FimH  
663 Antagonists: Phosphate Prodrugs Improve Oral Bioavailability. *J. Med. Chem.* **2016**, *59* (7), 3163-3182.

664 18. Kleeb, S.; Pang, L.; Mayer, K.; Eris, D.; Sigl, A.; Preston, R. C.; Zihlmann, P.; Sharpe, T.; Jakob, R.  
665 P.; Abgottspon, D.; Hutter, A. S.; Scharenberg, M.; Jiang, X.; Navarra, G.; Rabbani, S.; Smiesko, M.;  
666 Lüdin, N.; Bezençon, J.; Schwardt, O.; Maier, T.; Ernst, B., FimH Antagonists: Bioisosteres To Improve  
667 the in Vitro and in Vivo PK/PD Profile. *J. Med. Chem.* **2015**, *58* (5), 2221-2239.

668 19. Tomašić, T.; Rabbani, S.; Gobec, M.; Raščan, I. M.; Podlipnik, Č.; Ernst, B.; Anderluh, M.,  
669 Branched  $\alpha$ -d-mannopyranosides: a new class of potent FimH antagonists. *MedChemComm* **2014**, *5*  
670 (8), 1247-1253.

671 20. Romero, A.; Gabius, H.-J., Galectin-3: is this member of a large family of multifunctional lectins  
672 (already) a therapeutic target? *Exp. Opin. Ther. Patents* **2019**, *23* (10), 819-828.

673 21. Zetterberg, F. R.; MacKinnon, A.; Brimert, T.; Gravelle, L.; Johnsson, R. E.; Kahl-Knutson, B.;  
674 Leffler, H.; Nilsson, U. J.; Pedersen, A.; Peterson, K.; Roper, J. A.; Schambye, H.; Slack, R. J.; Tantawi, S.,  
675 Discovery and Optimization of the First Highly Effective and Orally Available Galectin-3 Inhibitors for  
676 Treatment of Fibrotic Disease. *J. Med. Chem.* **2022**, *65* (19), 12626-12638.

677 22. Bum-Erdene, K.; Collins, P. M.; Hugo, M. W.; Tarighat, S. S.; Fei, F.; Kishor, C.; Leffler, H.; Nilsson,  
678 U. J.; Groffen, J.; Grice, I. D.; Heisterkamp, N.; Blanchard, H., Novel Selective Galectin-3 Antagonists Are  
679 Cytotoxic to Acute Lymphoblastic Leukemia. *J. Med. Chem.* **2022**, *65* (8), 5975-5989.

680 23. Bratteby, K.; Torkelsson, E.; L'Estrade, E. T.; Peterson, K.; Shalgunov, V.; Xiong, M.; Leffler, H.;  
681 Zetterberg, F. R.; Olsson, T. G.; Gillings, N.; Nilsson, U. J.; Herth, M. M.; Erlandsson, M., In Vivo Veritas:  
682 18F-Radiolabeled Glycomimetics Allow Insights into the Pharmacological Fate of Galectin-3 Inhibitors.  
683 *J. Med. Chem.* **2020**, *63* (2), 747-755.

684 24. Mahanti, M.; Pal, K. B.; Kumar, R.; Schulze, M.; Leffler, H.; Logan, D. T.; Nilsson, U. J., Ligand  
685 Sulfur Oxidation State Progressively Alters Galectin-3-Ligand Complex Conformations To Induce  
686 Affinity-Influencing Hydrogen Bonds. *J. Med. Chem.* **2023**, *66* (21), 14716-14723.

687 25. Renaudet, O.; Roy, R., Multivalent scaffolds in glycoscience: an overview. *Chem. Soc. Rev.* **2013**,  
688 *42* (11), 4515-4517.

689 26. Boukerb, A. M.; Rousset, A.; Galanos, N.; Méar, J.-B.; Thépaut, M.; Grandjean, T.; Gillon, E.;  
690 Cecioni, S.; Abderrahmen, C.; Faure, K.; Redelberger, D.; Kipnis, E.; Dessein, R.; Havet, S.; Darblade, B.;  
691 Matthews, S. E.; de Bentzmann, S.; Guéry, B.; Cournoyer, B.; Imberty, A.; Vidal, S., Antiadhesive  
692 Properties of Glycoclusters against *Pseudomonas aeruginosa* Lung Infection. *J. Med. Chem.* **2014**, *57*  
693 (24), 10275-10289.

694 27. Ligeour, C.; Vidal, O.; Dupin, L.; Casoni, F.; Gillon, E.; Meyer, A.; Vidal, S.; Vergoten, G.; Lacroix,  
695 J.-M.; Souteyrand, E.; Imberty, A.; Vasseur, J.-J.; Chevolut, Y.; Morvan, F., Mannose-centered aromatic  
696 galactoclusters inhibit the biofilm formation of *Pseudomonas aeruginosa*. *Org. Biomol. Chem.* **2015**, *13*  
697 (31), 8433-8444.

698 28. Reymond, J.-L.; Bergmann, M.; Darbre, T., Glycopeptide dendrimers as *Pseudomonas*  
699 *aeruginosa* biofilm inhibitors. *Chem. Soc. Rev.* **2013**, *42* (11), 4814-4822.

700 29. Sharon, N., Carbohydrates as future anti-adhesion drugs for infectious diseases. *Biochim.*  
701 *Biophys. Acta* **2006**, *1760* (4), 527-537.

702 30. Pera, N. P.; Pieters, R. J., Towards bacterial adhesion-based therapeutics and detection  
703 methods. *MedChemComm* **2014**, *5* (8), 1027-1035.

704 31. Imberty, A.; Chabre, Y. M.; Roy, R., Glycomimetics and Glycodendrimers as High Affinity  
705 Microbial Anti-adhesins. *Chem. Eur. J.* **2008**, *14* (25), 7490-7499.

706 32. Sattin, S.; Bernardi, A., Glycoconjugates and Glycomimetics as Microbial Anti-Adhesives.  
707 *Trends Biotechnol.* **2016**, *34* (6), 483-495.

708 33. Corbett, P. T.; Leclaire, J.; Vial, L.; West, K. R.; Wietor, J.-L.; Sanders, J. K. M.; Otto, S., Dynamic  
709 Combinatorial Chemistry. *Chem. Rev.* **2006**, *106* (9), 3652-3711.

710 34. Li, J.; Nowak, P.; Otto, S., Dynamic Combinatorial Libraries: From Exploring Molecular  
711 Recognition to Systems Chemistry. *J. Am. Chem. Soc.* **2013**, *135* (25), 9222-9239.

712 35. Frei, P.; Hevey, R.; Ernst, B., Dynamic Combinatorial Chemistry: A New Methodology Comes of  
713 Age. *Chem. Eur. J.* **2019**, *25* (1), 60-73.

714 36. Canal-Martín, A.; Pérez-Fernández, R., Protein-Directed Dynamic Combinatorial Chemistry: An  
715 Efficient Strategy in Drug Design. *ACS Omega* **2020**, *5* (41), 26307-26315.

716 37. Ramström, O.; Lehn, J.-M., In Situ Generation and Screening of a Dynamic Combinatorial  
717 Carbohydrate Library against Concanavalin A. *ChemBioChem* **2000**, *1* (1), 41-48.

718 38. Ramström, O.; Lohmann, S.; Bunyapaiboonsri, T.; Lehn, J.-M., Dynamic Combinatorial  
719 Carbohydrate Libraries: Probing the Binding Site of the Concanavalin A Lectin. *Chem. Eur. J.* **2004**, *10*  
720 (7), 1711-1715.

721 39. Reeh, P.; de Mendoza, J., Dynamic Multivalency for Carbohydrate-Protein Recognition  
722 through Dynamic Combinatorial Libraries Based on FeII-Bipyridine Complexes. *Chem. Eur. J.* **2013**, *19*  
723 (17), 5259-5262.

724 40. Mahon, C. S.; Fascione, M. A.; Sakonsinsiri, C.; McAllister, T. E.; Bruce Turnbull, W.; Fulton, D.  
725 A., Templating carbohydrate-functionalised polymer-scaffolded dynamic combinatorial libraries with  
726 lectins. *Org. Biomol. Chem.* **2015**, *13* (9), 2756-2761.

727 41. Ponnuswamy, N.; Cougnon, F. B. L.; Clough, J. M.; Pantoş, G. D.; Sanders, J. K. M., Discovery of  
728 an Organic Trefoil Knot. *Science* **2012**, *338* (6108), 783-785.

729 42. Otto, S.; Furlan, R. L. E.; Sanders, J. K. M., Selection and Amplification of Hosts From Dynamic  
730 Combinatorial Libraries of Macrocyclic Disulfides. *Science* **2002**, *297* (5581), 590-593.

731 43. Brisig, B.; Sanders, J. K. M.; Otto, S., Selection and Amplification of a Catalyst from a Dynamic  
732 Combinatorial Library. *Angew. Chem. Int. Ed.* **2003**, *42* (11), 1270-1273.

733 44. Gianga, T.-M.; Audibert, E.; Trandafir, A.; Kociok-Köhn, G.; Pantoş, G. D., Discovery of an all-  
734 donor aromatic [2]catenane. *Chem. Sci.* **2020**, *11* (35), 9685-9690.

735 45. Adamski, P.; Eleveld, M.; Sood, A.; Kun, Á.; Szilágyi, A.; Czárán, T.; Szathmáry, E.; Otto, S., From  
736 self-replication to replicator systems en route to de novo life. *Nat. Rev. Chem.* **2020**, *4* (8), 386-403.

737 46. Orrillo, A. G.; Furlan, R. L. E., Sulfur in Dynamic Covalent Chemistry. *Angew. Chem. Int. Ed.* **2022**,  
738 *61* (26), e202201168.

739 47. Vial, L.; Perret, F.; Leclaire, J., Dyn[n]arenes: Versatile Platforms To Study the Interplay  
740 between Covalent and Noncovalent Bonds. *Eur. J. Org. Chem.* **2022**, e202101274.

741 48. Skowron, P.-T.; Dumartin, M.; Jeamet, E.; Perret, F.; Gourlaouen, C.; Baudouin, A.; Fenet, B.;  
742 Naubron, J.-V.; Fotiadu, F.; Vial, L.; Leclaire, J., On-Demand Cyclophanes: Substituent-Directed Self-  
743 Assembling, Folding, and Binding. *J. Org. Chem.* **2016**, *81* (2), 654-661.

744 49. Donnier-Maréchal, M.; Septavaux, J.; Jeamet, E.; Héloin, A.; Perret, F.; Dumont, E.; Rossi, J.-C.;  
745 Ziarelli, F.; Leclaire, J.; Vial, L., Diastereoselective Synthesis of a Dyn[3]arene with Distinct Binding  
746 Behaviors toward Linear Biogenic Polyamines. *Org. Lett.* **2018**, *20* (8), 2420-2423.

747 50. Dumartin, M.; Septavaux, J.; Donnier-Maréchal, M.; Jeamet, E.; Dumont, E.; Perret, F.; Vial, L.;  
748 Leclaire, J., The dark side of disulfide-based dynamic combinatorial chemistry. *Chem. Sci.* **2020**, *11* (31),  
749 8151-8156.

750 51. Zhang, Y.; Ourri, B.; Skowron, P.-T.; Jeamet, E.; Chetot, T.; Duchamp, C.; Belenguer, A. M.;  
751 Vanthuyne, N.; Cala, O.; Dumont, E.; Mandal, P. K.; Huc, I.; Perret, F.; Vial, L.; Leclaire, J., Self-assembly  
752 of achiral building blocks into chiral cyclophanes using non-directional interactions. *Chem. Sci.* **2023**,  
753 *14* (26), 7126-7135.

754 52. Jeamet, E.; Septavaux, J.; Héloin, A.; Donnier-Maréchal, M.; Dumartin, M.; Ourri, B.; Mandal,  
755 P.; Huc, I.; Bignon, E.; Dumont, E.; Morell, C.; Francoia, J.-P.; Perret, F.; Vial, L.; Leclaire, J., Wetting the  
756 lock and key enthalpically favours polyelectrolyte binding. *Chem. Sci.* **2019**, *10* (1), 277-283.

757 53. Vial, L.; Dumartin, M.; Donnier-Maréchal, M.; Perret, F.; Francoia, J.-P.; Leclaire, J., Chirality  
758 sensing and discrimination of lysine derivatives in water with a dyn[4]arene. *Chem. Commun.* **2016**, *52*  
759 (99), 14219-14221.

760 54. Vial, L.; Ludlow, R. F.; Leclaire, J.; Pérez-Fernández, R.; Otto, S., Controlling the Biological Effects  
761 of Spermine Using a Synthetic Receptor. *J. Am. Chem. Soc.* **2006**, *128* (31), 10253-10257.

762 55. Mével, M.; Bouzelha, M.; Leray, A.; Pacouret, S.; Guilbaud, M.; Penaud-Budloo, M.; Alvarez-  
763 Dorta, D.; Dubreil, L.; Gouin, S. G.; Combal, J. P.; Hommel, M.; Gonzalez-Aseguinolaza, G.; Blouin, V.;  
764 Moullier, P.; Adjali, O.; Deniaud, D.; Ayuso, E., Chemical modification of the adeno-associated virus  
765 capsid to improve gene delivery. *Chem. Sci.* **2020**, *11* (4), 1122-1131.

766 56. Kimura, T.; Yamamoto, A.; Namao, T., Preparation of Octakis  
767 (methylthio)octaethylphthalocyaninato Titanium (IV) Benzenedichalcogenolates. *Phosphorus Sulfur*  
768 *Silicon Relat. Elem.* **2010**, *185* (5-6), 1008-1013.

769 57. Cecioni, S.; Faure, S.; Darbost, U.; Bonnamour, I.; Parrot-Lopez, H.; Roy, O.; Taillefumier, C.;  
770 Wimmerová, M.; Praly, J.-P.; Imbert, A.; Vidal, S., Selectivity among Two Lectins: Probing the Effect of  
771 Topology, Multivalency and Flexibility of "Clicked" Multivalent Glycoclusters. *Chem. Eur. J.* **2011**, *17*  
772 (7), 2146-2159.

773 58. Houser, J.; Komarek, J.; Kostlanova, N.; Cioci, G.; Varrot, A.; Kerr, S. C.; Lahmann, M.; Balloy, V.;  
774 Fahy, J. V.; Chignard, M.; Imbert, A.; Wimmerova, M., A Soluble Fucose-Specific Lectin from  
775 *Aspergillus fumigatus* Conidia - Structure, Specificity and Possible Role in Fungal Pathogenicity. *PLoS*  
776 *One* **2013**, *8* (12), e83077.

777 59. Goyard, D.; Baldoneschi, V.; Varrot, A.; Fiore, M.; Imbert, A.; Richichi, B.; Renaudet, O.; Nativi,  
778 C., Multivalent Glycomimetics with Affinity and Selectivity toward Fucose-Binding Receptors from  
779 Emerging Pathogens. *Bioconjugate Chem.* **2018**, *29* (1), 83-88.

- 780 60. Lehot, V.; Brissonnet, Y.; Dussouy, C.; Brument, S.; Cabanettes, A.; Gillon, E.; Deniaud, D.;  
781 Varrot, A.; Le Pape, P.; Gouin, S. G., Multivalent Fucosides with Nanomolar Affinity for the *Aspergillus*  
782 *fumigatus* Lectin FleA Prevent Spore Adhesion to Pneumocytes. *Chem. Eur. J.* **2018**, *24* (72), 19243-  
783 19249.
- 784 61. Boukerb, A. M.; Decor, A.; Ribun, S.; Tabaroni, R.; Rousset, A.; Commin, L.; Buff, S.; Doléans-  
785 Jordheim, A.; Vidal, S.; Varrot, A.; Imberty, A.; Cournoyer, B., Genomic Rearrangements and Functional  
786 Diversification of *lecA* and *lecB* Lectin-Coding Regions Impacting the Efficacy of Glycomimetics Directed  
787 against *Pseudomonas aeruginosa*. *Front. Microbiol.* **2016**, *7*, 811. doi: 10.3389/fmicb.2016.00811.
- 788 62. Hauser, A. R., The type III secretion system of *Pseudomonas aeruginosa*: infection by injection.  
789 *Nat. Rev. Microbiol.* **2009**, *7* (9), 654-665.
- 790 63. Géloën, A.; Berger, E., Reduced Glutathione Decreases Cell Adhesion and Increases Cell  
791 Volume. *Arch. Clin. Biomed. Res.* **2022**, *6*, 880-888.
- 792 64. Engel, J.; Balachandran, P., Role of *Pseudomonas aeruginosa* type III effectors in disease. *Curr.*  
793 *Opin. Microbiol.* **2009**, *12* (1), 61-66.

794

# Dynamic combinatorial chemistry for the multiplexed identification of glyco-dyn[n]arenes in an anti-adhesive strategy against *Pseudomonas aeruginosa*

Fanny Demontrond,<sup>a</sup> Yoann Pascal,<sup>a</sup> Marion Donnier-Maréchal,<sup>a</sup> Corentin Raillon,<sup>a</sup> Baptiste Luton,<sup>b</sup> Clara De la Tramblais,<sup>c</sup> Laurent Vial,<sup>a</sup> David Gueyrard,<sup>a</sup> Benoit Cournoyer,<sup>b</sup> Julien Leclaire,<sup>a</sup> and Sébastien Vidal<sup>a,c\*</sup>

<sup>a</sup> Institut de Chimie et Biochimie Moléculaires et Supramoléculaires, UMR 5246, CNRS, Université Claude Bernard Lyon 1, Université de Lyon, INSA Lyon, CPE Lyon, Villeurbanne, 69622, France

<sup>b</sup> UMR Ecologie Microbienne, CNRS 5557, INRAE 1418, Research Group «Bacterial Opportunistic Pathogens and Environment», VetAgro Sup, Aisle 3, 1st Floor, 69280 Marcy L'Etoile, France

<sup>c</sup> Institut de Chimie des Substances Naturelles, UPR 2301, CNRS, Université Paris-Saclay, Gif-sur-Yvette, 91198, France, [sebastien.vidal@cnrs.fr](mailto:sebastien.vidal@cnrs.fr)

## Supporting Information

Figures S1 to S6	Page S2
Materials and methods	Page S7
Synthesis and characterization of new molecules	Page S8
Equilibration and purification of glycosylated dyn[3,4]arenes	Page S31
Dynamic combinatorial libraries	Page S32
Isothermal titration calorimetry (raw data)	Page S34
Toxicity assays on PAO1	Page S39
Toxicity assays on A549 epithelial cells	Page S40
Aggregation bacterial cell assays	Page S40

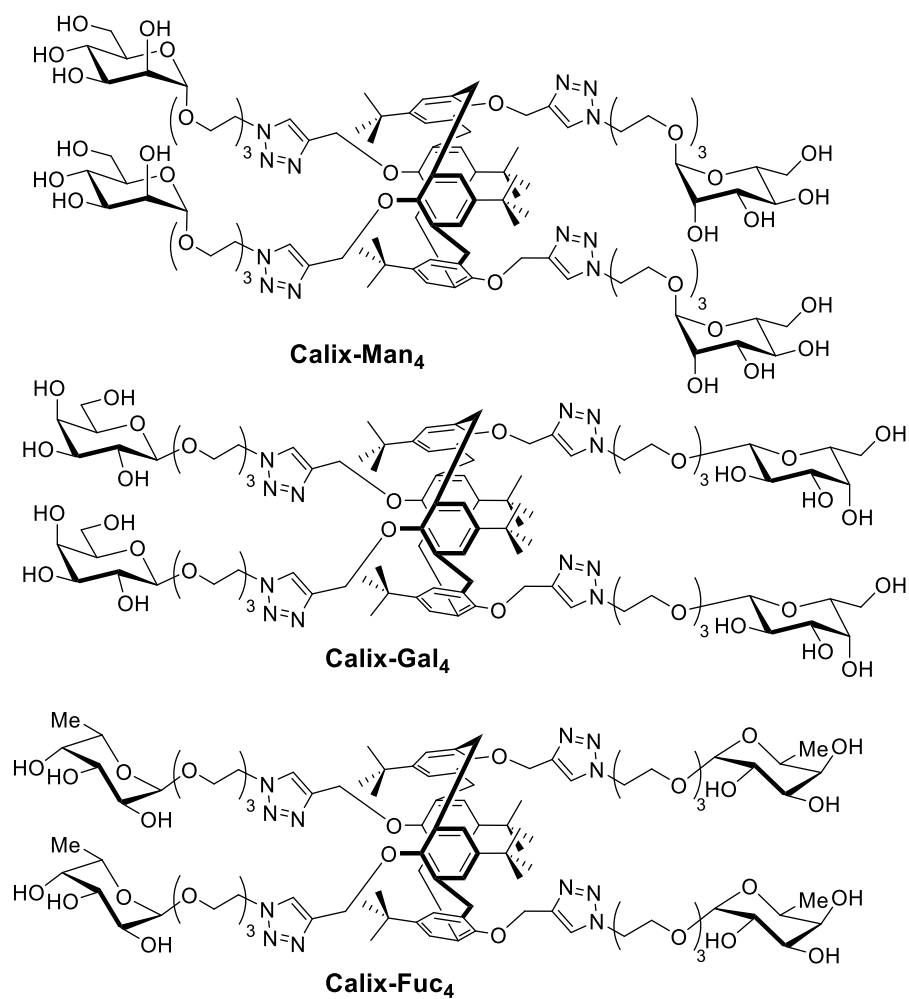


**Figure S1.** Structure of the tetraivalent calixarene-based glycoclusters **Calix-Man<sub>4</sub>**, **Calix-Gal<sub>4</sub>** and **Calix-Fuc<sub>4</sub>**

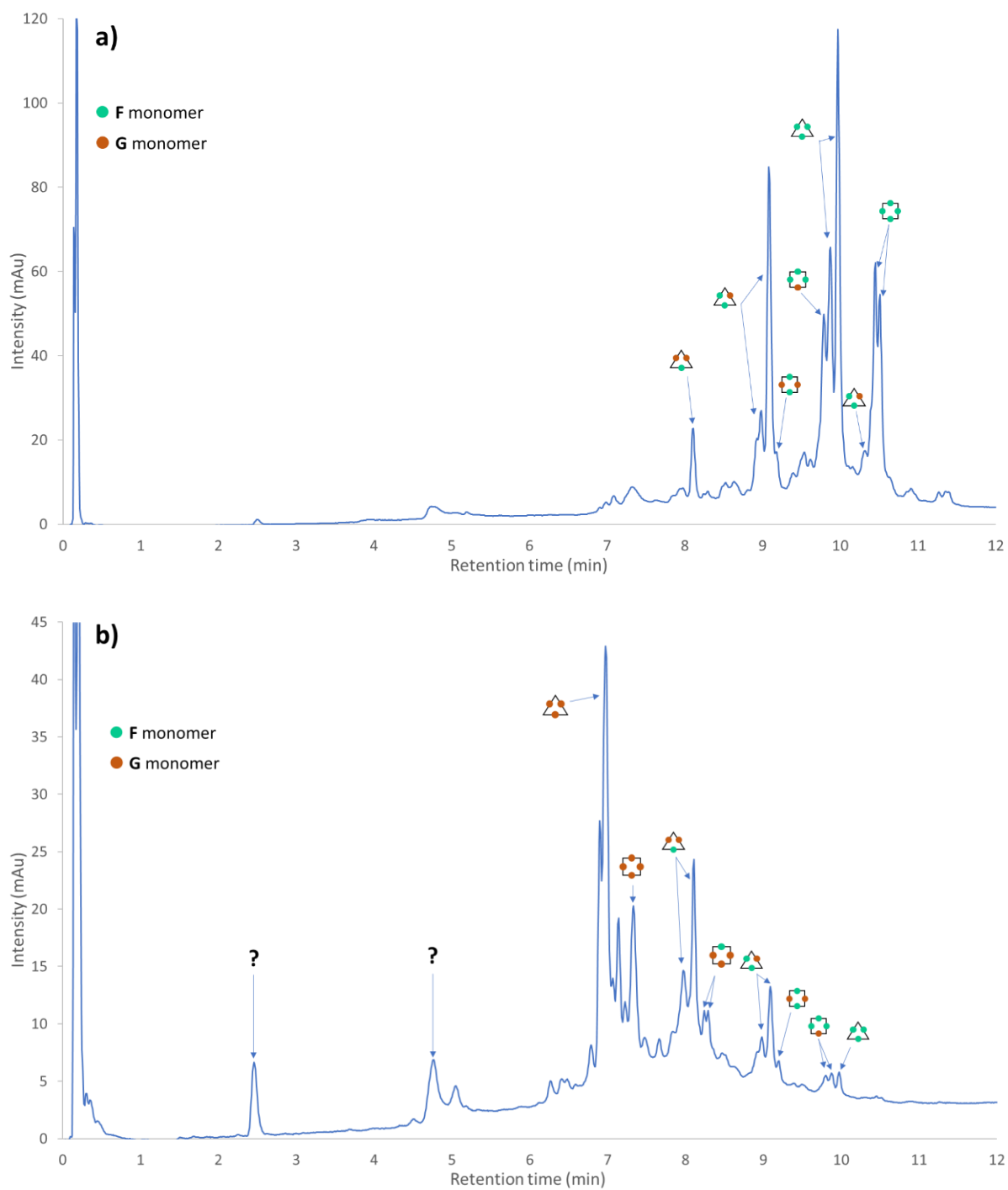


**Figure S2.** UHPLC analysis of the **G/F** (1:1, 0.4 mM) DCL after incubation with LecB (0.4 mM) with the (a) precipitate and (b) supernatant



**Figure S3.** Picture of the precipitate and supernatant samples obtained for the AFL-(G+F)-DCL

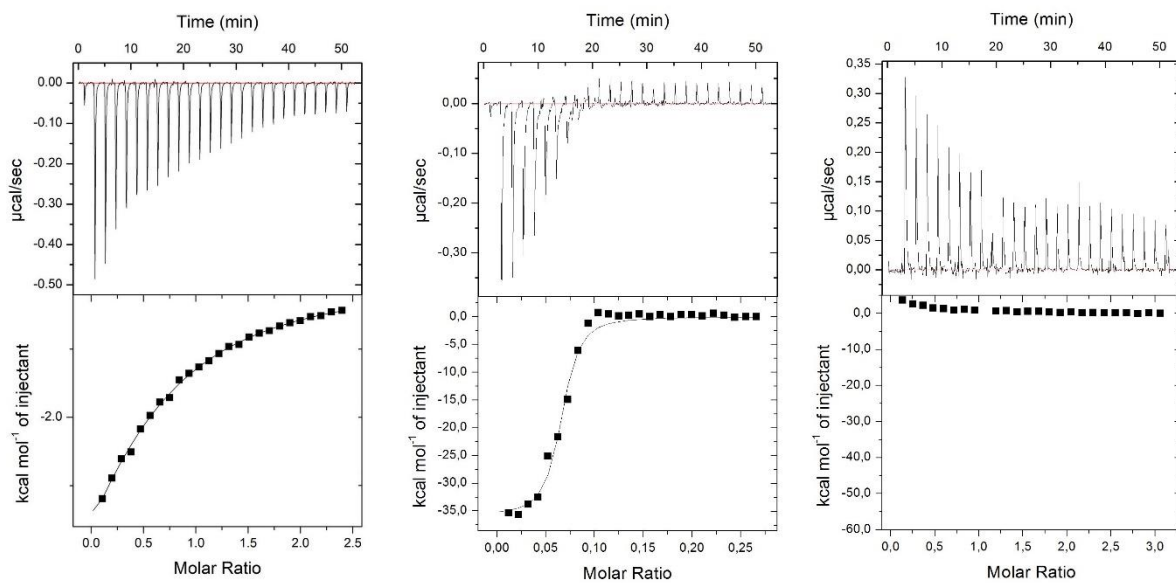


**Figure S4.** Isothermal titration microcalorimetry (ITC) analysis of the binding properties toward LecA (0.1 mM) for  $\beta$ -D-GalOMe (1.8 mM, left panel) and the association titration curve obtained with a 1:1 binding model (lower left panel). ITC data obtained for injections of  $G_3/G_4$  (0.2 mM, 1:1) into a solution of LecA (0.1 mM) and the associated titration curve (center panel). ITC data obtained for injections of  $F_3/F_4$  (0.575 mM, 1:1) into a solution of LecA (0.05 mM) and the associated titration curve (right panel).



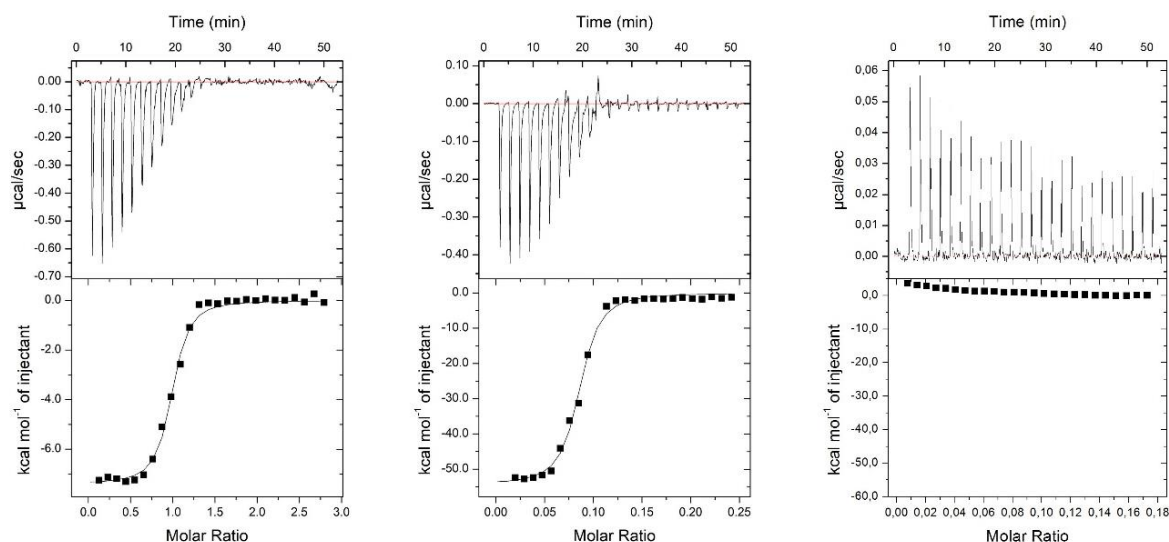


**Figure S5.** Isothermal titration microcalorimetry (ITC) analysis of the binding properties toward LecB (0.112 mM) for  $\alpha$ -L-FucOMe (1.67 mM, left panel) and the association titration curve obtained with a 1:1 binding model (lower left panel). ITC data obtained for injections of  $F_3/F_4$  (0.072 mM, 1:1) into a solution of LecB (0.112 mM) and the associated titration curve (center panel). ITC data obtained for injections of  $G_3/G_4$  (0.209 mM, 1:1) into a solution of LecB (0.112 mM) and the associated titration curve (right panel).

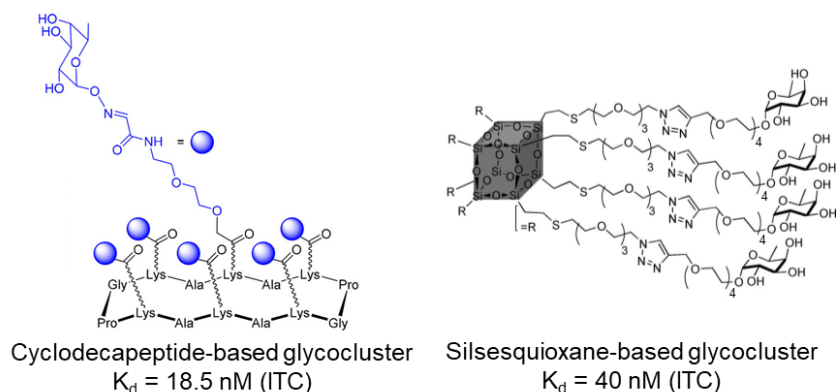


**Figure S6.** Hexavalent cyclodecapeptide-based and silsesquioxane-based glycoclusters used as a comparison with the  $F_3/F_4$  fucosylated dyn[n]arenes.

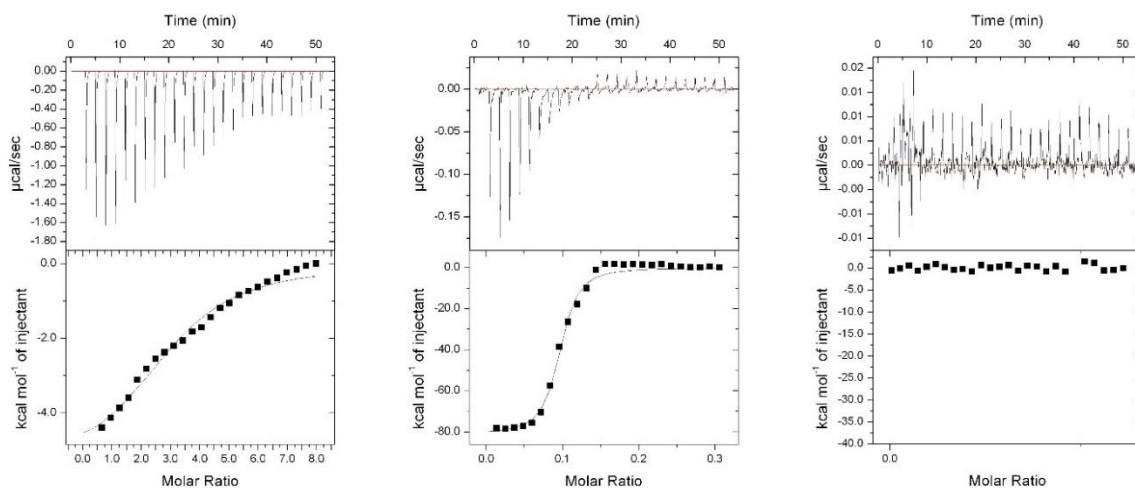


**Figure S7.** Isothermal titration microcalorimetry (ITC) analysis of the binding properties toward AFL (0.05 mM) for  $\alpha$ -L-FucOMe (3 mM, left panel) and the association titration curve obtained with a 1:1 binding model (lower left panel). ITC data obtained for injections of  $F_3/F_4$  (0.012 mM, 1:1) into a solution of AFL (0.05 mM) and the associated titration curve (center panel). ITC data obtained for injections of  $G_3/G_4$  (0.012 mM, 1:1) into a solution of AFL (0.01 mM) and the associated titration curve (right panel).

## Materials and methods

Commercial reagents were used without further purification. Solvents were dried using standard methods. All reactions were carried out under argon. Column chromatography was performed using silica gel (40–63  $\mu\text{m}$ ). Reactions were monitored via TLC on a silica gel aluminum plate and visualized under UV light (254 nm).

$^1\text{H}$ ,  $^{13}\text{C}$ , DEPT, COSY, HSQC, HMBC experiments were performed on Bruker spectrometers: AV 300, AVL 300, AV 400 and AV 500 at 298K at the CCRMN of the University of Lyon. The chemical shifts are indicated in ppm (parts per million) in reference to the residual solvent peak (*J. Org. Chem.*, **1997**, *62*, 7512-7515). Coupling constants ( $J$ ) are indicated in Hz (Hertz). The abbreviations used for the multiplicity are: s (singlet), b (broad), d (doublet), dd (doublet of doublet), t (triplet), td (triplet of doublet), q (quadruplet), m (multiplet).

Low resolution mass spectrometry was performed on a LCQ advantage (50-20 000  $m/z$ ) apparatus from Thermofinnigan. High resolution mass spectrometry was performed on a MicrOTOFQ II (50-20 000  $m/z$ ) apparatus from Bruker. Electrospray ionization was used in all cases.

Lyophilization was carried out in a CHRIST Alpha 2-4 LDPlus apparatus or on a CHRIST Alpha 3-4 LSC Basic system.

C18 Chromatography was performed on automated systems such as CombiFlash Companion system from Serlabo Technologies, Puriflash 5.020 apparatus from Interchim or Pure C-805 from Buchi using C18 Reversed-Phase column cartridges.

Preparative high-performance liquid chromatographies were performed on a Shimadzu LC20 semi-preparative system equipped with a binary pump, a manual injection manifold, dual wavelength UV detector. The chromatographic separation was performed at RT on various columns. The chromatograms were recorded at 210 and 250 nm.

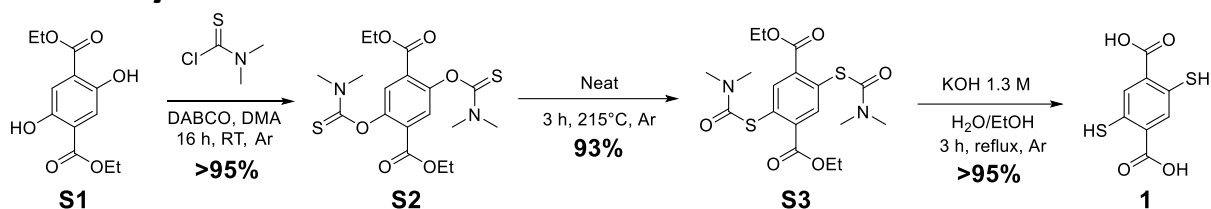
Filtration with membrane could be performed on hydrophilic (0.45  $\mu\text{m}$  pore size, hydrophilic polyethersulfone, 47 mm diameter, ref: HPWP04700) or hydrophobic (Membrane Durapore, PVDF hydrophobic, 0.22  $\mu\text{m}$  pore size, 47 mm diameter, ref: GVHP04700) membranes purchased from Merck Millipore

HPLC analyses were performed on a UHPLC Thermo Scientific Dionex UltiMate 3000 system equipped with a binary pump, an auto-sampler, a variable wavelength UV detector. The chromatographic separation was performed at 30°C on various columns. The chromatograms were recorded at 210 and 254 nm. High resolution mass spectrometry was performed on a QTOF Impact II (50-20 000  $m/z$ ) apparatus from Bruker. **Column:** Thermo Scientific Accucore C8 80 Å, 2.1×50 mm, 2.6  $\mu\text{m}$  and **Gradient** in Table S1 below.

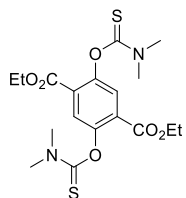
**Table S1.** Gradient for HPLC analyses

Time (min)	Flow (mL/min)	H <sub>2</sub> O + 0.1% TFA	MeCN + 0.1% TFA
0	0.800	100	0
15	0.800	70	30
18	0.800	0	100
19	0.800	0	100
19.5	0.800	100	0
22	0.800	100	0

## Synthesis and characterization of new molecules



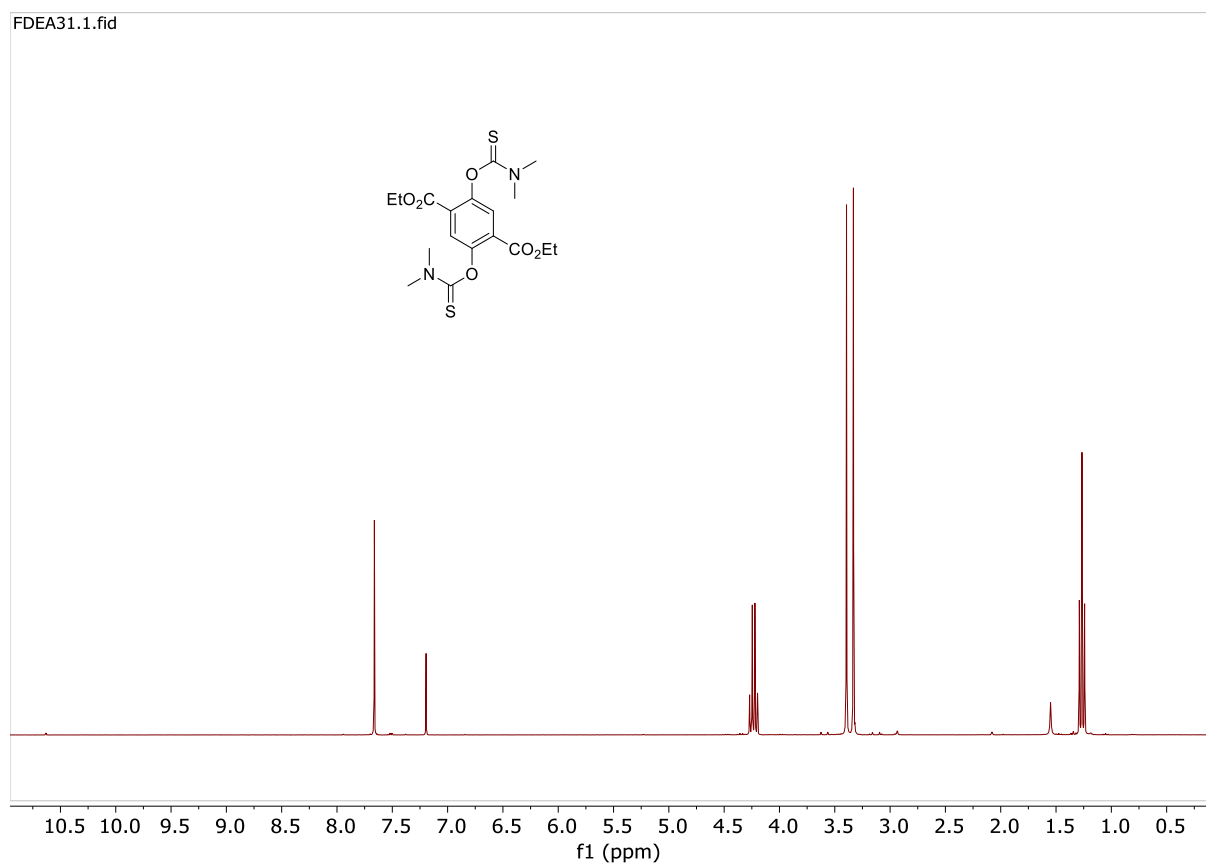
### Diethyl 2,5-bis(dimethylthiocarbamoyloxy)terephthalate (**S2**)



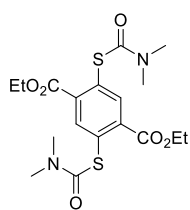
To a solution of **S1** diethyl 2,5-dihydroxyterephthalate (10 g, 39 mmol, 1 eq.) in dry DMA (100 mL) was added dropwise at 0°C a solution of dimethylthiocarbamoyl chloride (19 g, 157 mmol, 4 eq.) and DABCO (18 g, 157 mmol, 4 eq.) in dry DMA (50 mL). The mixture was stirred under nitrogen at room temperature for 24 h. The precipitate was filtrated and washed extensively with water (4×250 mL). The solid was dried under vacuum to give compound **S2** as a white powder (17 g, 38 mmol, >95%).

$^1\text{H NMR}$  (300 MHz,  $\text{CDCl}_3$ )  $\delta$  ppm = 7.74 (s, 2H, Ar), 4.31 (q,  $J = 7.2$  Hz, 4H,  $\text{CH}_2$ ), 3.47 (s, 6H,  $\text{NCH}_3$ ), 3.41 (s, 6H,  $\text{NCH}_3$ ), 1.34 (t,  $J = 7.2$  Hz, 6H,  $\text{CH}_3$ )

The data were in agreement with the literature reference. *J. Am. Chem. Soc.*, **2006**, *128*, 10253-10257



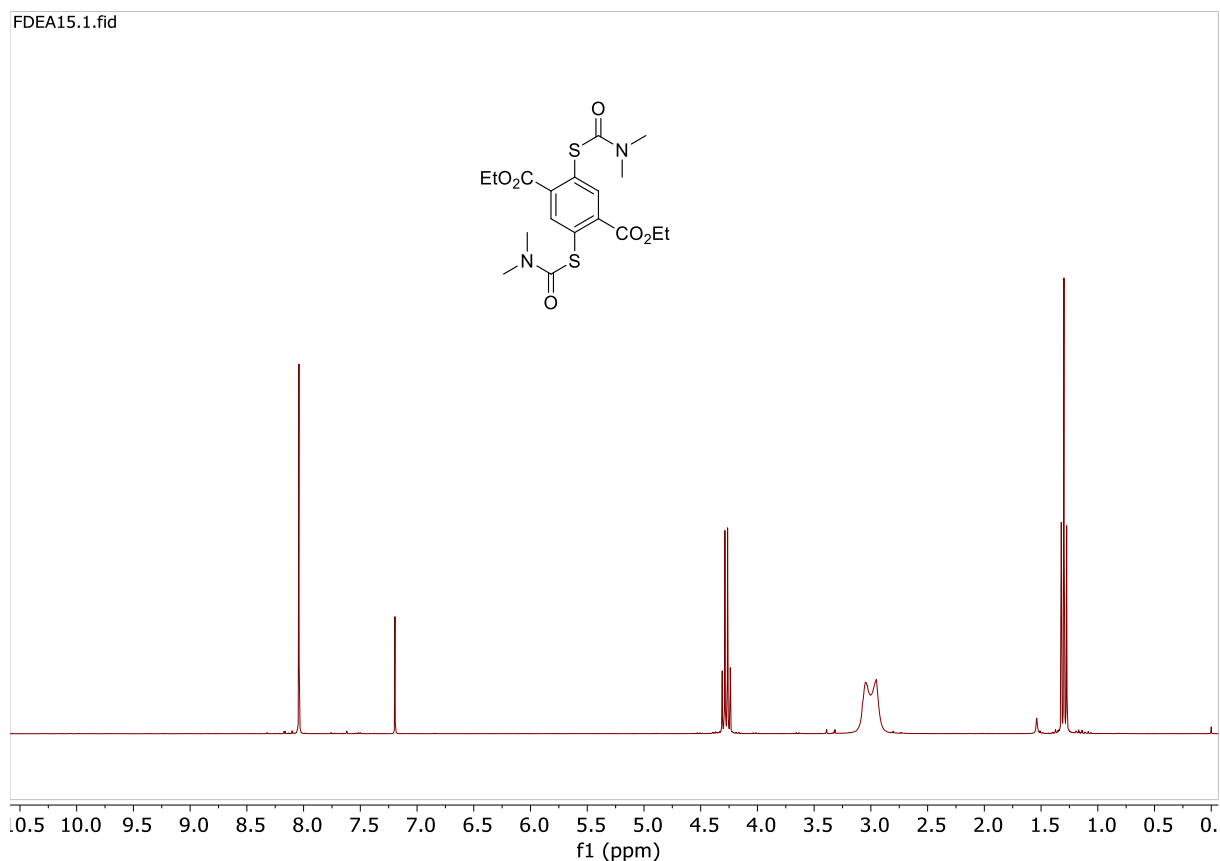
### Diethyl 2,5-bis(dimethylcarbamoylsulfanyl)terephthalate (**S3**)



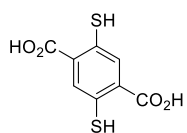
Diethyl 2,5-bis(dimethylthiocarbamoyloxy)terephthalate **S2** (3,6 g, 8.21 mmol) was heated under neat conditions at 210°C for 2 h. The solid was cooled at 90°C. Then, ethanol was added (120 mL) and the mixture was cooled at 0°C overnight. The precipitate was washed with cooled ethanol (2×45 mL) and dried under vacuum to give compound **S3** as a beige powder (3.3 g, 7.62 mmol, 93%).

$^1\text{H NMR}$  (300 MHz,  $\text{CDCl}_3$ )  $\delta$  ppm = 8.09 (s, 2H, Ar), 4.32 (q,  $J = 7.2$  Hz, 4H,  $\text{CH}_2$ ), 3.10 (brs, 6H,  $\text{NCH}_3$ ), 2.99 (br s, 6H,  $\text{NCH}_3$ ), 1.34 (t,  $J = 7.2$  Hz, 6H,  $\text{CH}_3$ )

The data were in agreement with the literature reference. *J. Am. Chem. Soc.*, **2006**, *128*, 10253-10257



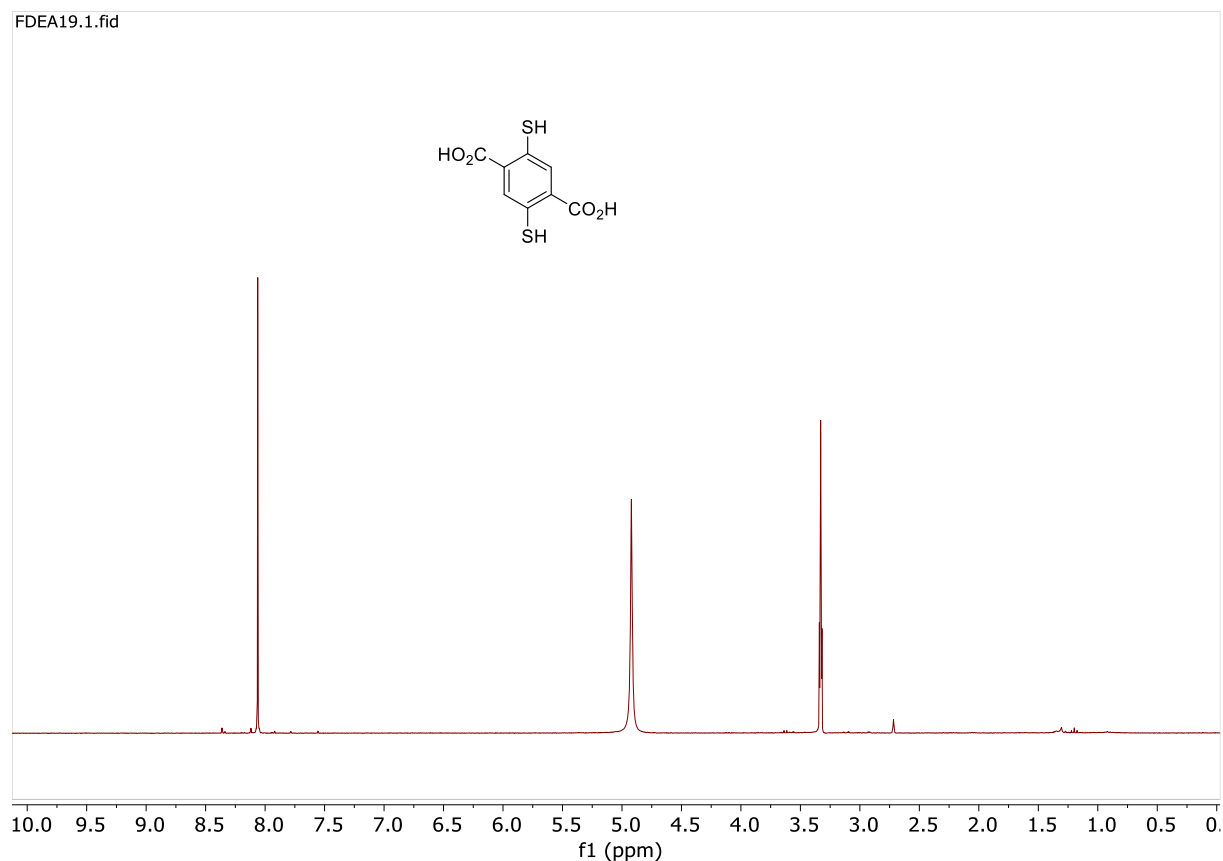
### 2,5-Dimercaptoterephthalic acid (**1**)



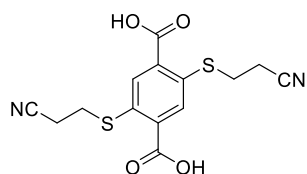
A solution of diethyl diethyl 2,5-bis(dimethylcarbamoylsulfanyl)terephthalate **S3** (2.9 g, 6.7 mmol, 1 eq.) in degassed 1.3 M KOH (7.3 g, 130.3 mmol, 17 eq.) in EtOH/H<sub>2</sub>O (1:1, 100 mL) was heated under reflux under an inert atmosphere for 3 h. The reaction mixture was cooled in an ice-bath, and concentrated HCl (30 mL) was added until pH 1. A bright yellow precipitate was formed, filtered, and washed extensively with water, yielding compound **1** as a yellow solid (1.5 g, 6.6 mmol, >95%).

<sup>1</sup>H NMR (300 MHz, CD<sub>3</sub>OD) δ = 8.06 (s, 2H, Ar)

The data were in agreement with the literature reference. *J. Am. Chem. Soc.*, **2006**, *128*, 10253-10257



## 2,5-Di[(2-cyanoethyl)thio]terephthalic acid (**2**)

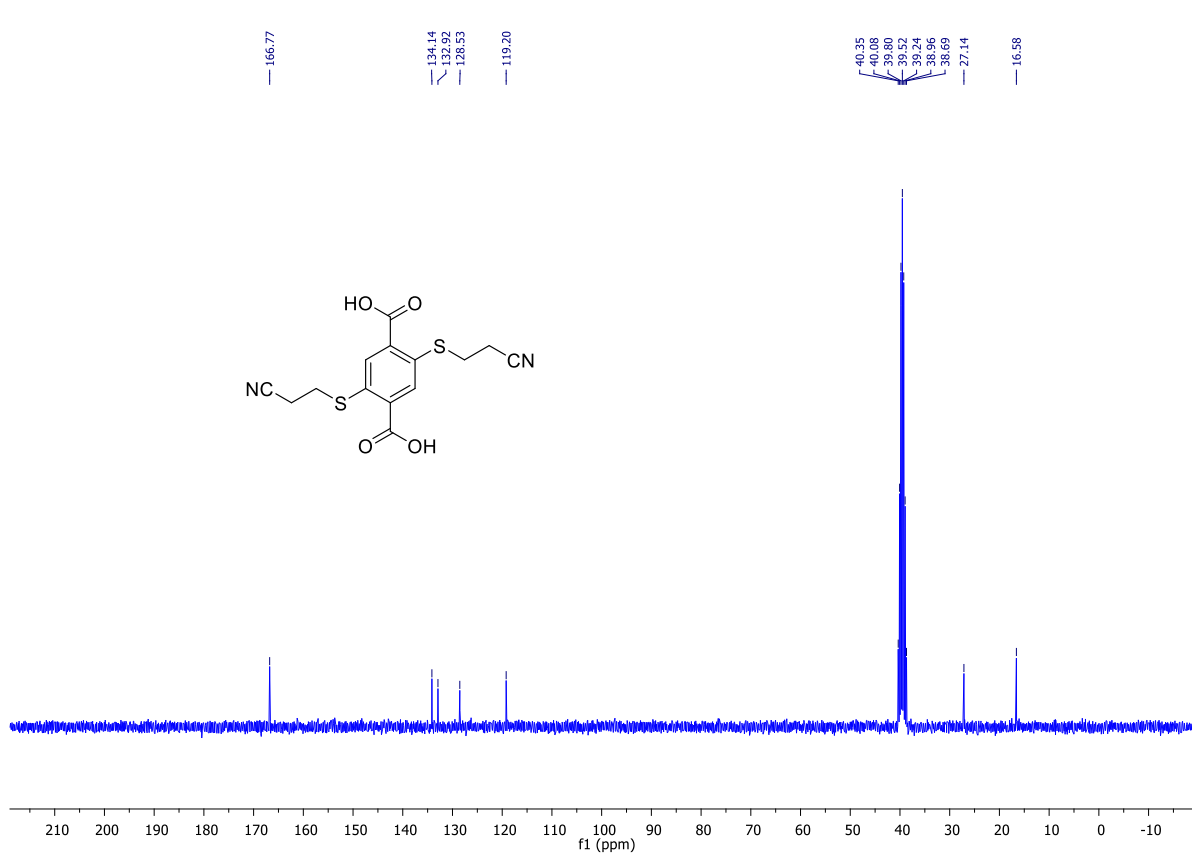
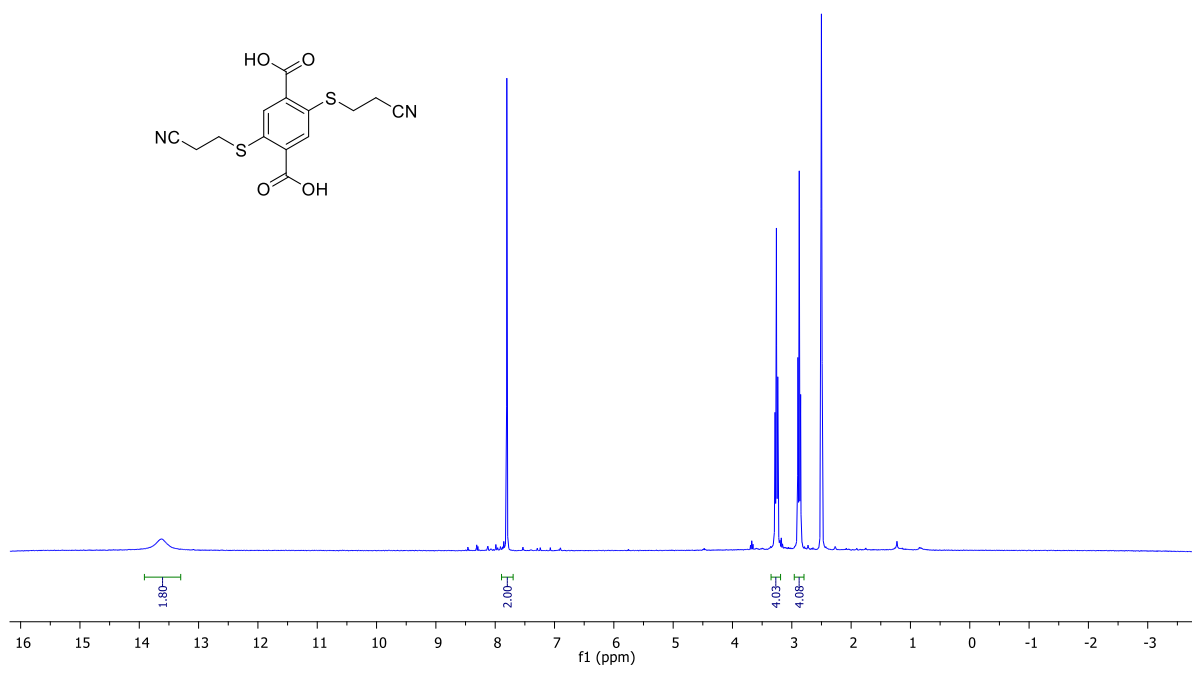


2,5-Dimercaptoterephthalic acid **1** (0.965 g, 4.2 mmol, 1 eq.) was dissolved in degassed THF (20 mL) and heated to 70°C. Then, resulting mixture was added on a suspension of NaH (60% in mineral oil, 1.047 g, 26.2 mmol, 6.2 eq.) in degassed anhydrous THF (10 mL). The suspension was stirred at r.t. during 1 h then 3-bromopropionitrile (4 mL, 48.2 mmol, 12 eq.) was added dropwise at r.t. The mixture was heated at 70°C for 16 h. The solvent was evaporated and the yellow solid crude residue was suspended in CHCl<sub>3</sub> (50 mL) then filtered off using a hydrophobic membrane (5 μm). The solid was dried under vacuum then poured into 1 M HCl (40 mL). The precipitate was filtered off using a hydrophilic membrane (5 μm) and washed with water (5×20 mL). The solid was dried under vacuum to afford 2,5-di[(2-cyanoethyl)thio]terephthalic acid **2** (1.417 g, 4.2 mmol, >95%) as a bright yellow amorphous solid.

<sup>1</sup>H NMR (300 MHz, DMSO-d<sub>6</sub>): 13.62 (bs, 2H, CO<sub>2</sub>H), 7.80 (s, 2H, H<sub>ar</sub>), 3.26 (t, *J* = 6.8 Hz, 4H, SCH<sub>2</sub>), 2.87 (t, *J* = 6.8 Hz, 4H, CH<sub>2</sub>CN)

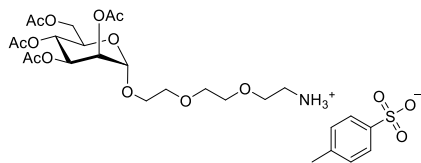
<sup>13</sup>C NMR (75 MHz, DMSO-d<sub>6</sub>): 166.7 (CO<sub>2</sub>H), 134.1 (CS), 132.9 (CCO<sub>2</sub>H), 128.5 (CH<sub>ar</sub>), 119.2 (CH<sub>2</sub>CN), 27.1 (SCH<sub>2</sub>), 16.5 (CH<sub>2</sub>CN)

HR-ESI-MS (positive mode) *m/z* : calcd. for C<sub>14</sub>H<sub>12</sub>N<sub>2</sub>NaO<sub>4</sub>S<sub>2</sub> [M+Na]<sup>+</sup> 359.0131, found 359.0145





**1-Ammonium-3,6-dioxaoct-8-yl 2,3,4,6-tetra-O-acetyl- $\alpha$ -D-mannopyranoside *p*-toluenesulfonate (4-Man)**



A solution of azide **3-Man** (13.56 g, 26.83 mmol, 1 eq.) and *p*TsOH (4.77 g, 27.70 mmol, 1 eq.) in dry MeOH (500 mL) with Pd/C 10% (1.4 g, 10%w) was placed under H<sub>2</sub> atmosphere (1 bar). The reaction was monitored by TLC and stirred until completion. After 45 min, the mixture was filtered on a pad of celite and

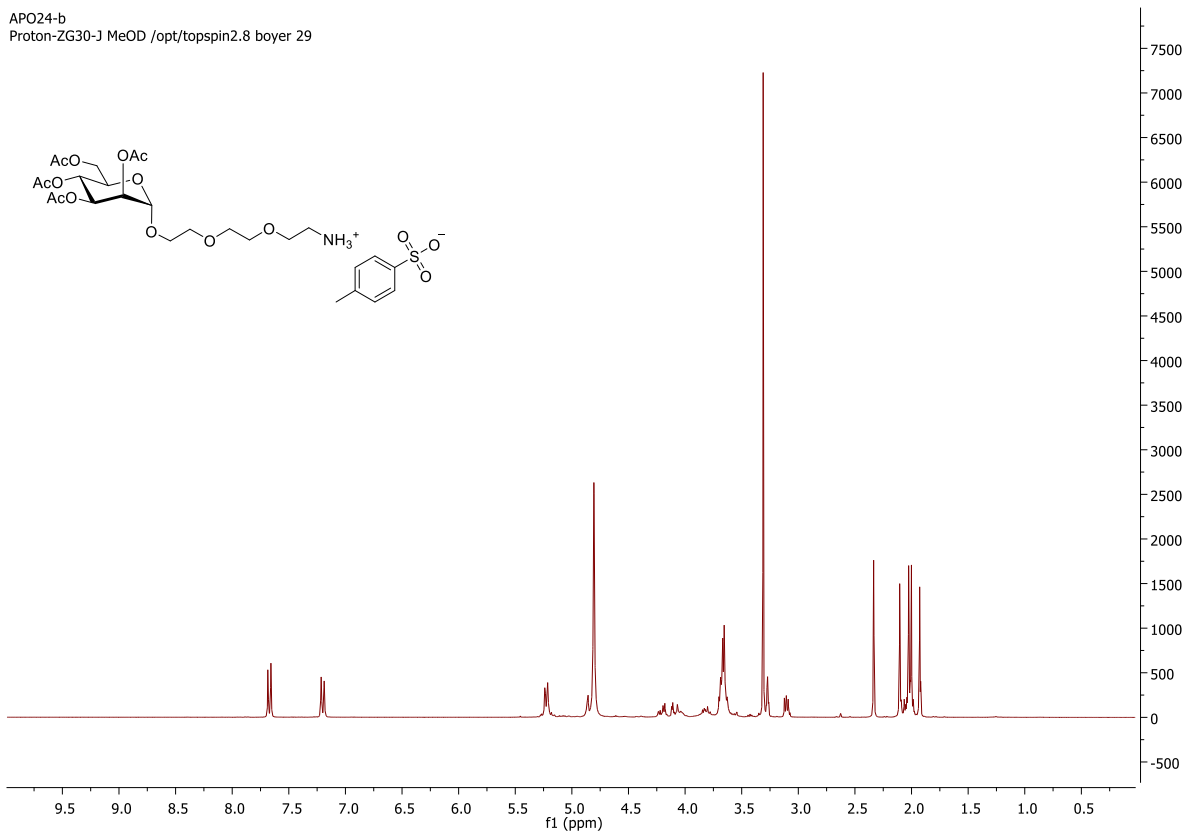
washed with MeOH and the solvent was evaporated to afford the desired product ammonium **4-Man** *p*TsOH salt (16.15 g, 24.78 mmol, 92%) as a green amorphous solid.

<sup>1</sup>H NMR (300 MHz, CD<sub>3</sub>OD): 7.67 (d, *J* = 8.1 Hz, 2H, CH<sub>Ar</sub>), 7.20 (d, *J* = 7.8 Hz, 2H, CH<sub>Ar</sub>), 5.23 (dd, *J* = 7.8, 2.1 Hz, 3H, H<sub>2</sub>, H<sub>3</sub>, H<sub>4</sub>), 4.86 (d, *J* = 1.2 Hz, 1H, H<sub>1</sub>), 4.19 (m, 1H, H<sub>5</sub>), 4.08 (m, 2H, H<sub>6</sub>), 3.87-3.78 (m, 2H, CH<sub>2</sub>OMan), 3.70-3.63 (m, 8H, 4xCH<sub>2</sub>O), 3.14 (br, 2H, CH<sub>2</sub>N), 2.33 (s, 3H, C<sub>Ar</sub>CH<sub>3</sub>), 2.10, 2.04, 1.99, 1.92 (s, 4x3H, COCH<sub>3</sub>).

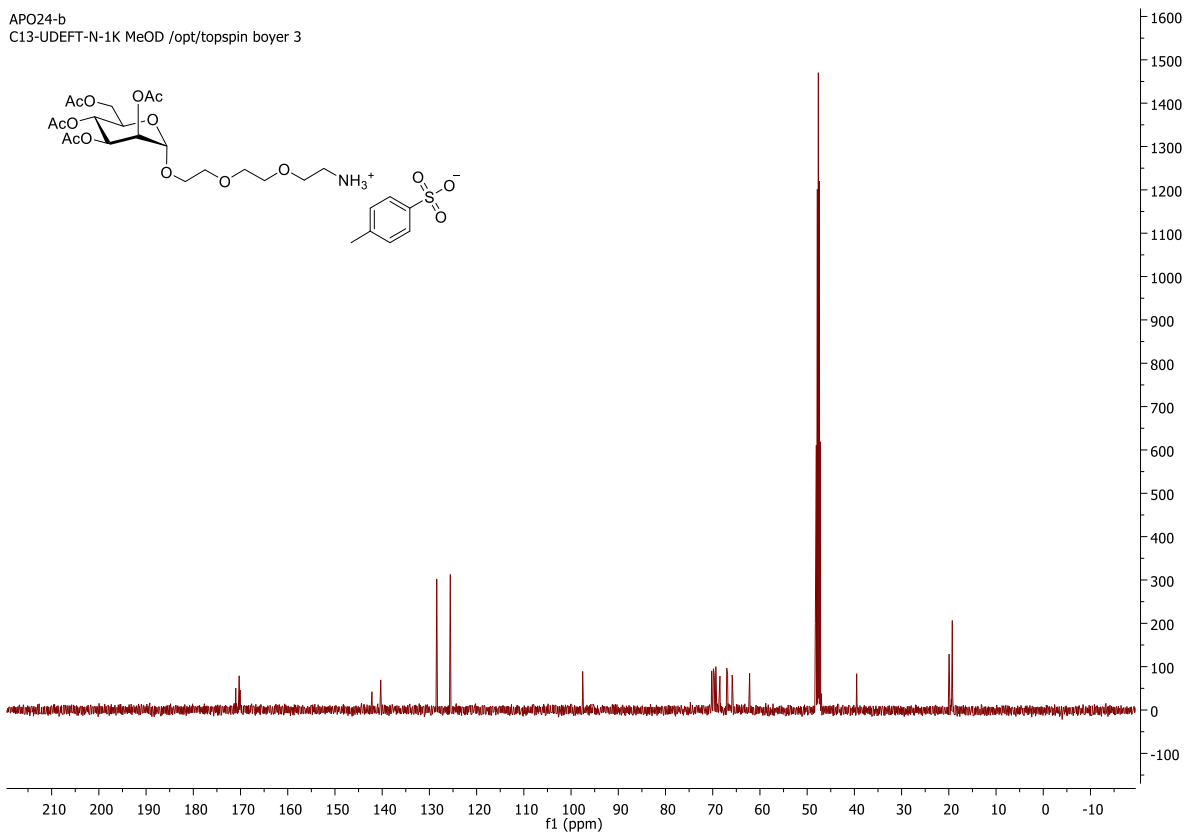
<sup>13</sup>C NMR (300 MHz, CD<sub>3</sub>OD): 171.0, 172.3, 171.9, 170.1 (4xCOCH<sub>3</sub>), 142.2 (C<sub>Ar</sub>CH<sub>3</sub>), 140.3 (C<sub>Ar</sub>SO<sub>3</sub>), 128.4 (2xC, C<sub>Ar</sub>), 125.6 (2xC, C<sub>Ar</sub>), 97.5 (C<sub>1</sub>), 70.22, 69.8, 69.7 (3xCH<sub>2</sub>O), 69.4 (C<sub>2</sub>), 69.3 (C<sub>3</sub>), 68.5 (C<sub>5</sub>), 67.0 (CH<sub>2</sub>O), 66.8 (CH<sub>2</sub>OMan), 65.9 (C<sub>4</sub>), 62.2 (C<sub>6</sub>), 39.5 (CH<sub>2</sub>N), 19.9, 19.30, 19.26, 19.2 (4xCOCH<sub>3</sub>).

HR-ESI-MS (positive mode) *m/z*: calcd. for C<sub>20</sub>H<sub>34</sub>NO<sub>12</sub>: [M]<sup>+</sup> = 480.2076, found 480.2074.

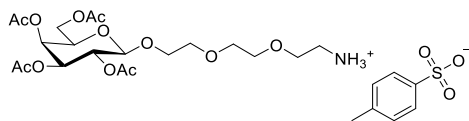
APO24-b  
Proton-ZG30-J MeOD /opt/topspin2.8 boyer 29



APO24-b  
C13-UDEFT-N-1K MeOD /opt/topspin boyer 3



### 1-Ammonium-3,6-dioxaoct-8-yl 2,3,4,6-tetra-*O*-acetyl- $\beta$ -D-galactopyranoside *p*-toluenesulfonate (4-Gal)



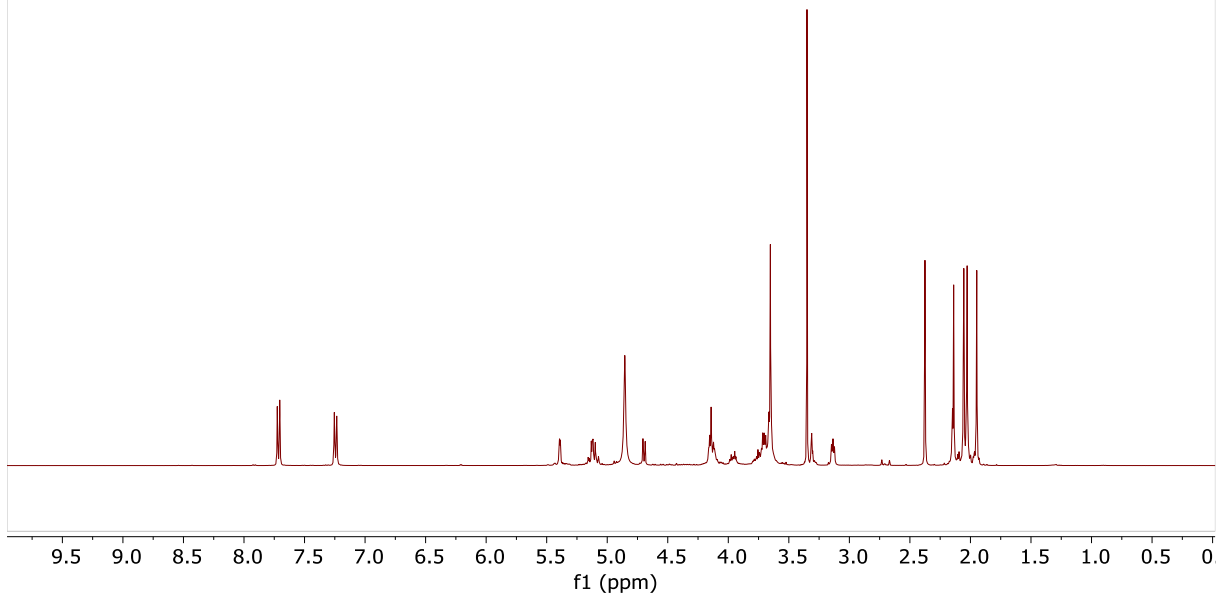
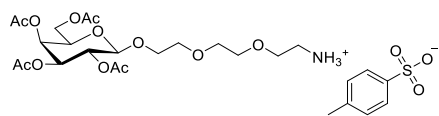
A solution of azide **3-Gal** (777 mg, 1.31 mmol, 1 eq.) and *p*TsOH (250 mg, 1.32 mmol, 1 eq.) in dry MeOH (65 mL) with Pd/C 10% (99 mg, 10%w) was placed under H<sub>2</sub> atmosphere (1 bar). The reaction was monitored by TLC and stirred until completion. After 20 min, the mixture was filtered on a pad of celite and washed with MeOH and the solvent was evaporated to afford the desired product ammonium **4-Gal** and *p*TsOH salt (850 mg, 1.3 mmol, >95%) as a green amorphous solid.

<sup>1</sup>H NMR (400 MHz, CD<sub>3</sub>OD): 7.71 (d, *J* = 8.2 Hz, 2H, CH<sub>Ar</sub>), 7.25 (d, *J* = 8.2 Hz, 2H, CH<sub>Ar</sub>), 5.39 (dd, *J* = 3.1, 1.0 Hz, 1H, H<sub>4</sub>), 5.15-5.07 (m, 2H, H<sub>2</sub> + H<sub>3</sub>), 4.69 (d, *J* = 7.3 Hz, 1H, H<sub>1</sub>), 4.22-4.07 (m, 3H, H<sub>6</sub> + CH<sub>2</sub>OGal), 4.01-3.91 (m, 1H, H<sub>5</sub>), 3.78-3.63 (m, 9H, 4xCH<sub>2</sub>O + CH<sub>2</sub>OGal), 3.13 (bs, 2H, CH<sub>2</sub>N), 2.37 (s, 3H, C<sub>Ar</sub>CH<sub>3</sub>), 2.14, 2.05, 2.03, 1.95 (s, 4xCOCH<sub>3</sub>)

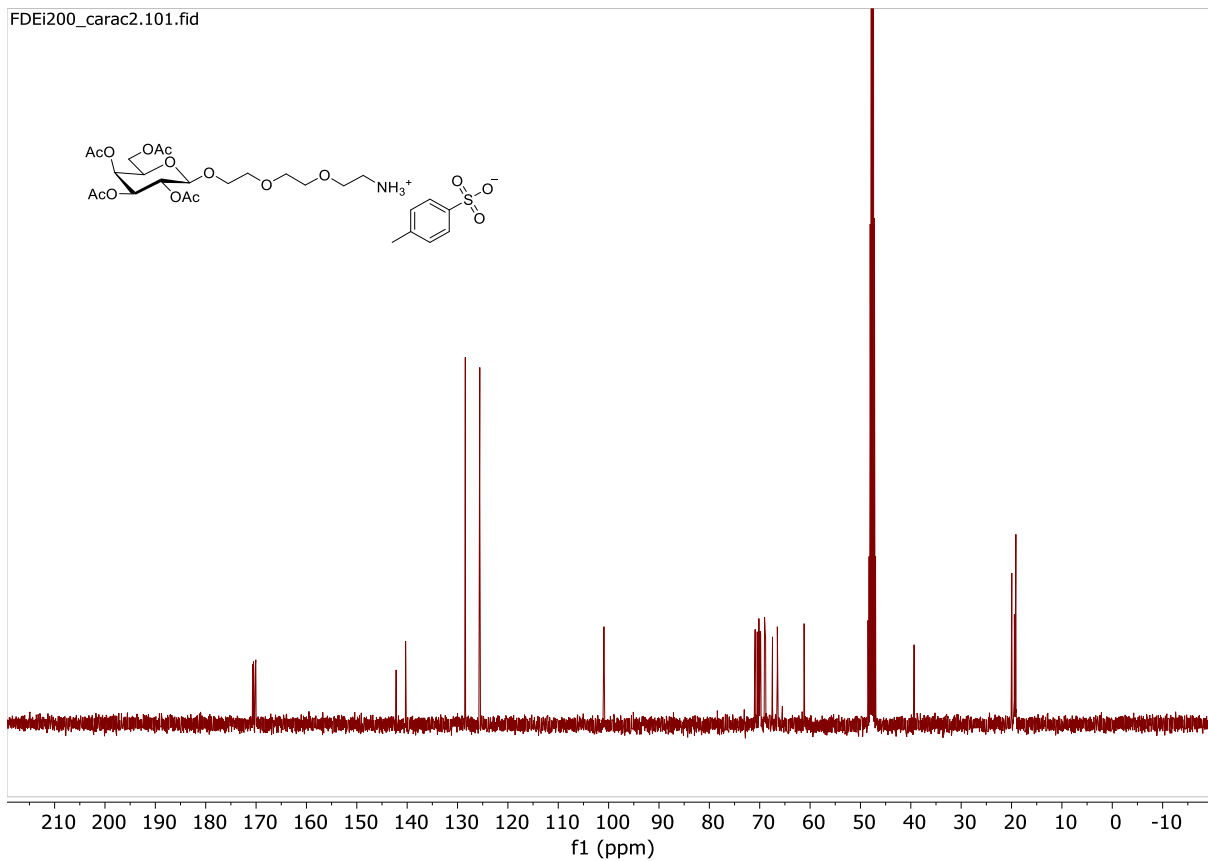
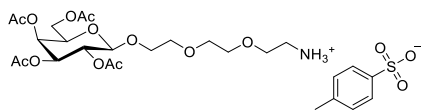
<sup>13</sup>C NMR (100 MHz, CD<sub>3</sub>OD): 172.1, 171.9, 171.5, 171.4 (4xC, COCH<sub>3</sub>), 143.6 (CCH<sub>3</sub>), 141.7 (CSO<sub>3</sub>), 129.8 (2xC, C<sub>Ar</sub>), 126.9 (2xC, C<sub>Ar</sub>), 102.3 (C<sub>1</sub>), 72.3, 71.8, 71.5, 71.3, 70.2 (5xC, CH<sub>2</sub>O + CH<sub>2</sub>OGal), 71.2 (C<sub>5</sub>), 70.4, 68.8 (C<sub>2</sub> + C<sub>3</sub>), 67.9 (C<sub>4</sub>), 62.5 (C<sub>6</sub>), 40.7 (CH<sub>2</sub>N), 21.3, 20.8, 20.6, 20.5 (5xC, COCH<sub>3</sub> + CCH<sub>3</sub>).

HR-ESI-MS (positive mode) *m/z* : calcd. for C<sub>20</sub>H<sub>34</sub>NO<sub>12</sub> : [M]<sup>+</sup> = 480.2076, found 480.2073.

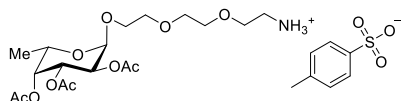
FDEi200\_carac2.100.fid



FDEi200\_carac2.101.fid



### 1-Ammonium-3,6-dioxaoct-8-yl 2,3,4-tri-*O*-acetyl- $\alpha$ -L-fucopyranoside *p*-toluenesulfonate (**4-Fuc**)



A solution of azide **3-Fuc** (1.014 g, 2.27 mmol, 1 eq.) and *p*TsOH (0.433 g, 2.28 mmol, 1 eq.) in dry MeOH (100 mL) with Pd/C 10% (79 mg, 10%w) was placed under H<sub>2</sub> atmosphere (1 bar). The reaction was monitored by TLC and stirred until completion. After

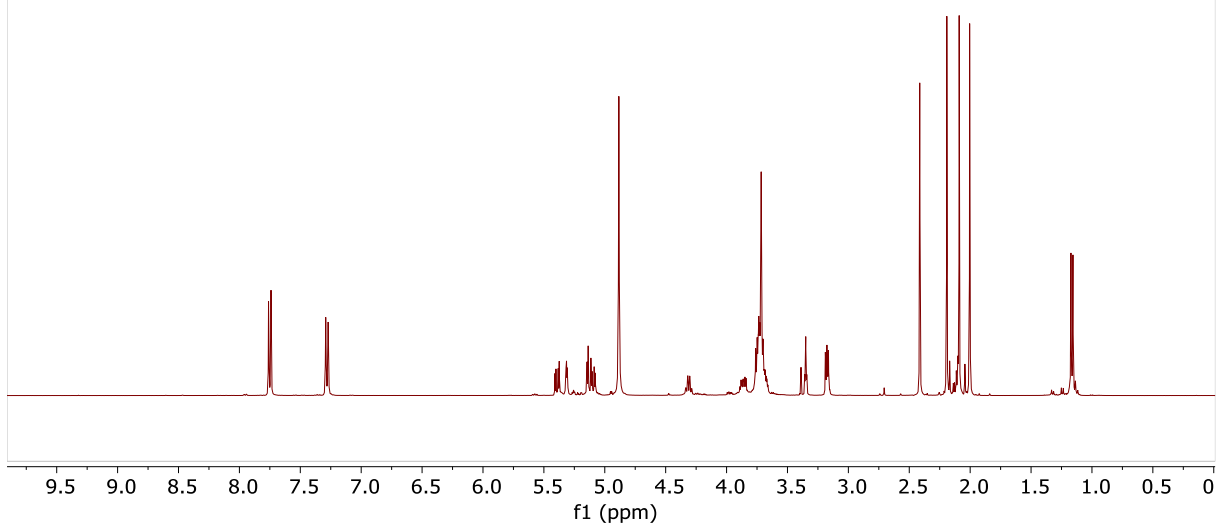
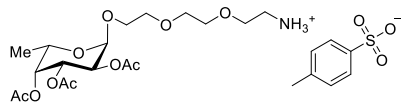
25 min, the mixture was filtered on a pad of celite and washed with MeOH and the solvent was evaporated to afford the desired product ammonium **4-Fuc** *p*TsOH salt (1.279 g, 2.15 mmol, 95%) as a green amorphous solid.

<sup>1</sup>H NMR (400 MHz, CD<sub>3</sub>OD): 7.71 (d, *J* = 8.2 Hz, 2H, CH<sub>Ar</sub>), 7.24 (d, *J* = 8.2 Hz, 2H, CH<sub>Ar</sub>), 5.35 (dd, *J* = 10.7, 3.4 Hz, 1H, H<sub>3</sub>), 5.27 (dd, *J* = 3.5, 1.4 Hz, 1H, H<sub>2</sub>), 5.11-5.04 (m, 2H, H<sub>1</sub> + H<sub>2</sub>), 4.27 (qd, *J* = 6.5, 1.4 Hz, 1H, H<sub>5</sub>), 3.84-3.80 (m, 1H, CH<sub>2</sub>OFuc), 3.72-3.66 (m, 9H, 4xCH<sub>2</sub>O + CH<sub>2</sub>OFuc), 3.14 (bs, 2H, CH<sub>2</sub>N), 2.37 (s, 3H, C<sub>Ar</sub>CH<sub>3</sub>), 2.15, 2.05, 1.96 (s, 4xCOCH<sub>3</sub>)

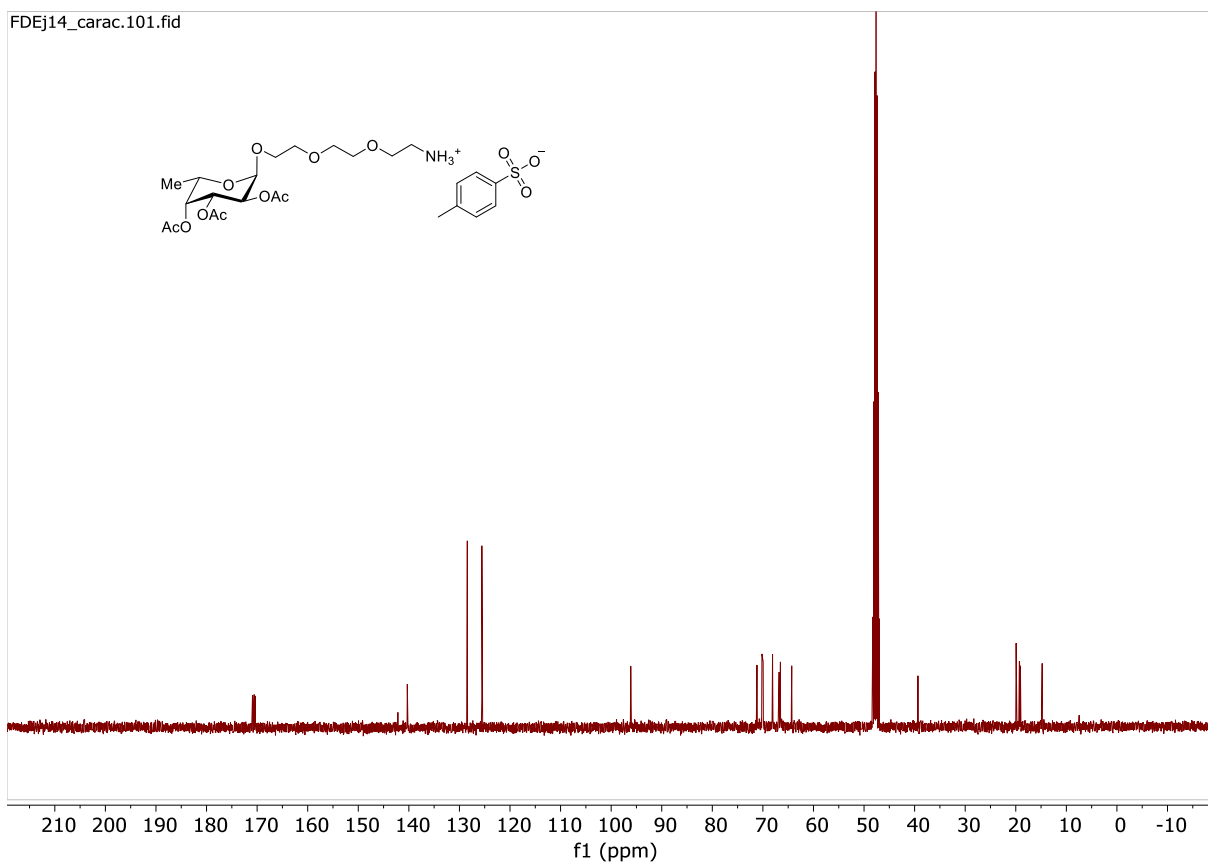
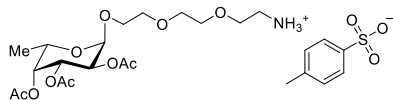
<sup>13</sup>C NMR (100 MHz, CD<sub>3</sub>OD): 172.3, 172.0, 171.8 (3xC, COCH<sub>3</sub>), 143.6 (C<sub>Ar</sub>CH<sub>3</sub>), 141.7 (C<sub>Ar</sub>SO<sub>3</sub>), 129.8 (2xC<sub>Ar</sub>), 127.0 (2xC<sub>Ar</sub>), 97.5 (C<sub>1</sub>), 72.6 (C<sub>4</sub>), 71.6, 71.4, 71.3 (3xCH<sub>2</sub>), 69.5 (C<sub>3</sub>), 69.4 (C<sub>2</sub>), 68.2 (FucOCH<sub>2</sub>CH<sub>2</sub>), 67.9 (FucOCH<sub>2</sub>CH<sub>2</sub>), 65.7 (C<sub>5</sub>), 40.7 (CH<sub>2</sub>N), 21.3 (C<sub>Ar</sub>CH<sub>3</sub>), 20.7, 20.6, 20.5 (3xCOCH<sub>3</sub>), 16.2 (C<sub>6</sub>).

HR-ESI-MS (positive mode) *m/z* : calcd. for C<sub>18</sub>H<sub>32</sub>NO<sub>10</sub> : [M]<sup>+</sup> = 422.2021, found 422.2014.

FDEj14\_carac.100.fid



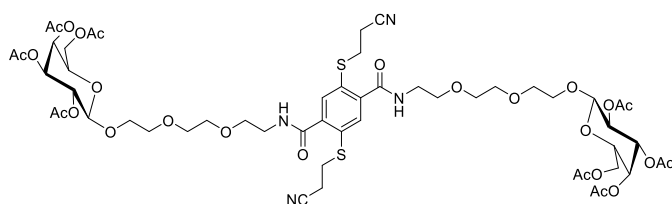
FDEj14\_carac.101.fid



## General procedure for the formation of amides

2,5-Di[(2-cyanoethyl)thio]terephthalic acid **2** (1 eq.), HOBT•H<sub>2</sub>O (2.6 eq.) and EDCI•HCl or EDCI (2.6 eq.) were suspended under inert atmosphere (Ar) in dry CH<sub>2</sub>Cl<sub>2</sub> affording a heterogeneous yellow solution. Amine **4** (2.6 eq.) dissolved in dry CH<sub>2</sub>Cl<sub>2</sub> was added dropwise, *i*Pr<sub>2</sub>NEt (2.6 eq.) was then added and the stirring was continued during 18 h. The solvent was evaporated off and the crude residue was purified by flash silica gel column chromatography (CH<sub>2</sub>Cl<sub>2</sub>/MeOH 97:3) to afford the desired amide **5**.

### 2,5-Di[(2-cyanoethyl)thio]-*N,N*-di[3,6-dioxo-8-(2,3,4,6-tetra-*O*-acetyl-β-D-galactopyranosyloxy)-oct-1-yl]terephthalamide (**5-Gal**)



Prepared according to the general procedure from diacid **2** (614 mg, 1.827 mmol, 1 eq.), HOBT•H<sub>2</sub>O (728 mg, 4.727 mmol, 2.6 eq.), EDCI (840 μL, 4.727 mmol, 2.6 eq.) in CH<sub>2</sub>Cl<sub>2</sub> (100 mL), *i*Pr<sub>2</sub>NEt (840 μL, 4.822 mmol, 2.7 eq.) and amine **4-Gal**

(3.100 g, 4.757 mmol, 2.6 eq.) in CH<sub>2</sub>Cl<sub>2</sub> (50 mL) affording compound **5-Gal** (1.244 g, 54%) as a brown oil.

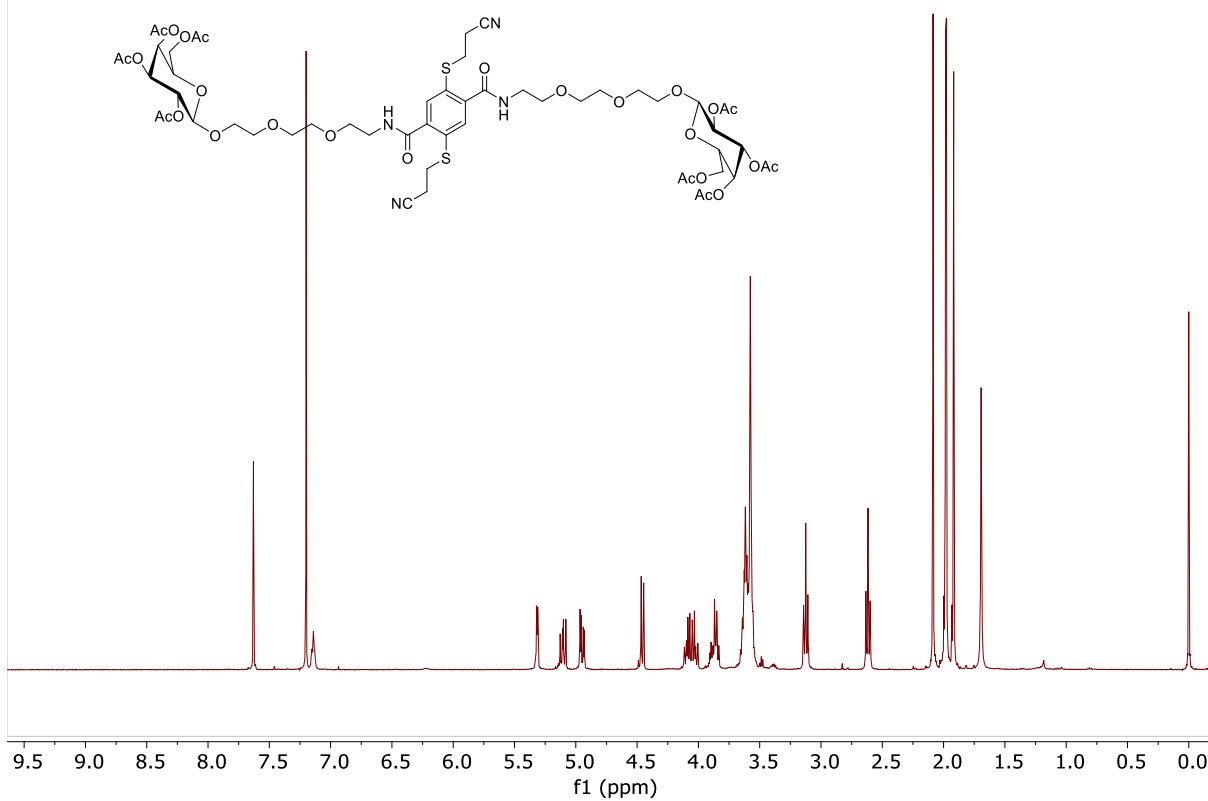
*R*<sub>f</sub> = 0.5 (CHCl<sub>3</sub>/MeOH, 19:1)

<sup>1</sup>H NMR (400 MHz, CDCl<sub>3</sub>): 7.69 (s, 2H, H<sub>ar</sub>), 7.16 (t, *J* = 5.2 Hz, 2H, NH), 5.37 (d, *J* = 3.4 Hz, 2H, H<sub>4</sub>), 5.17 (dd, *J* = 7.9; 10.5 Hz, 2H, H<sub>2</sub>), 5.00 (dd, *J* = 3.4; 10.5 Hz, 2H, H<sub>3</sub>), 4.51 (d, *J* = 7.9 Hz, 2H, H<sub>1</sub>), 4.18-4.05 (m, 4H, H<sub>6</sub> + H<sub>6'</sub>), 3.98-3.88 (m, 4H, CH<sub>2</sub>OGal + H<sub>5</sub>), 3.75-3.60 (m, 22H, CH<sub>2</sub>OGal + 4×OCH<sub>2</sub> + NHCH<sub>2</sub>), 3.19 (t, *J* = 7.0 Hz, 4H, SCH<sub>2</sub>), 2.68 (t, *J* = 7.0 Hz, 4H, CH<sub>2</sub>CN), 2.14; 2.05; 2.04; 1.98 (4×6H, COCH<sub>3</sub>)

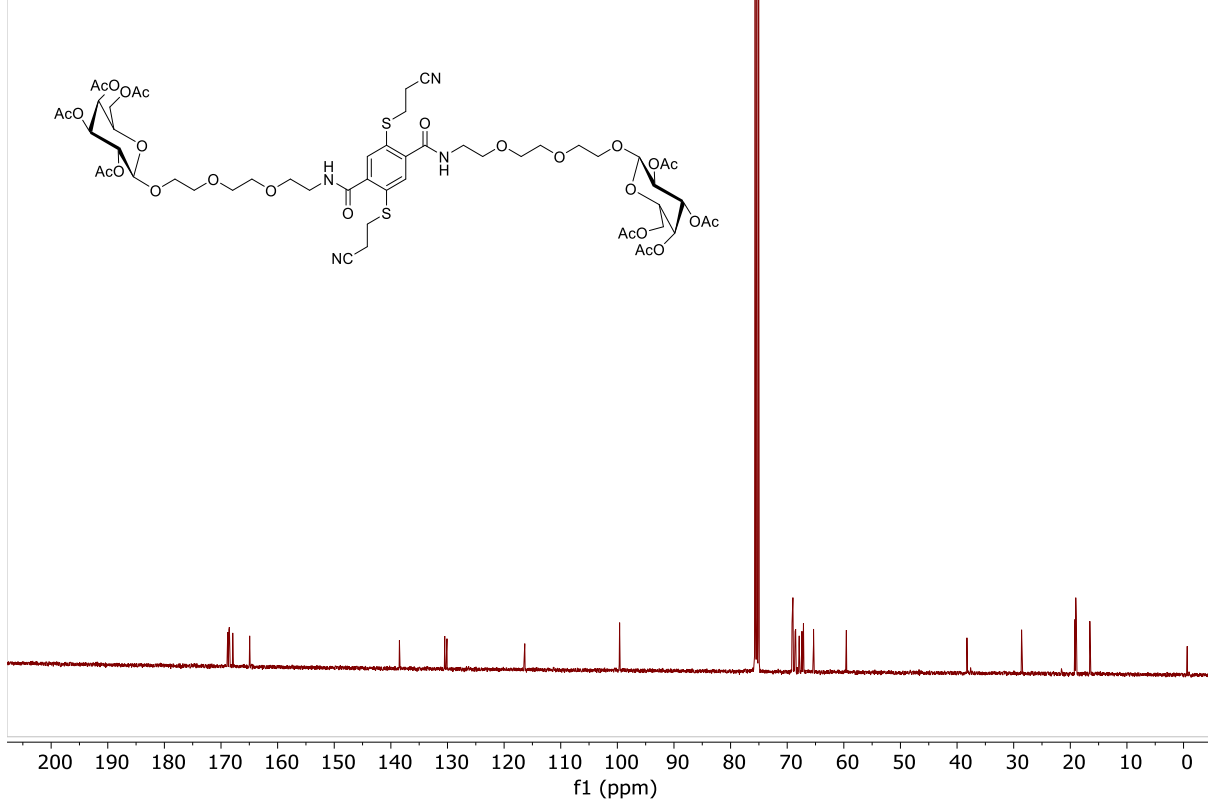
<sup>13</sup>C NMR (100 MHz, CDCl<sub>3</sub>): 170.6; 170.4; 170.3; 169.7 (4×COCH<sub>3</sub>), 166.7 (CONH), 140.3 (CCONH), 132.3 (CH<sub>ar</sub>), 131.9 (CS), 118.1 (CN), 101.4 (C<sub>1</sub>), 70.9 (C<sub>3</sub>), 70.80; 70.4; 70.3; 69.7 (4×C, OCH<sub>2</sub>), 70.79 (C<sub>5</sub>), 69.2 (CH<sub>2</sub>OGal), 68.9 (C<sub>2</sub>), 67.1 (C<sub>4</sub>), 61.3 (C<sub>6</sub>), 40.1 (NHCH<sub>2</sub>), 30.4 (SCH<sub>2</sub>), 21.0; 20.85; 20.84; 20.7 (4×COCH<sub>3</sub>), 18.3 (CH<sub>2</sub>CN)

HR-ESI-MS (positive mode) *m/z*: calcd. for C<sub>54</sub>H<sub>74</sub>N<sub>4</sub>Na<sub>2</sub>O<sub>26</sub>S<sub>2</sub> [M+2Na]<sup>2+</sup> = 652.1909, found 652.1909.

YP55.1.fid

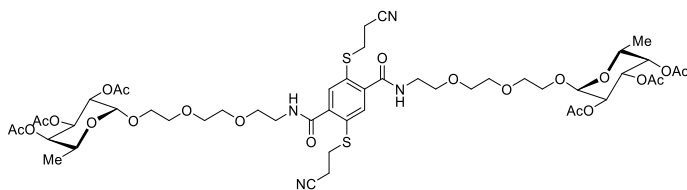


YP55.2.fid





**2,5-Di[(2-cyanoethyl)thio]-*N,N*-di[3,6-dioxa-8-(2,3,4-tri-*O*-acetyl- $\alpha$ -L-fucopyranosyloxy)-oct-1-yl]terephthalamide (5-Fuc)**



Prepared according to the general procedure from diacid **2** (312 mg, 0.926 mmol, 1 eq.), HOBt•H<sub>2</sub>O (370 mg, 2.42 mmol, 2.6 eq.), EDCI (430  $\mu$ L, 2.42 mmol, 2.6 eq.) in CH<sub>2</sub>Cl<sub>2</sub> (25 mL), *i*Pr<sub>2</sub>Net (420  $\mu$ L,

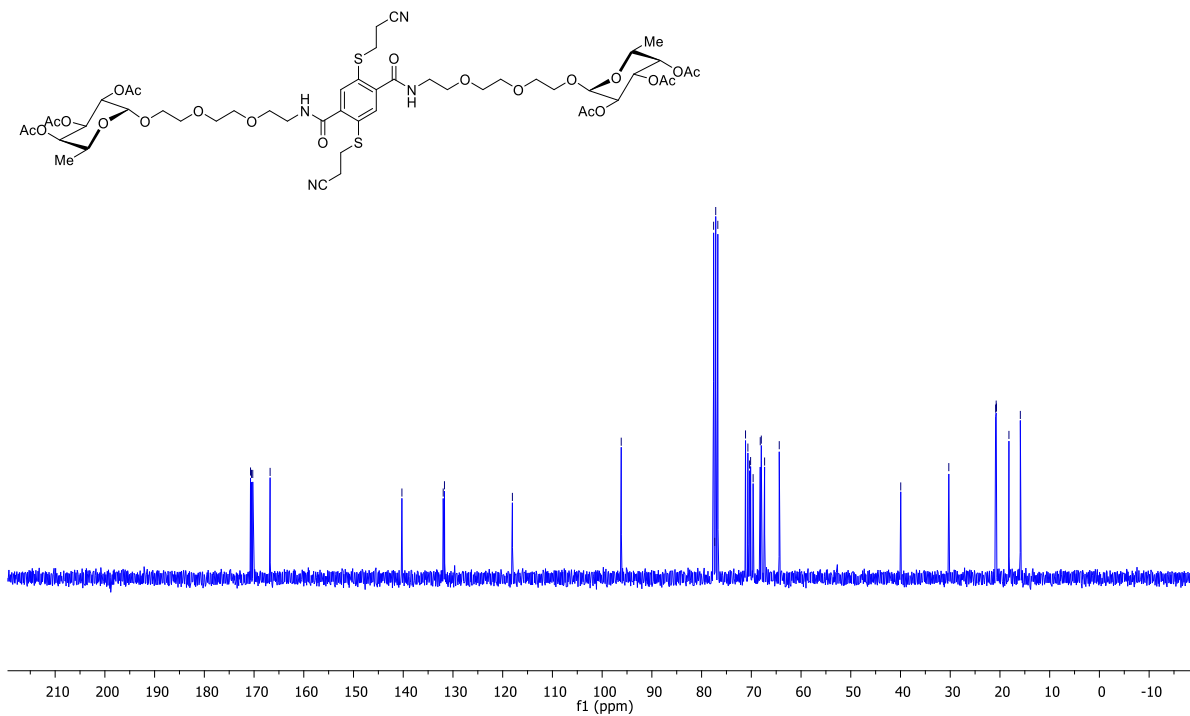
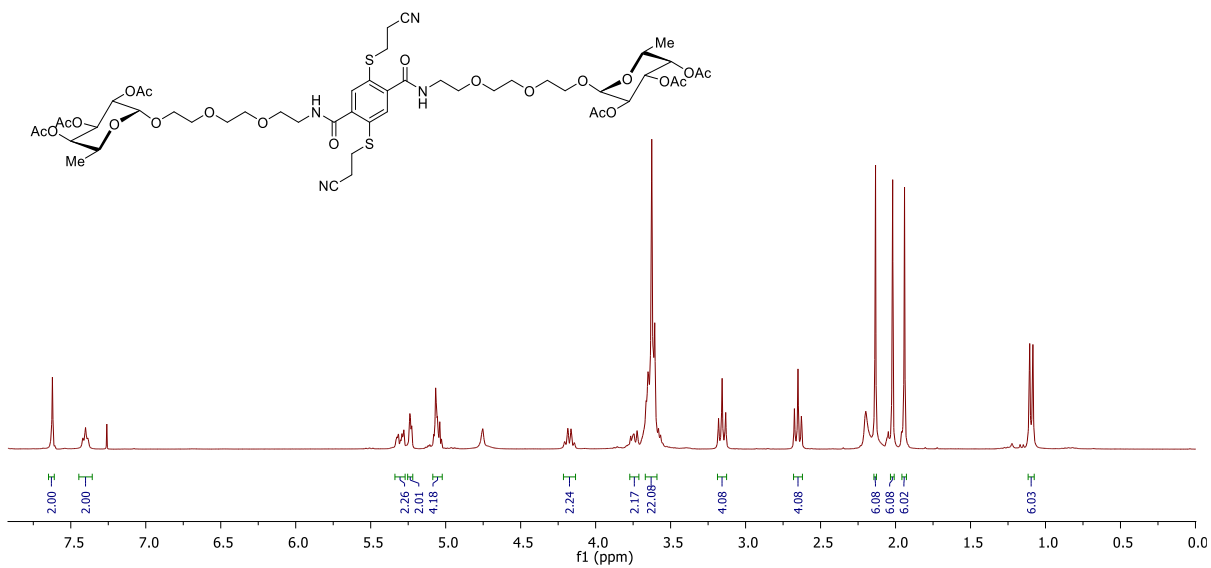
2.42 mmol, 2.6 eq.) and amine **4-Fuc** (1.405 g, 2.36 mmol, 2.5 eq.) in CH<sub>2</sub>Cl<sub>2</sub> (25 mL) affording the desired product **5-Fuc** (584 mg, 55%) as a brown oil.

*R*<sub>f</sub> = 0.5 (CHCl<sub>3</sub>/MeOH, 19:1)

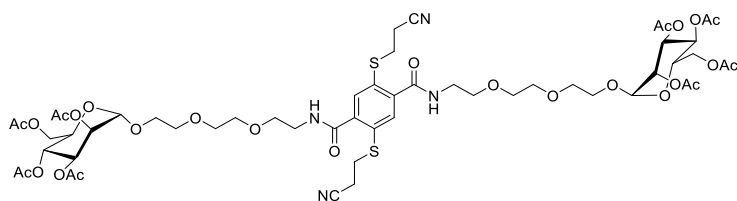
<sup>1</sup>H NMR (300 MHz, CDCl<sub>3</sub>): 7.62 (s, 2H, H<sub>ar</sub>), 7.25 (br, 2H, NH), 5.33-5.26 (m, 2H), 5.22 (m, 2H), 5.09-5.00 (m, 4H), 4.17 (q, *J* = 6.6 Hz, 2H, H<sub>5</sub>), 3.75-3.67 (m, 2H, CH<sub>2</sub>OFuc), 3.67-3.55 (m, 22H, CH<sub>2</sub>OFuc + 4×OCH<sub>2</sub> + NHCH<sub>2</sub>), 3.14 (t, *J* = 7.0 Hz, 4H, SCH<sub>2</sub>), 2.64 (t, *J* = 7.0 Hz, 4H, CH<sub>2</sub>CN), 2.12; 2.01; 1.92 (3×6H, COCH<sub>3</sub>), 1.08 (d, *J* = 6.6 Hz, H<sub>6</sub>).

<sup>13</sup>C NMR (75 MHz, CDCl<sub>3</sub>): 170.7; 170.5; 170.3 (3×COCH<sub>3</sub>), 166.7 (CONH), 140.3 (CCONH), 132.0 (CH<sub>ar</sub>), 131.7 (CS), 118.1 (CN), 96.2 (C<sub>1</sub>), 71.2 (C<sub>4</sub>), 70.7; 70.4; 70.1; 69.6 (4×OCH<sub>2</sub>), 68.2 (C<sub>2</sub> or C<sub>3</sub>), 68.0 (C<sub>2</sub> or C<sub>3</sub>), 67.3 (CH<sub>2</sub>OFuc), 64.4 (C<sub>5</sub>), 40.0 (NHCH<sub>2</sub>), 30.2 (SCH<sub>2</sub>), 20.9; 20.76; 20.70 (3×COCH<sub>3</sub>), 18.2 (CH<sub>2</sub>CN), 15.9 (C<sub>6</sub>).

HR-ESI-MS (positive mode) *m/z* : calcd. for C<sub>50</sub>H<sub>71</sub>N<sub>4</sub>O<sub>22</sub>S<sub>2</sub> [M+H]<sup>+</sup> = 785.2835, found 785.2831.



**2,5-Di[(2-cyanoethyl)thio]-*N,N*-di[3,6-dioxo-8-(2,3,4,6-tetra-*O*-acetyl- $\alpha$ -D-mannopyranosyloxy)-oct-1-yl]terephthalamide (5-Man)**



Prepared according to the general procedure from diacid **2** (291 mg, 0.87 mmol, 1 eq.), HOBt monohydrate (354 mg, 2.31 mmol, 2.6 eq.), EDCI•HCl (400  $\mu$ L, 2.26 mmol, 2.6 eq.) in  $\text{CH}_2\text{Cl}_2$  (40 mL), *i*Pr<sub>2</sub>NEt (350  $\mu$ L, 2.01, 2.3 eq.)

and amine **4-Man** (1.398 g, 2.35 mmol, 2.7 eq.) in  $\text{CH}_2\text{Cl}_2$  (35 mL) affording the desired product **5-Man** (598 mg, 55%) as a brown oil.

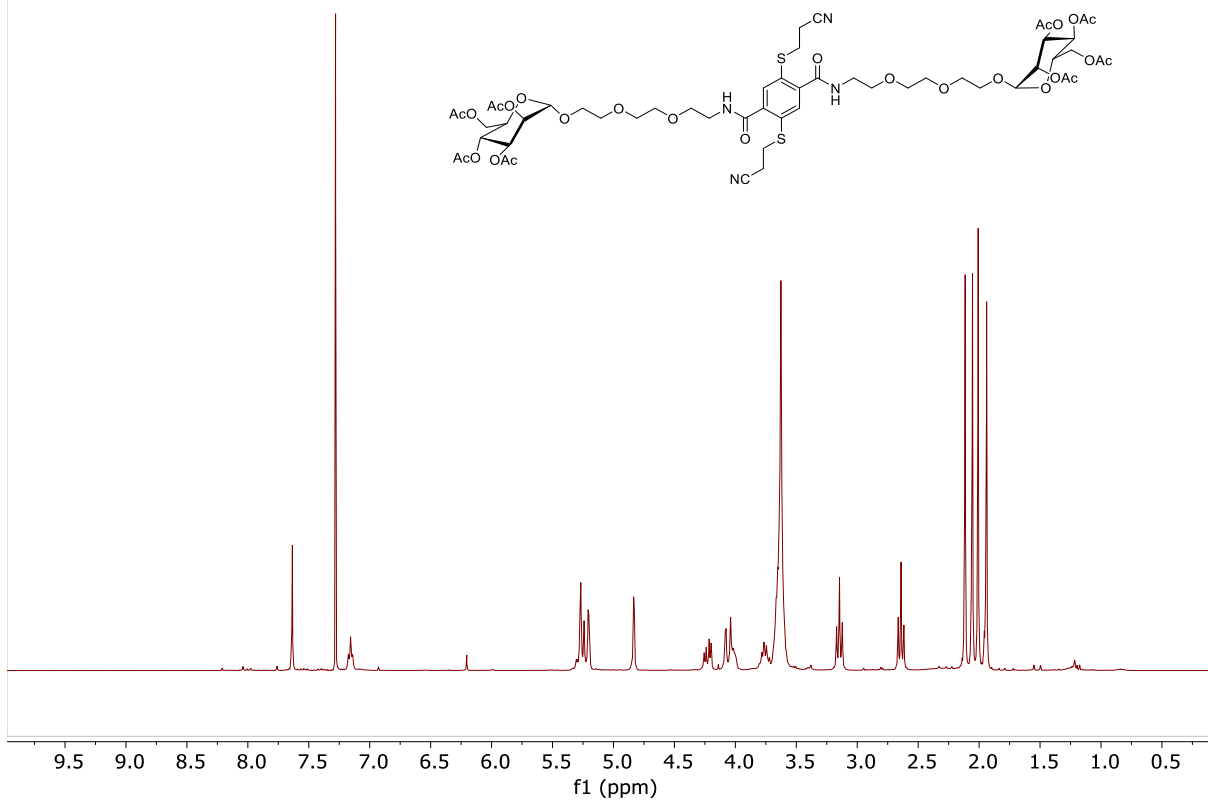
*R*<sub>f</sub> = 0.5 ( $\text{CHCl}_3/\text{MeOH}$ , 19:1)

<sup>1</sup>H NMR (300 MHz,  $\text{CDCl}_3$ ): 7.67 (s, 2H,  $\text{CH}_{\text{ar}}$ ), 7.14 (br, 2H, NH), 5.33-5.25 (m, 4H,  $\text{H}_3 + \text{H}_4$ ), 5.22 (dd, *J* = 1.6; 3.0 Hz, 2H,  $\text{H}_2$ ), 4.85 (d, *J* = 1.6 Hz, 2H,  $\text{H}_1$ ), 4.25 (dd, *J* = 4.9; 12.1 Hz, 2H,  $\text{H}_6$ ), 4.10-3.95 (m, 4H,  $\text{H}_5 + \text{H}_6'$ ), 3.83-3.73 (m, 2H,  $\text{CH}_2\text{OMan}$ ), 3.73-3.59 (m, 22H,  $\text{CH}_2\text{OMan} + 4 \times \text{OCH}_2 + \text{NHCH}_2$ ), 3.17 (t, *J* = 7.0 Hz, 4H,  $\text{SCH}_2$ ), 2.66 (t, *J* = 7.0 Hz, 4H,  $\text{CH}_2\text{CN}$ ), 2.13; 2.07; 2.02; 1.96 (4 $\times$ 6H,  $\text{COCH}_3$ ).

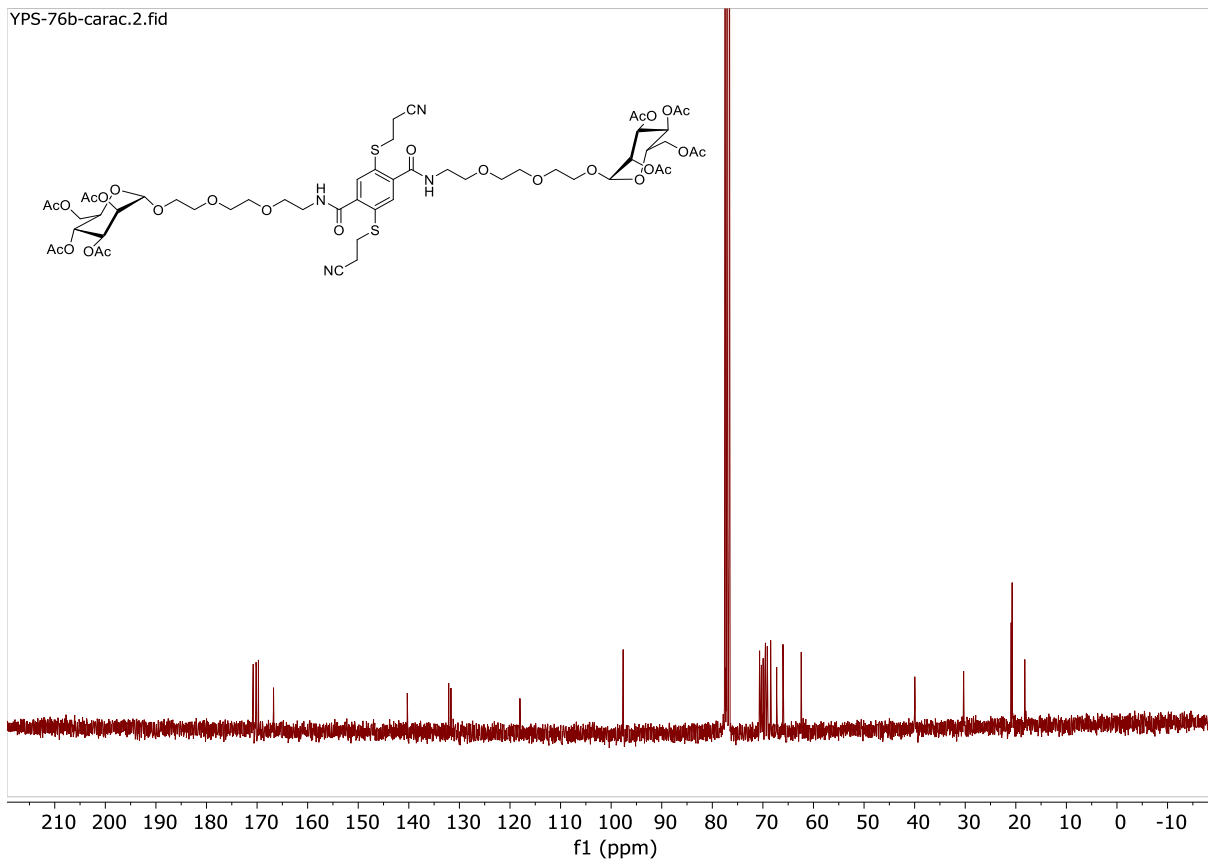
<sup>13</sup>C NMR (75 MHz,  $\text{CDCl}_3$ ): 170.8; 170.3; 170.2; 169.8 (4 $\times$ C,  $\text{COCH}_3$ ), 166.8 (CONH), 140.4 (CCONH), 132.2 ( $\text{CH}_{\text{ar}}$ ), 131.7 (CS), 118.1 (CN), 97.7 ( $\text{C}_1$ ), 70.7; 70.4; 70.0; 69.7 (4 $\times$ C,  $\text{OCH}_2$ ), 69.6 ( $\text{C}_2$ ), 69.2 ( $\text{C}_3$  or  $\text{C}_4$ ), 68.5 ( $\text{C}_5$ ), 67.3 ( $\text{CH}_2\text{OMan}$ ), 66.1 ( $\text{C}_3$  or  $\text{C}_4$ ), 62.5 ( $\text{C}_6$ ), 40.0 ( $\text{NHCH}_2$ ), 30.4 ( $\text{SCH}_2$ ), 21.0; 20.88; 20.84; 20.82 (4 $\times$ C,  $\text{COCH}_3$ ), 18.3 ( $\text{CH}_2\text{CN}$ ).

HR-ESI-MS (positive mode) *m/z*: calcd. for  $\text{C}_{54}\text{H}_{74}\text{N}_4\text{NaO}_{26}\text{S}_2$  [ $\text{M}+\text{Na}$ ]<sup>+</sup> = 1281.3925, found 1281.3927.

YPSi-18a.1.fid



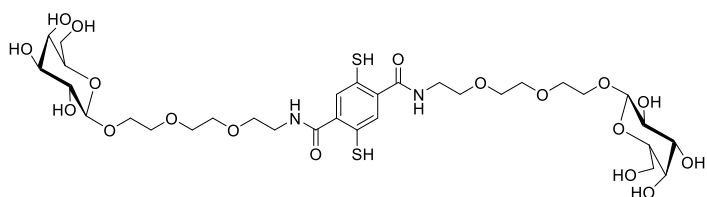
YPS-76b-carac.2.fid



## General procedure for deprotection of 2-cyanoethyl and acetate

Protected 1,4-dithiophenol **5** (1 eq.) and CsOH•H<sub>2</sub>O (20 eq.) were dissolved in degassed THF/MeOH (1:1, 10 mL) under inert atmosphere. The mixture was stirred at r.t. for 3 h then HCl 2 N was carefully added until pH 4. Solvent was evaporated. The residue was purified by a 4 g C18 silica gel column chromatography (Gradient: 4 CV 100% H<sub>2</sub>O + 0.25 % TFA, 10 CV 100 % MeOH + 0.25 % TFA, 4 CV 100 % MeOH + 0.25 % TFA, 4 CV 100 % H<sub>2</sub>O + 0.25% TFA). Methanol was removed via a rotary evaporator and the remaining water was removed using a freeze-dryer affording the desired unprotected product **6**.

## 2,5-Mercapto-*N,N*-di[3,6-dioxa-8-(β-D-galactopyranosyloxy)-oct-1-yl]terephthalamide (**6-Gal**)



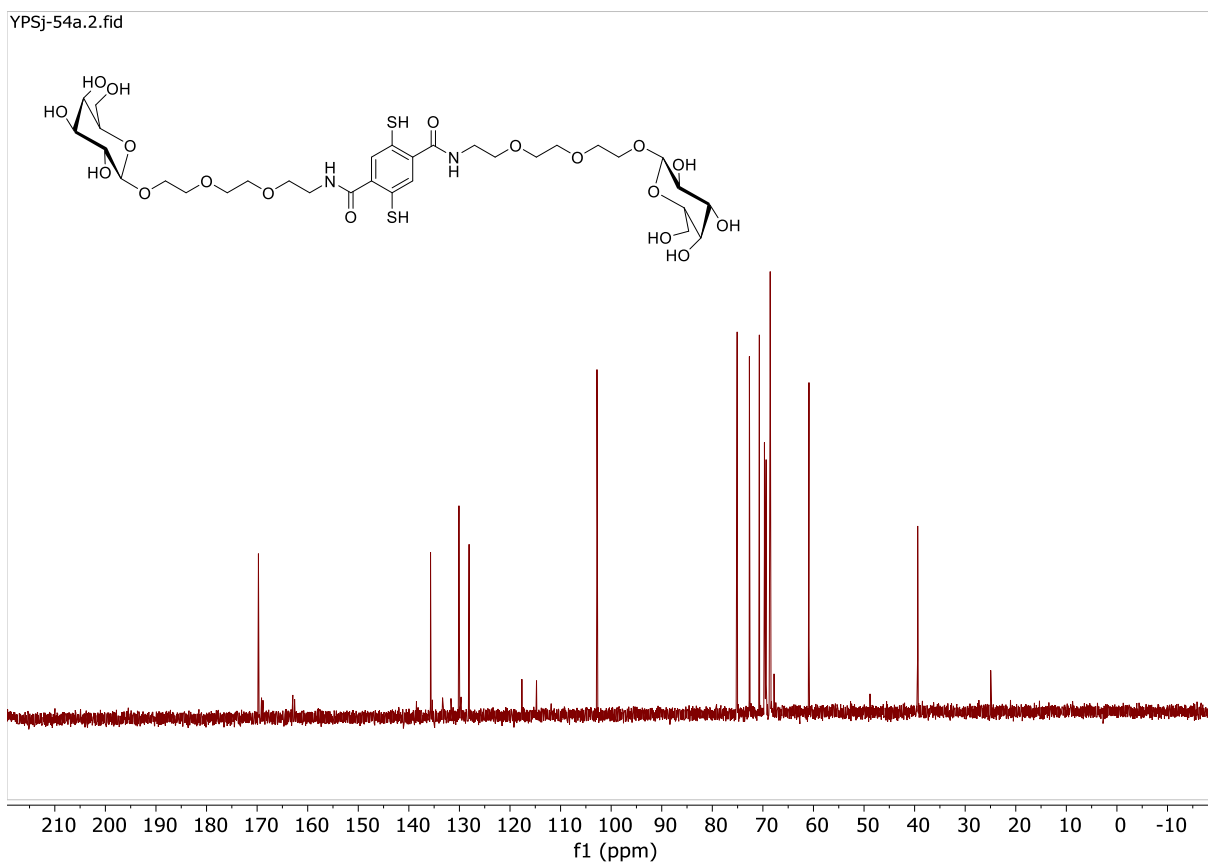
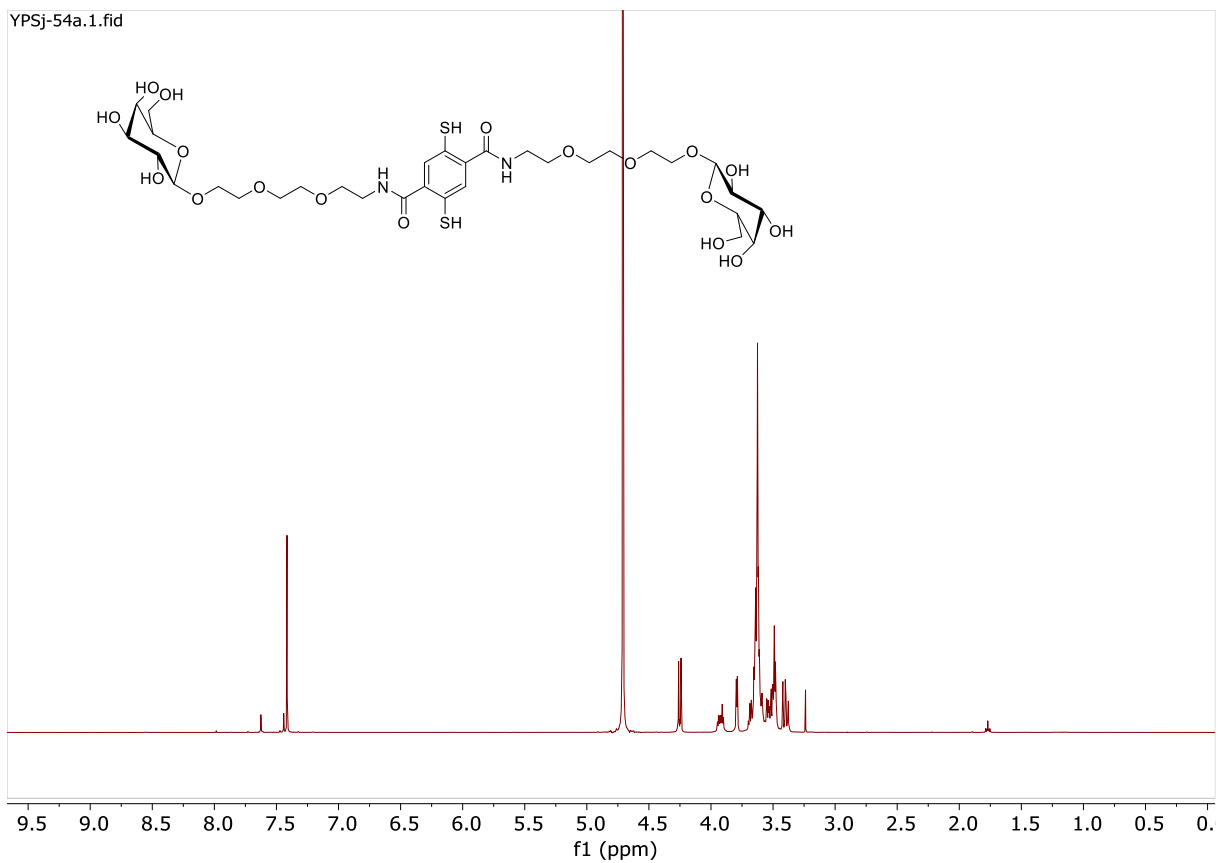
Prepared according to the general procedure from compound **5-Gal** (360 mg, 0.286 mmol, 1 eq.) and CsOH•H<sub>2</sub>O (868 mg, 2.47 mmol, 8.6 eq.) in THF/MeOH (1:1, 30 mL) affording the

desired 1,4-dithiophenol **6-Gal** (189 mg, 80%) as a white foam.

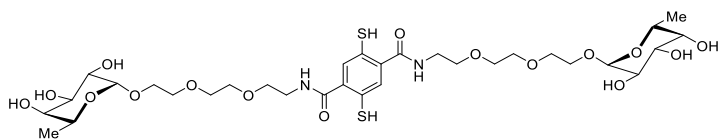
<sup>1</sup>H NMR (400 MHz, D<sub>2</sub>O + εTFA): 7.50 (s, 2H, CH<sub>ar</sub>), 4.33 (d, *J* = 7.8 Hz, 2H, H<sub>1</sub>), 4.05-3.97 (m, 2H, CH<sub>2</sub>OGal), 3.87 (d, *J* = 3.5 Hz, 2H, H<sub>4</sub>), 3.80-3.64 (m, 22 H), 3.63-3.55 (m, 8H), 3.47 (dd, *J* = 7.8; 9.9 Hz, 2H, H<sub>2</sub>).

<sup>13</sup>C NMR (100 MHz, D<sub>2</sub>O + εTFA): 169.7 (CONH), 135.7 (CCONH), 130.0 (CH<sub>ar</sub>), 128.0 (CS), 102.8 (C<sub>1</sub>), 75.0; 72.6; 70.7; 68.5 (4×C, C<sub>2</sub> or C<sub>3</sub> or C<sub>4</sub> or C<sub>5</sub>), 69.69; 69.60; 69.3; 68.6; 68.5 (5×C, CH<sub>2</sub>), 60.8 (C<sub>6</sub>), 39.3 (NHCH<sub>2</sub>).

HR-ESI-MS (positive mode) *m/z* : calcd. for C<sub>32</sub>H<sub>52</sub>N<sub>2</sub>NaO<sub>18</sub>S<sub>2</sub> [M+Na]<sup>+</sup> = 839.2549, found 839.2552.



## 2,5-Mercapto-*N,N*-di[3,6-dioxa-8-( $\alpha$ -L-fucopyranosyloxy)-oct-1-yl]terephthalamide (**6-Fuc**)



Prepared according to the general procedure from compound **5-Fuc** (115 mg, 0.1 mmol, 1 eq.) and CsOH•H<sub>2</sub>O (311 mg, 1.85 mmol, 18.5 eq.) in

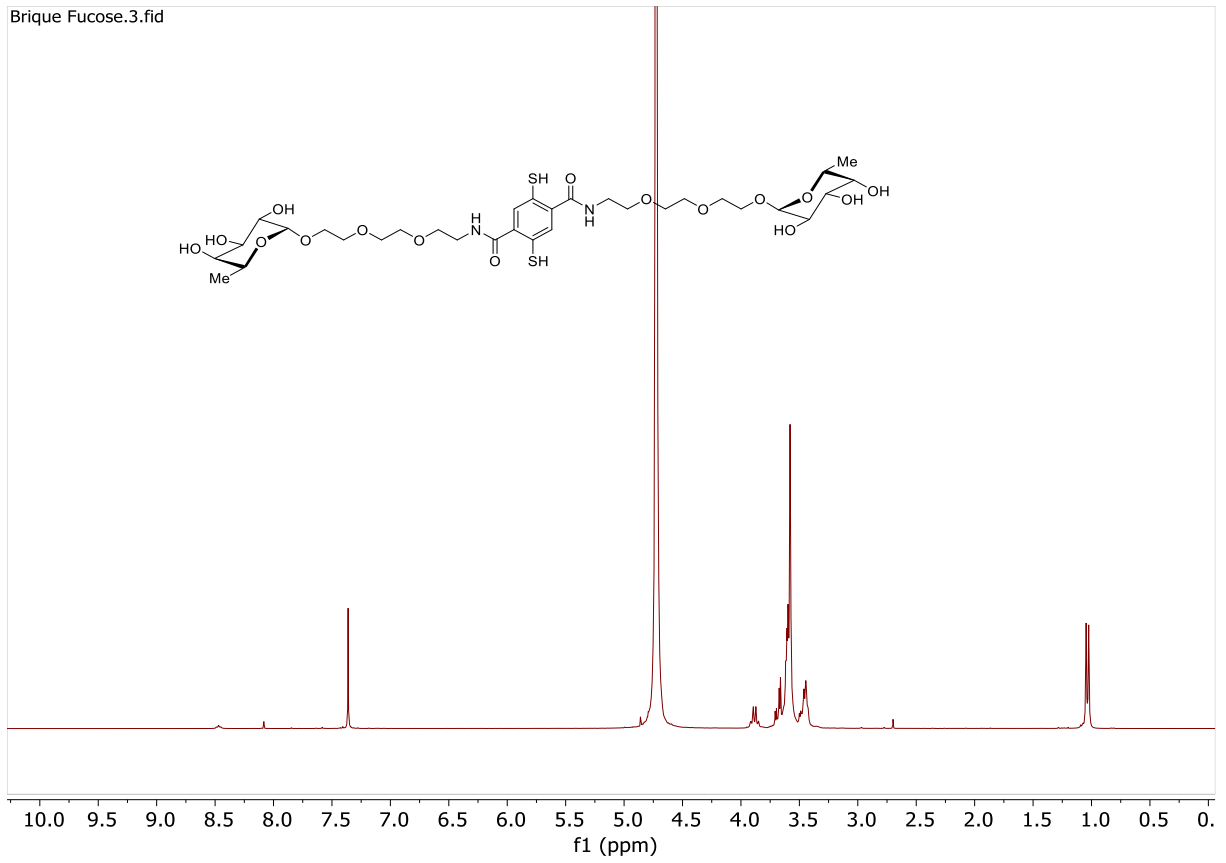
THF/MeOH (1:1, 9 mL) affording the desired 1,4-dithiophenol **6-Fuc** (54 mg, 68%).

<sup>1</sup>H NMR (400 MHz, D<sub>2</sub>O +  $\epsilon$ TFA): 7.50 (s, 2H, CH<sub>ar</sub>), 4.84 (d, *J* = 3.9 Hz, 2H, H<sub>1</sub>), 4.0-2 (q, *J* = 6.6 Hz, 2H, H<sub>5</sub>), 3.82-3.64 (m, 24 H, H<sub>2</sub> + H<sub>3</sub> + H<sub>4</sub> + CH<sub>2</sub>OFuc + 4×CH<sub>2</sub>O), 3.64-3.53 (m, 6H, CH<sub>2</sub>OFuc + NHCH<sub>2</sub>), 1.16 (d, *J* = 6.6 Hz, 6H, H<sub>6</sub>).

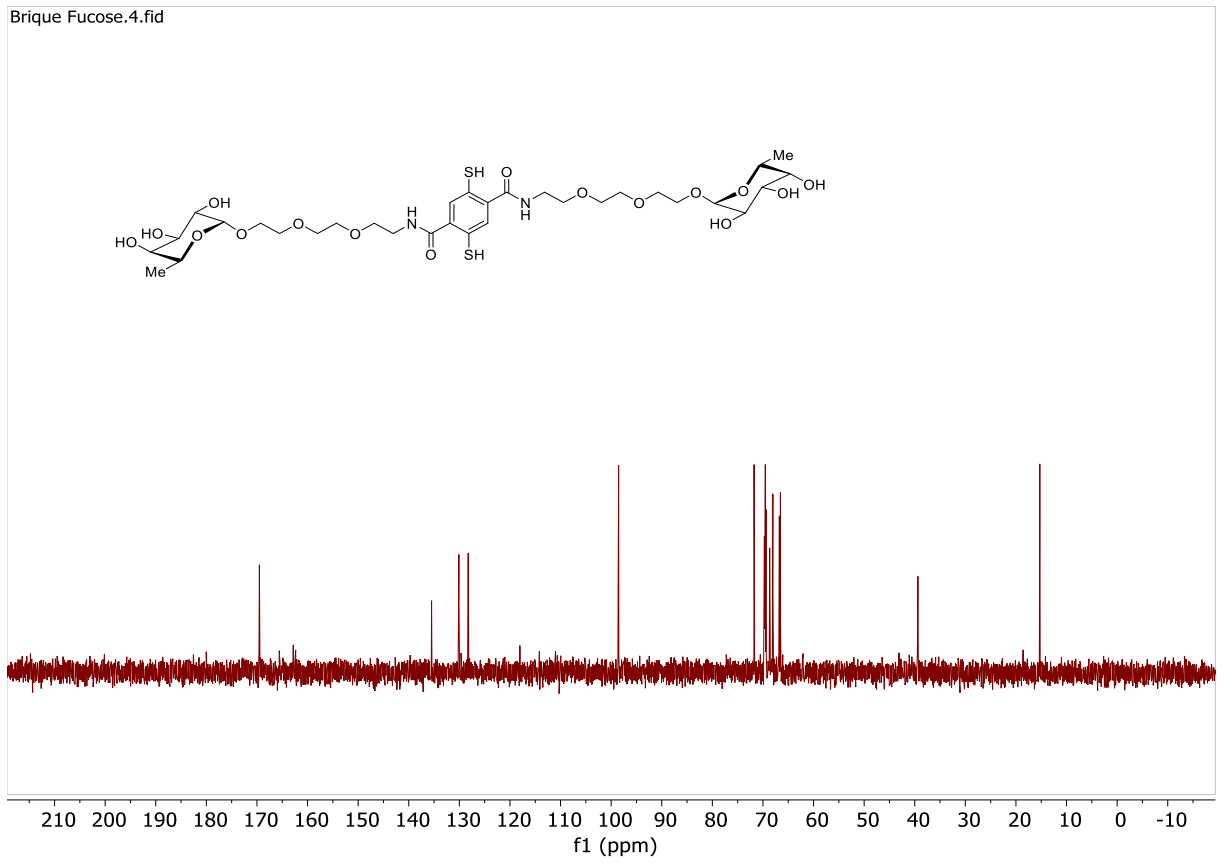
<sup>13</sup>C NMR (100 MHz, D<sub>2</sub>O +  $\epsilon$ TFA): 169.7 (CONH), 135.7 (CCONH), 130.1 (CH<sub>ar</sub>), 128.2 (CS), 98.6 (C<sub>1</sub>), 71.8; 69.5; 68.0 (C<sub>2</sub> or C<sub>3</sub> or C<sub>4</sub>), 69.7; 69.6; 69.4; 68.7 (4×CH<sub>2</sub>O), 66.8 (CH<sub>2</sub>OFuc), 66.6 (C<sub>5</sub>), 39.3 (NHCH<sub>2</sub>), 15.3 (C<sub>6</sub>).

HR-ESI-MS (positive mode) *m/z*: calcd. for C<sub>32</sub>H<sub>53</sub>N<sub>2</sub>O<sub>16</sub>S<sub>2</sub> [M+H]<sup>+</sup> = 785.2831, found 785.2835.

Brique Fucose.3.fid

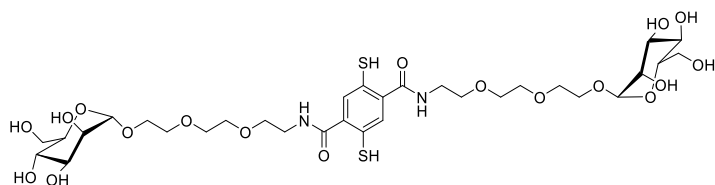


Brique Fucose.4.fid





## 2,5-Mercapto-*N,N*-di[3,6-dioxa-8-( $\alpha$ -D-mannopyranosyloxy)-oct-1-yl]terephthalamide (**6-Man**)



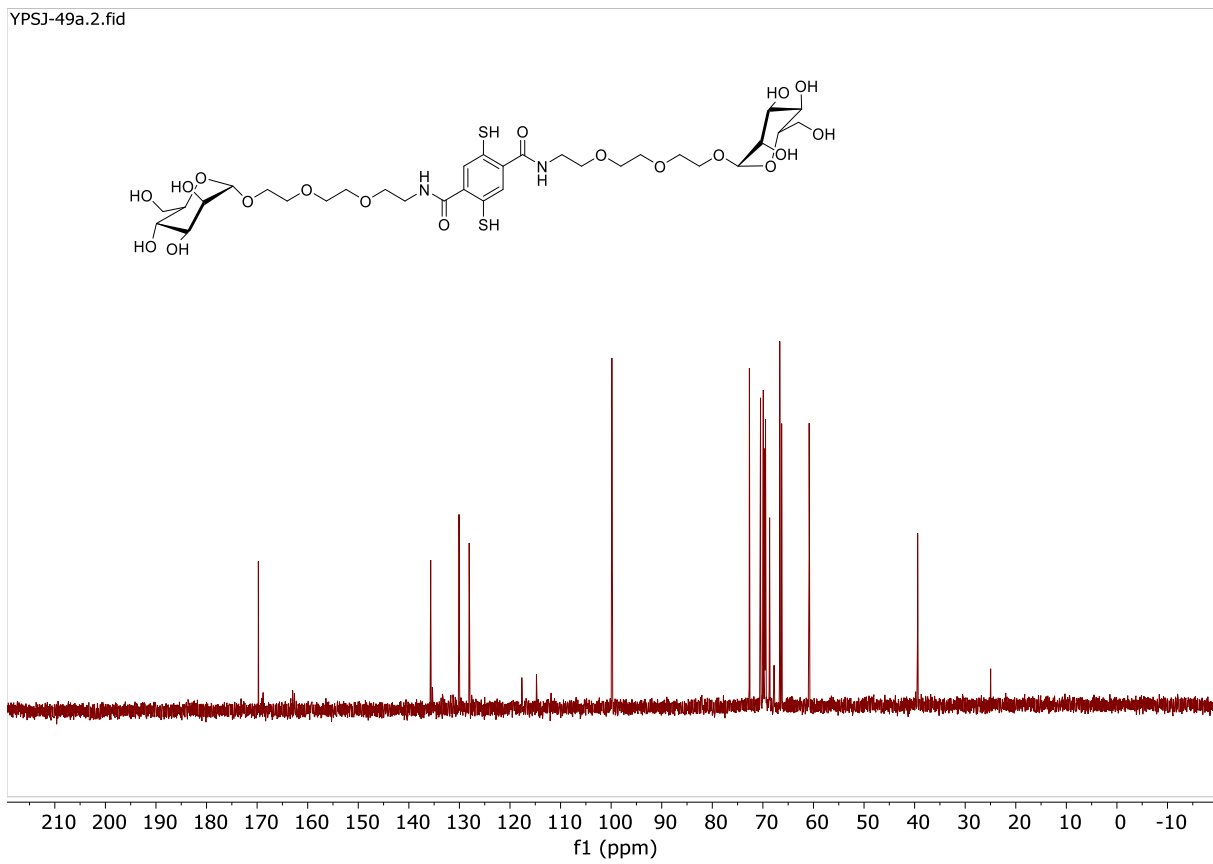
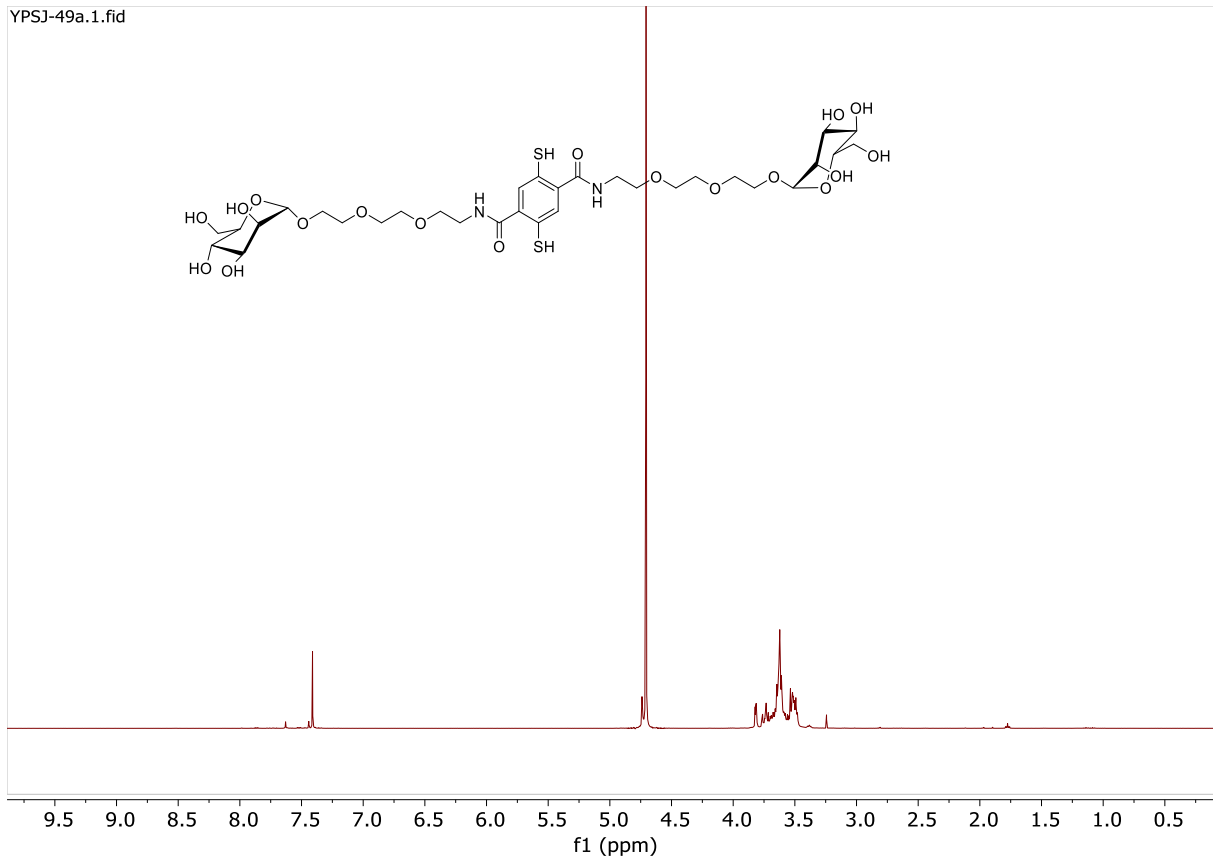
Prepared according to the general procedure from compound **5-Man** (58 mg, 0.046 mmol, 1 eq.) and CsOH•H<sub>2</sub>O (157 mg, 0.935 mmol, 18.5 eq.) in THF/MeOH (1:1, 6 mL) affording the desired 1,4-dithiophenol **6-Man** (25 mg,

67%) as a white foam.

<sup>1</sup>H NMR (400 MHz, D<sub>2</sub>O +  $\epsilon$ TFA): 7.94 (s, 2H, CH<sub>ar</sub>), 4.82 (d, *J* = 1.7 Hz, 2H, H<sub>1</sub>), 3.90 (dd, *J* = 1.7 Hz, 2H, H<sub>2</sub>), 3.87-3.53 (m, 34 H).

<sup>13</sup>C NMR (100 MHz, D<sub>2</sub>O +  $\epsilon$ TFA): 169.7 (CONH), 135.6 (CCONH), 130.0 (CH<sub>ar</sub>), 128.0 (CS), 99.8 (C<sub>1</sub>), 72.6; 70.4; 69.9; 66.6 (4×C, C<sub>1</sub> or C<sub>2</sub> or C<sub>3</sub> or C<sub>4</sub>), 69.6; 69.47; 69.44; 68.6; 66.2 (5×C, OCH<sub>2</sub>), 60.8 (C<sub>6</sub>), 39.4 (CH<sub>2</sub>NH).

HR-ESI-MS (positive mode) *m/z* : calcd. for C<sub>32</sub>H<sub>52</sub>N<sub>2</sub>NaO<sub>18</sub>S<sub>2</sub> [M+Na]<sup>+</sup> = 839.2549, found 839.2552.



## Equilibration and purification of glycosylated dyn[3,4]arenes **M<sub>3</sub>/M<sub>4</sub>, G<sub>3</sub>/G<sub>4</sub> and F<sub>3</sub>/F<sub>4</sub>**

1,4-Dithiophenol **6** (100 mg, 4 mM) was dissolved in Tris buffer (Tris 200 mM, NaCl<sub>2</sub> 100 mM, CaCl<sub>2</sub> 100 μM) and was equilibrated at RT with stirring in a closed vial during 48 to 72 h. Progress of the reaction was monitored by UHPLC. The equilibrated DCL was then freeze-dried and the crude product was purified by reversed phase silica gel column chromatography (40-g C18 cartridge, Gradient: 4 CV 100% H<sub>2</sub>O + 0.1% TFA, 15 CV to increase from 0 to 100% MeOH + 0.1% TFA, 4 CV 100% MeOH + 0.1% TFA). The fractions of the column were analysed one-by-one by UHPLC and combined accordingly. Methanol was evaporated off with the heating bath set at a maximum of 25°C. The remaining water was removed using a freeze-dryer affording the desired glycosylated dyn[3,4]arenes.

### **Preparation of M<sub>3</sub>/M<sub>4</sub>**

Prepared according the general procedure from **6-Man** (151 mg, 4 mM) and affording **M<sub>3</sub>/M<sub>4</sub>** (63 mg, 42%) as a slightly yellow powder.

### **Preparation of G<sub>3</sub>/G<sub>4</sub>**

Prepared according the general procedure from **6-Gal** (236 mg, 4 mM) and affording **G<sub>3</sub>/G<sub>4</sub>** (70 mg, 30%) as a slightly yellow powder.

### **Preparation of F<sub>3</sub>/F<sub>4</sub>**

Prepared according the general procedure from **6-Fuc** (316 mg, 4 mM) and affording **F<sub>3</sub>/F<sub>4</sub>** (238 mg, 75%) as a very slightly yellow powder.

## Dynamic combinatorial libraries

### General procedure for the preparation of DCLs without lectin

In a typical experiment, the 1,4-dithiophenols (4 mM overall) were dissolved in TRIS buffer (200 mM, NaCl 100 mM, CaCl<sub>2</sub> 100 μM, pH 7.4). The mixture was allowed to equilibrate by stirring (400 rpm) in an open vial at r.t. The reaction was monitored by HPLC by injection of 4 μL of the DCL solution. UV absorbance was recorded at 210 and 254 nm.

### General procedure for the preparation of DCLs without multiple lectins:

In a typical experiment, 1,4-dithiophenols **6** (4 mM overall) were suspended in TRIS buffer (200 mM, NaCl 100 mM, CaCl<sub>2</sub> 100 μM, pH 7.4). The mixture was equilibrated by stirring in an open vial at room temperature (Figure S8). After 24 h, four DCLs were prepared in open vials. In the first one (Ref), the original DCL was diluted 10 times with buffer solution affording a library composed of 1,4-thiophenols (0.4 mM overall). The other ones were diluted ten times with buffer and lectin (LecA, LecB or AFL) was added resulting in a library composed of 1,4-dithiophenols **6** (0.4 mM overall) and lectin (0.4 mM). After 24 h, the Ref DCL was diluted 2× with 1M HCl and analyzed by UHPLC (**Sample 1**) by injection of 25 μL of the sample. Meanwhile, the DCLs were centrifuged (2 min, 10 000 rpm). The supernatants were collected and diluted 2× with 1M HCl and analyzed by HPLC (**Sample 2**, **Sample 4** and **Sample 6**) by injection of 25 μL of the sample. The precipitates were diluted in buffer and 1M HCl (1:1 v/v) to afford the same volume as the Ref DCL and analyzed by HPLC (**Sample 3**, **Sample 5** and **Sample 7**) by injection of 25 μL of the sample.

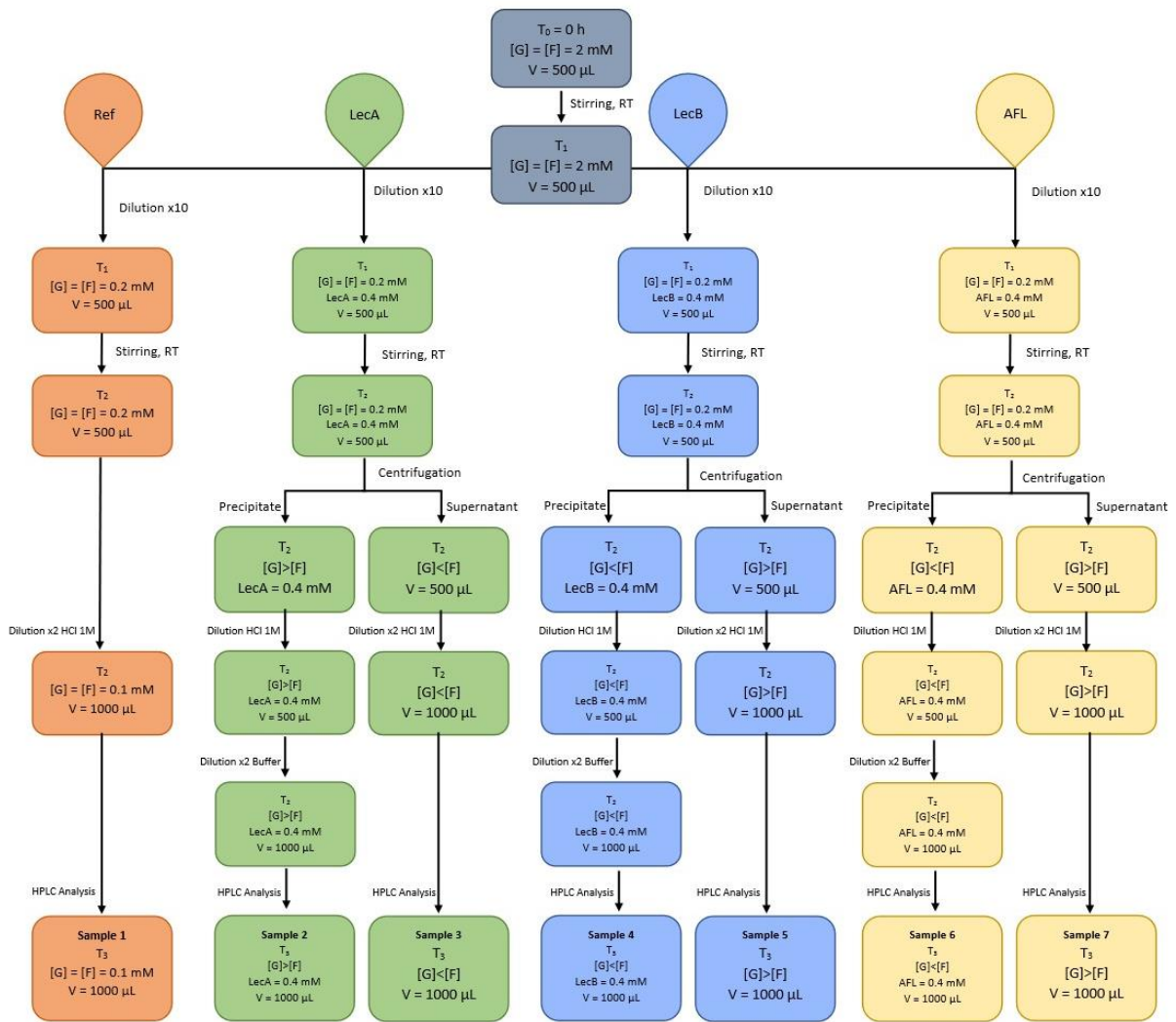


**Figure S8.** Protocol for DCL of G/F with and without lectin: reference (orange), LecA (green), LecB (blue) and AFL (yellow)

## Isothermal Titration Calorimetry (raw data)

ITC experiments were performed with a microcal calorimeter Malvern ITC200. Temperature was set to 298 K. In every experiment, the host solution is at concentration [Host] in a Tris buffer (200 mM, NaCl 100 mM, CaCl<sub>2</sub> 100 μM, pH 7.4) and placed in the cell (200 μL), while the guest at the concentration [Guest] and is placed in the syringe (40 μL). Then, successive aliquots of guest solution were added thanks to a computer-automated injector with 2 min intervals. Heat changes were recorded after each addition. The first injection was discarded from each dataset to remove effect of guest diffusion across the syringe tip during the equilibration process. For the following tables, thermodynamic parameters were obtained from binding model of the MicroCal ITC Origin software. n is for stoichiometry. Raw data are converted from kcal to kJ applying a factor of 4.184.

### ConA vs M<sub>3</sub>/M<sub>4</sub>

**Table S2.** ITC data for the binding properties of M<sub>3</sub>/M<sub>4</sub> towards ConA

	[ConA] mM	[M <sub>3</sub> /M <sub>4</sub> ] mM	n	Kd (nM)	ΔH	-TΔS	ΔG
					(kJ/mol)	(kJ/mol)	(kJ/mol)
ConA vs M <sub>3</sub> /M <sub>4</sub> #1	0.12	0.2	0.09	250	-123	7.2	-37.6
ConA vs M <sub>3</sub> /M <sub>4</sub> #2	0.12	0.2	0.06 6	279	-70.6	2.8	-37.4
ConA vs M <sub>3</sub> /M <sub>4</sub> #3	0.12	0.2	0.11 2	250	-110	6.1	-37.6
ConA vs M <sub>3</sub> /M <sub>4</sub> #4	0.12	0.2	0.11 2	397	-122.6	7.2	-36.5
Average			0.09	294	-106.6	5.8	-37.3

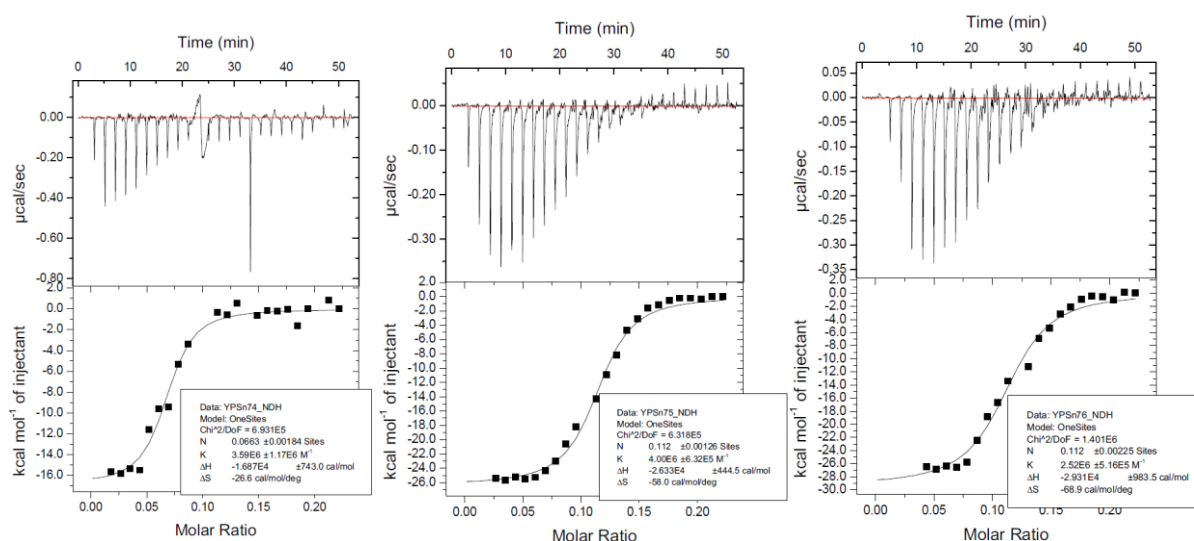


**Figure S9.** Isothermal titration microcalorimetry (ITC) analysis of the binding properties toward ConA (0.12 mM) for M<sub>3</sub>/M<sub>4</sub> (0.2 mM, top panels) and the association titration curve obtained with a 1:1 binding model (bottom panels).

## LecA vs G<sub>3</sub>/G<sub>4</sub>

**Table S3.** ITC data for the binding properties of G<sub>3</sub>/G<sub>4</sub> towards LecA

	[LecA] mM	[G <sub>3</sub> /G <sub>4</sub> ] mM	n	Kd (nM)	ΔH	-TΔS	ΔG
					(kJ/mol)	(kJ/mol)	(kJ/mol)
LecA vs G <sub>3</sub> /G <sub>4</sub> #1	0.049	0.4	0.12	214	-167	129	-38.1
LecA vs G <sub>3</sub> /G <sub>4</sub> #2	0.049	0.4	0.08	174	-150	111	-38.6
LecA vs G <sub>3</sub> /G <sub>4</sub> #3	0.049	0.4	0.10	168	-158	119	-38.7
Average			0.10	185	-158.3	119.7	-38.5

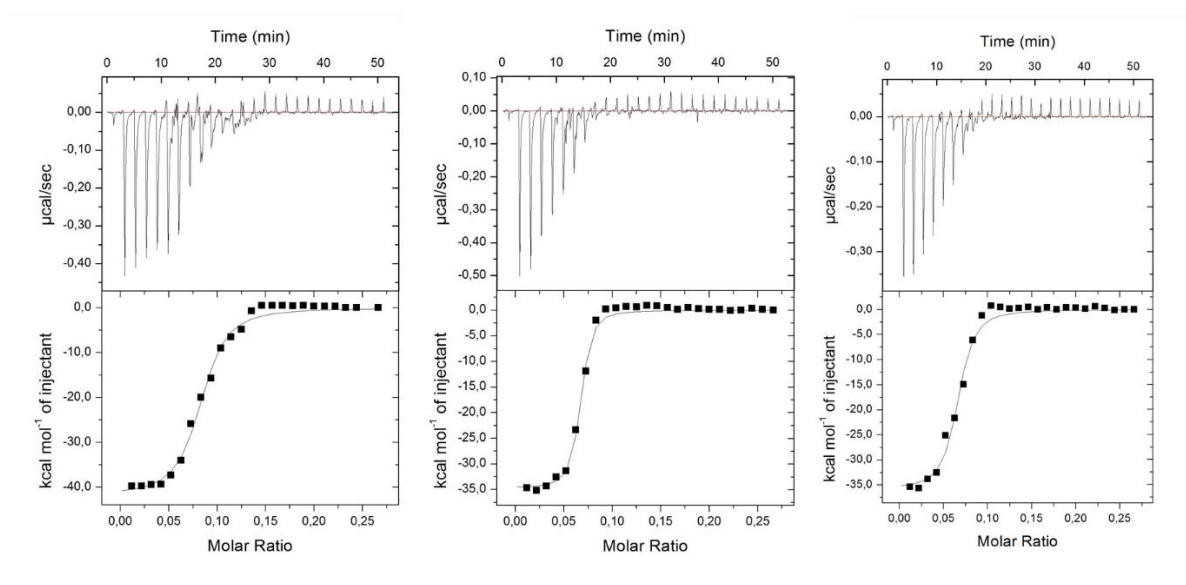


**Figure S10.** Isothermal titration microcalorimetry (ITC) analysis of the binding properties toward LecA (0.049 mM) for G<sub>3</sub>/G<sub>4</sub> (0.4 mM, top panels) and the association titration curve obtained with a 1:1 binding model (bottom panels).

## LecB vs F<sub>3</sub>/F<sub>4</sub>

**Table S4.** ITC data for the binding properties of F<sub>3</sub>/F<sub>4</sub> towards LecB

	[LecB] mM	[F <sub>3</sub> /F <sub>4</sub> ] mM	n	Kd (nM)	ΔH	-TΔS	ΔG
					(kJ/mol)	(kJ/mol)	(kJ/mol)
LecB vs F <sub>3</sub> /F <sub>4</sub> #1	0.0829	0.145	0.12	8	-218.6	-172.0	-46.3
LecB vs F <sub>3</sub> /F <sub>4</sub> #2	0.0829	0.145	0.10	155	-230.8	-192.0	-38.8
LecB vs F <sub>3</sub> /F <sub>4</sub> #3	0.0829	0.145	0.08	108	-227.8	-188.3	-39.7
Average			0.10	90	-225.8	-184.1	-41.6

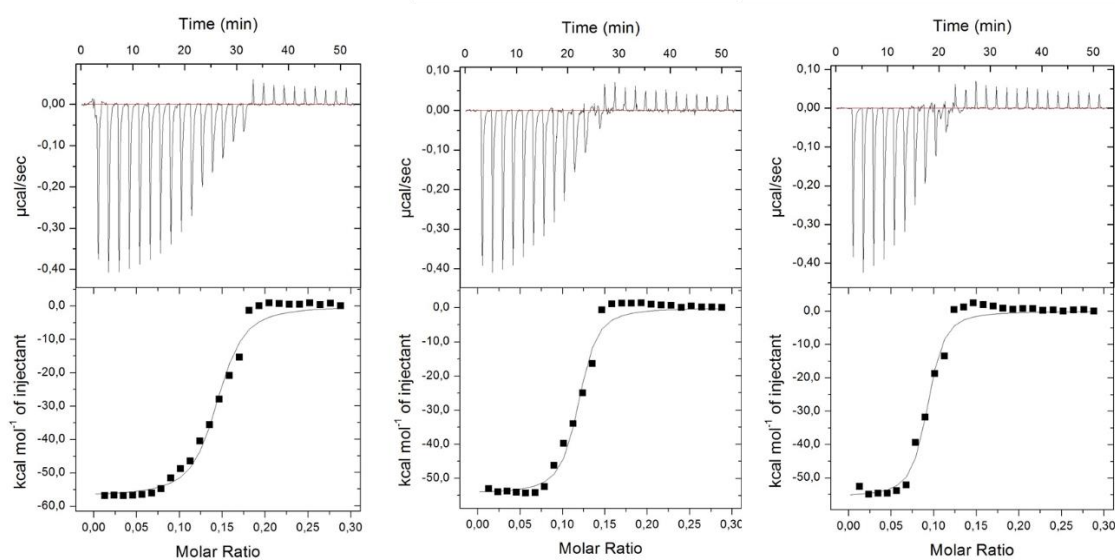


**Figure S11.** Isothermal titration microcalorimetry (ITC) analysis of the binding properties toward LecB (0.0829 mM) for F<sub>3</sub>/F<sub>4</sub> (0.145 mM, top panels) and the association titration curve obtained with a 1:1 binding model (bottom panels).



## AFL vs $\alpha$ FucOMe

**Table S5.** ITC data for the binding properties of  $\alpha$ FucOMe towards AFL

	[AFL] mM	[ $\alpha$ FucOMe] mM	n	Kd (nM)	$\Delta$ H	$-T\Delta$ S	$\Delta$ G
					(kJ/mol)	(kJ/mol)	(kJ/mol)
AFL vs $\alpha$ FucOMe	0.05	3.00	2.98	40300	-32.8	7.7	-25.1

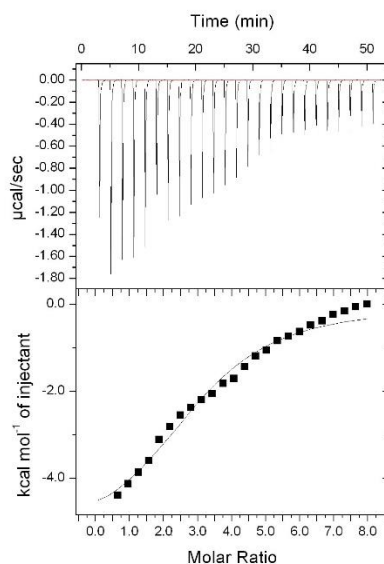


**Figure S12.** Isothermal titration microcalorimetry (ITC) analysis of the binding properties toward AFL (0.05 mM) for  $\alpha$ FucOMe (3 mM, top panel) and the association titration curve obtained with a 1:1 binding model (bottom panel).

## AFL vs F<sub>3</sub>/F<sub>4</sub>

**Table S6.** ITC data for the binding properties of F<sub>3</sub>/F<sub>4</sub> towards AFL

	[AFL] mM	[F <sub>3</sub> /F <sub>4</sub> ] mM	n	Kd (nM)	ΔH	-TΔS	ΔG
					(kJ/mol)	(kJ/mol)	(kJ/mol)
AFL vs F <sub>3</sub> /F <sub>4</sub> #1	0.01	0.023	0.08	30	-335.0	292	-43.0
AFL vs F <sub>3</sub> /F <sub>4</sub> #2	0.02	0.076	0.14	46	-335.0	293	-41.9
Average			0.11	38	-335.0	292.5	-42.4

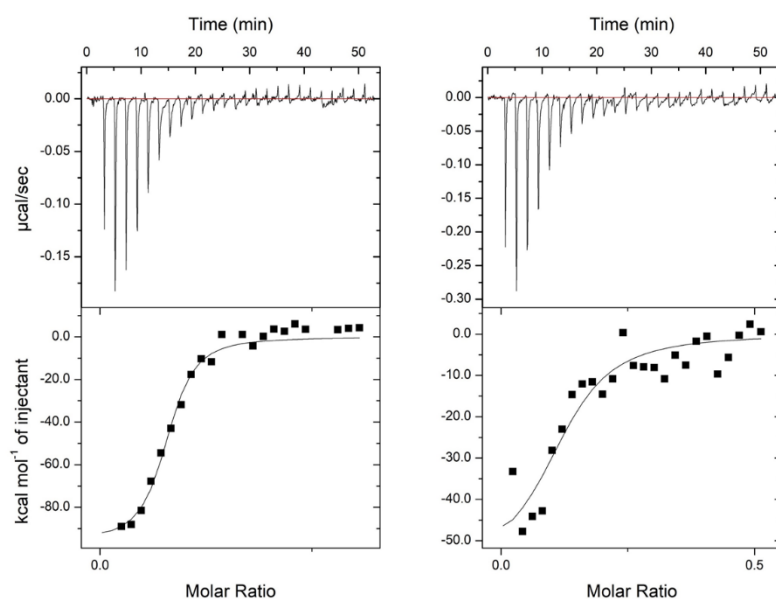


**Figure S13.** Isothermal titration microcalorimetry (ITC) analysis of the binding properties toward AFL (0.01 mM) for F<sub>3</sub>/F<sub>4</sub> (0.023 and 0.076 mM, top panels) and the association titration curve obtained with a 1:1 binding model (bottom panels).

## Toxicity assays on PAO1

*P. aeruginosa* strain PAO1 (the main strain model used in virulence analyses) was grown in Luria-Bertani Broth overnight at 37°C with an orbital shaker. Growing cells at OD<sub>600</sub> of 0.3 – 0.6 (beginning of the exponential growth phase) were washed three times with a PBS solution (pH 7.3), and used in the following assays.

These *P. aeruginosa* cells were swabbed over the surface of Muller-Hinton II agar plates and exposed to dynarene concentrations ranging from 100 µM to 10 mM (using 10 µL solutions spotted over the growing cells). These plated cells did not show any inhibition zones due to exposure to these dynarene spotted concentrations.

Live-Dead assays monitoring dead cells (permeable to propidium iodide - PI) in PBS: *P. aeruginosa* cells exposed to the dynarene glycoclusters generated in this study further confirmed this absence of toxicity over more than 4 h incubation time.

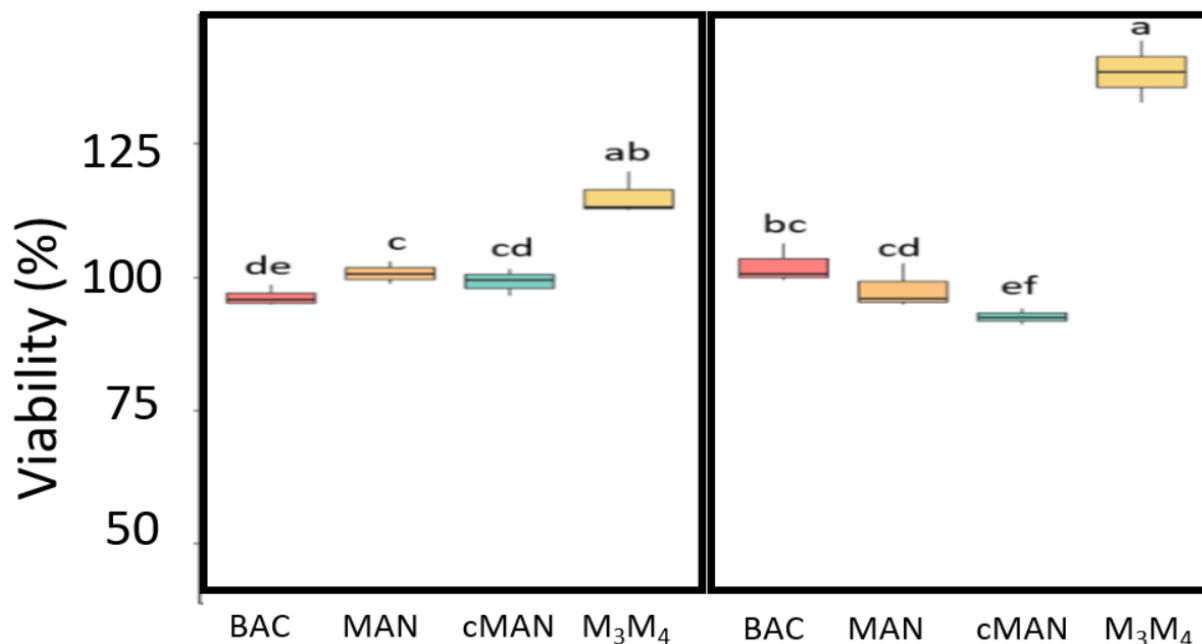


**Figure S14.** Boxplot analysis of the relation between the relative viability of *P. aeruginosa* PAO1 cell suspensions exposed to mannosylated glycoconjugates (BAC = PAO1 alone, MAN = methyl  $\alpha$ -D-mannopyranoside, cMAN = mannosylated calixarene-based glycoclusters, see Figure S1). The G/R ratios obtained from TECAN fluorescence microplate monitoring after 15 min, 1 h, 4 h and 24 h. Samples were prepared and stained as indicated in the LIVE/DEAD® BacLight™ Bacterial Viability Kits. The integrated intensities of the green ( $535 \pm 25$  nm) and red ( $620 \pm 10$  nm) emission of suspensions excited at  $485 \pm 20$  nm were acquired, and the green/red fluorescence ratios (RatioG/R) were calculated for each proportion of live/dead *P. aeruginosa* cells. Each point represents the mean of twelve measurements replicated three times using independent bacterial broths. Boxplots with distinct letter codes showed significant differences ( $p$ -values < 0.05 using Kruskal-Wallis (KW) Dunn tests)

## Toxicity on A549 epithelial cells

A549 Cell lines (ATCC, Massanas, VA, USA) used in the assays were grown in flasks with a culture media Dulbecco's Modified Eagle's Medium (DMEM) with 4.5 g/L glucose (HG), 10% (v/v) fetal calf serum (FCS) (DMEM-calf high glucose) and a 1% penicillin/streptomycin mixture (Sigma Aldrich, Saint-Quentin Fallavier, France). These flasks were incubated at 37°C with 5% (v/v) CO<sub>2</sub>. The cell culture growth media was changed every 2-3 days. A549 cells were treated with 0.05% (m/v) trypsin-EDTA (Thermo Fisher Scientific, New Hampshire, USA) and cells in suspension were counted using a Scepter cell counter (Merk Millipore), diluted in culture media then seeded into E96-microtiter plates.

Realtime cell analyses (RTCA) on A549 cell monolayers were performed after 48-72 h cell growth until at least 80% confluency. These cells were then exposed to PAO1 cells pre-treated during 15 min with 1 mM of **X<sub>3</sub>/X<sub>4</sub>** dynarene glycoclusters and diluted 10% in cell culture media without antibiotics (Multiplicity of infection MOI 10).

RTCA of A549 cell adhesion were performed with epithelial cells in suspension in culture media without antibiotics pre-incubated with 4.13 μM **X<sub>3</sub>/X<sub>4</sub>** dynarene glycoclusters or with PAO1 cells pre-treated during 15 min with 1 mM of **X<sub>3</sub>/X<sub>4</sub>** dynarene glycoclusters (MOI10) before loading onto microtiter plates.

RTCA were performed onto an xCELLigence SP station (ACEA Biosciences, San Diego, USA) using RTCA software 2.1. Data are expressed as Delta Cell Indexes (DCI). For each well the DCI at a given time is the difference between a reference DCI value (time of treatment t<sub>0</sub>) and the Cell index at Delta time (DCI<sub>ti</sub> = CI + (1- DCI<sub>ti-t0</sub>)). At the end of experiments, A549 cells were fixed with formalin 5% for cell imaging. Experiments were performed in Ibidi glass dishes (Cliniscience, Nanterre, France) for Nanolive (Nanolive SA, Lausanne, Switzerland) 3D-cell imaging and 96-wells plates for x4 imaging and automated cell counts using a Cytation 3 platform (Biotek Instruments Winooski, VT, USA). A549 cells were labeled with Dapi (10 ng/mL, Sigma Aldrich), Phalloïdin-TRITC 7.5 μM, (Sigma Aldrich) and/or Dihydrorhodamine-123 2.5 μg/mL (DHR, Applied Bioprobes, ThermoFisher Scientific) in PBS 0.1% Triton and washed twice in PBS before cell imaging.

## Aggregation bacterial cell assays

Multivalent **X<sub>3</sub>/X<sub>4</sub>** dynarenes (galactose, fucose et mannose) were dissolved in a PBS solution (25 mM stock solutions). PBS has an osmolarity of 315 mOs, and is physiologically compatible with living cells and proteins. *P. aeruginosa* cells and ligands were mixed (short vortexing and spinning) in order to obtain 100 μM to 1 mM final concentrations of **X<sub>3</sub>/X<sub>4</sub>** dynarenes at OD<sub>600</sub> of 1 (using exponential phase cells OD<sub>600</sub> 0.4-0.6 cell cultures) in 1 mL of final reaction volume of PBS. These reaction mixtures were kept at room temperature (22-23°C) for 15 minutes at slow agitation (30 rpm), and then analysed in a small size Malvern glass support containing 6 mL PBS.